SCUOLA NORMALE SUPERIORE DI PISA

Ph. D. Thesis

Synthesis, optical characterization and computational study of novel organic fluorophores

Giulia Marianetti

SUPERVISOR

Prof. Vincenzo Barone

2017

Contents

Abstract

Over the last three decades lot of interest has been devoted to light harvesting technologies. Recent findings on global warming and energy nonrenewable resources push us to alternative means of storing energy. Sunlight stands indeed as an ideal asset to take advantage of. In this insight Luminescent Solar Concentrators (LSCs) represent a way to decrease the cost of solar photovoltaics. LSC devices usually consist in a thin slab of transparent material (glass or polymer) doped with a fluorescent dye. Upon solar irradiation, a fraction of the emitted light, through means of internal reflection, is collected at the edges of the device where photovoltaic cells are located. Compared to traditional concentrators, which make use of mirrors and lenses, these devices show numerous advantages, such as theoretical higher concentration factors, the ability to work with both diffuse and incident light and no need for tracking devices or cooling apparatuses. Organic fluorescent dyes bearing π-conjugated electron-donor and -acceptor moieties exhibit intramolecular charge-transfer (ICT) properties, and can therefore show the optical properties required by LSCs such as high quantum yield and high Stokes shift. On account of this, the present dissertation will discuss the synthesis, UV-Vis characterization and computational study of a set of novel unsymmetrical and symmetrical push-pull azole-based dyes. These compounds are characterized by a 1,3-azole 2,5 substituted with two aromatic moieties bearing electron withdrawing (EWG) or electron donating (EDG) groups. Remarkably, the introduction of an heteroaromatic ring usually improves the thermal and chemical stability and the overall polarizability of the fluorophore.

The studied compounds were prepared through a robust synthetic pathway involving a palladium and copper-promoted direct C-H arylation reaction as key step. We took into account the effect of the peripheral electron poor funtionality as well as the nature of the central heteroaromatic core. In order to rationalize the experimental results we carried out TD-DFT studies, that allowed us to proper understand the charge tranfer occuring during the electronic transition. After selecting the best fluorophores for our aim, we investigated its efficiency in an LSC prototypes.

The studied summerized above were object of the following publications and communications:

Papers:

1. *"Highly regioselective C-5 Alkynylation of Imidazoles by One-pot Sequential Bromination and Sonogashira Cross Coupling"* F. Bellina, M. Lessi, G. Marianetti, A. Panattoni *Tetrahedron Letters* **2015**, 56 (25), 3855
2. *"Toward the Design of Alkynylimidazole Fluorophores: Computational and Experimental*

Characterization of Spectroscopic Features in Solution and in Poly(methyl methacrylate)" M. Biczysco, V. Barone, J. Bloino, T. Fornaro, C. Latouche, F. Bellina, M. Lessi, G. Marianetti, A. Panattoni, P. Minei, A. Pucci *Phys. Chem. Chem. Phys.* **2015**, DOI: 10.1039/C5CP03047A

3. "*Tuning of dye optical properties by environmental effects: A QM/MM and experimental study*" G. Del Frate, F. Bellina, G. Mancini, G. Marianetti, P. Minei, A. Pucci, V. Barone *Phys. Chem. Chem. Phys.* **2016**, 18, 9724

4. "Colourless p-phenylene-spaced bis-azoles for luminescent concentrators" F. Bellina, M. Lessi, C. Manzini, G. Marianetti, C. Pezzetta, E. Fanizza, A. Panattoni, P. Minei, V. Barone, A. Pucci *Dyes and Pigments* **2016**, 134, 118

Posters and oral communications:

1. Poster and flash presentation: "*Azole-based Fluorophores via Regioselective Pd-catalyzed Direct C-H Arylation Reactions*" Winter School of Organic Chemistry, Bressanone, February 2014. G. Marianetti, M. Lessi, C. Manzini, L.Perego, C. Pezzetta, P. Minei, A. Pucci, G. Ruggeri, F. Bellina. *Winner of SCI-Organic Chemistry Division prize.*

2. Poster: "*Azole-based fluorophores via regioselective Palladium catalyzed arylation reactions*" G. Marianetti, M. Lessi, C. Manzini, L.Perego, C. Pezzetta, P. Minei, A. Pucci, F. Bellina Organometallic Chemistry Directed Towards Organic Synthesis, IUPAC International Symposium 2015 Sitges.

3. Poster and flash presentation: "*2,5-Diaryl substituted azoles as promising organic fluorescent dyes for luminescent solar concentrators*" Sigma Aldrich Young Chemists Symposium, October 2015 G. Marianetti,F. Bellina, V. Barone, M. Lessi, P. Minei, A. Pucci. *Winner of Best Flash Presentation prize.*

4. Oral communication: "*New Azole-based Fluorophores: Synthesis, Optical Properties and Computational Study*" at Workshop Year of Light, Pisa, February 2015. M. Lessi, C. Manzini, L.Perego, G. Marianetti, C. Pezzetta, F. Bellina.

1. Introduction

Over the last three decades, a lot of organic π-conjugated molecules have been found to exhibit extremely interesting chromophoric behaviour. Since the optical response of these molecular materials is mainly governed by the structural characteristics of the constituent chromophores, the search for novel molecules with thrilling optical features at desirable wavelengths represents a highly active area of research at present.

In fact, nowadays organic molecules with a delocalized π-system of electrons represent attractive targets for applications in advanced functional materials. Thanks to their ease of preparation, well-defined and tuneable structure, molecular arrangement, and adjustable, peculiar and unique properties, (hetero)aromatic π-conjugated systems are a remarkable feature of materials science. Recently, organic π-conjugated structures have become an extensively explored, expanding area of organic chemistry, and have found widespread applications across various sectors of current research. Among the many different areas where this kind of compounds can find application there are: organic electronics and optoelectronics,[1-3] conductors,[4] photovoltaics[5, 6] and solar photon conversion.[7] Given the development in the above-mentioned fields, and in parallel to widely explored inorganic analogues, organic devices such as light-emitting diodes (OLED),[8] organic solar cells (OSC),[9] dye-sensitizing solar cells (DSSC)[10] and luminescent solar concentrators (LSC)[11, 12] belong to well established and known applications of π-conjugated molecules.

Quite often, the choice of the best candidate for the application of interest is hardly achievable through chemical intuition alone, since the effect on the optical features of the chromophore (i.e. absorption and emission maxima, Stokes shift and quantum yield) by changing the nature of functional groups is not easily predictable.[13] Therefore theoretical investigations on possible structure-to-property relationships are very important for the design and synthesis of optical materials with optimized performance. It is important to underline that several structural factors, such as the electron richness of the π-conjugation center, the strength of donor and/or acceptor substituents, the planarity of the π-conjugation center, the molecular symmetry, and the dimensionality of charge transfer networks are particularly significant.[14-20]

Since most experiments and real applications are usually performed in condensed phases such as highly concentrated solutions, thin films or doped polymers, the complication of inter-molecular and environmental interactions makes the theoretical study of the relationship between the structure and collective properties a challenging matter.

This study is aimed at devolping new classes of interesting organic dyes, wich can be employed

in energetic devices. It is important to address such a complicated subject not only from an empirical point of view, but also from a more sophisticated theoretical perspective, since many important physico-chemical properties of molecular systems can be predicted using computational techniques. In this insight density functional theory (DFT) has become very important in theoretical modeling. Many molecular properties can be calculated from exchange-correlation functions in comparison with traditional ab initio methods,[21] and recent examples have shown that it is possible to evaluate the optical properties of molecules correctly and accurately through means of DFT and time-dependent DFT (TD-DFT) methods.[22, 23] Through means of computational analysis it is possible to gain a systematic approach which offers the possibility to get a better understanding of the physico-chemical properties responsible for the observed optical features. In fact, computational methods give an insight on the structural and stereo-electronic molecular properties, in both the ground and excited electronic states.[24-27] The effect of the molecular environment can be mimicked for instance by means of Polarizable Continuum Models (PCM)[28] or more complex matrices where the chromophores can be incorporated.[29-32] This work, thus, shows how useful it is to employ computational tools that can provide a reliable mean to predict spectroscopic features, and can help understanding experimental results.

This thesis starts with a general overview on push-pull organic chromophores, to then explore their possible fields of application. In the end of this section attention will be devoted to heteroaromatic push-pull chromophores that constitute the primary interest for this dissertation.

1.1 Push-pull Organic Chromophores

The basic molecular structure for a push-pull organic chromophore can be described as follows: a π-system (or linker) end-capped with an electron donor (D) and an electron acceptor (A) moieties. D–A interaction, or so-called intramolecular charge-transfer (ICT) (**Figure 1**), in such D–π–A molecules accounts for even more distinct optoelectronic properties.[33]
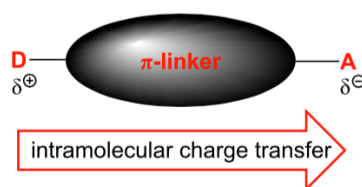
Figure 1: Schematic representation of ICT mechanism.

Thanks to the D–A interaction, a new low-energy molecular orbital (MO) is formed. Through irradiation with visible light facile excitation of the electrons within the new MO can be reached, and therefore push–pull molecules generally show a coloured aspect and are referred to as internal charge-

transfer (ICT) chromophores.[14-16] This ICT phenomenon is also responsible for the polarization of the push–pull chromophore and the presence of a molecular dipole. The extent of the ICT can be expressed by two limiting resonance forms,[33, 34] as shown in **Figure 2** for a simple D–π–A model based on nitroaniline. The impact of the ICT on the optical properties of π-conjugated molecules can be shown by the UV/Vis absorption spectra measured for aniline, nitrobenzene, 4- nitroaniline and 3-nitroaniline (**Figure 2**).[33] For the first two compounds only absorption in the UV region is being observed, 4-nitroaniline showed a pretty different behaviour: an intense and bathochromically shifted longest-wavelength absorption maxima (CT-band). On the other hand, 3-nitroaniline showed only a decreased CT-band as a result of a non-conjugating arrangement of the amino group (D) and the nitro functionality (A).[33]
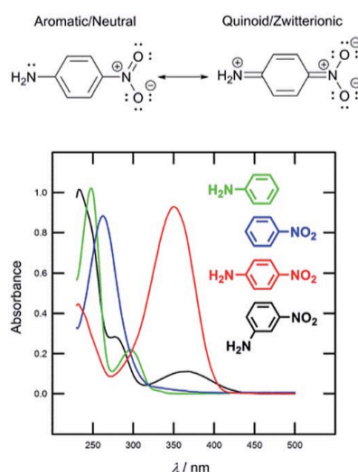
Figure 2: Limiting resonance forms and UV/Vis spectra for model D-π–A systems based on nitroaniline.

Typical electron donors (D) are represented by the substituents with +M/+I effects such as OH, NH_2, OR and NR_2, heteroaromatic moieties such as thiophene[35] as well as some metallocenes.[36, 37] On the other hand, the most used electron acceptors (A) involve substituents featuring -M/-I effects such as NO_2, CN, CHO and electron deficient heterocyclic compounds such as azines,[38] benzothiazole[39] and imidazole.[23, 40] **Table 1**[33] compares the electronic properties of selected electron withdrawing and donating groups used as A/D parts of push–pull molecules through the Hammett[41] σ_p and Pytela[42] σ^i substitution constants.

As shown in **Table 1** nitro/cyano and *N,N*-dimethylamino are among the strongest and most widely used electron acceptors and donors, respectively, and this can be explained through the above-mentioned constants σ_p and σ^i. Beside these groups, less common (perfluoro)sulfo(a)nyl and ferrocenyl groups also impart notable electronic effects (resonance and inductive) to push–pull molecules, as indicated by their high σ_p constants.

Acceptors			Donors		
Subst.	σ_p	σ^i	Subst.	σ_p	σ^i
NO$_2$	0.78	0.606	NMe$_2$	−0.83	0.089
CN	0.66	0.525	NHMe	−0.70	0.094
CHO	0.42	0.385	NH$_2$	−0.66	0.089
COMe	0.50	0.286	NHPh	−0.56	—
COPh	0.43	—	NPh$_2$	−0.22	—
COOH	0.45	0.264	OH	−0.37	0.157
COOMe	0.45	0.274	OMe	−0.27	0.220
CF$_3$	0.54	0.372	OPh	−0.03	0.278
COCF$_3$	0.80	—	SMe	0.00	0.217
C$_6$F$_5$	0.27	—	2-Thienyl	0.05	—
SO$_2$Me	0.72	0.551	Fc	−0.18	—
SO$_2$CN	1.26	—			
SO$_2$CF$_3$	0.96	—			
SF$_5$	0.68	—			
Pyridin-4-yl	0.44	—			
Benzoxazol-2-yl	0.33	—			
Benzothiazol-2-yl	0.29	—			

Table 1: Comparison in electronic properties of different functional groups.

Compared to *N,N*-dialkylamino (σ_p = -0.83), the wildely employed *N,N*-diphenyl(aryl)amino group (σ_p = -0.56) possesses a lower donating ability, most likely due to a partial delocalization of the amine lone electron pair to the appended aryls, which are generally arranged in a nonplanar manner.[33]

In most push–pull chromophores the π-conjugated path is created by a combination of multiple bonds (olefinic and acetylenic scaffolding)[14-16] and aromatic (mostly benzenoids)[14-16] or heteroaromatic spacers.[38, 40] Push–pull molecules can display several different molecular arrangements. The most simple, yet widely diffused is the linear one (D–π–A), but more complex structures such as quadrupolar symmetrical (D–π–A–π–D or A–π–D–π–A) and octupolar/tripodal ((D–π)$_3$–A or (A–π)$_3$–D) systems have been described too. It is worth mentioning that quadrupolar structures were introduced mainly to minimize the dipole induced intermolecular interactions that can lead to fluorescence quenching. In addition to these classical organizations, there are extraordinary arrangements reported in literature, such as V,[43] Y,[40] H[44] and X-shapes.[45]

The ICT, the corresponding HOMO–LUMO gap, and the optical response can be tailored by (i) attaching electron donors and acceptors of various electronic nature, (ii) assuring efficient D–A interaction, (iii) extension, composition and spatial arrangement of the π-linker, (iv) reducing the bond-length alternation of the π-system and (v) planarization of the entire molecule.[46-48]

Besides the aforementioned general use of organic π-conjugated molecules find predominant application as chromophores in many different fields in particular given the possibility to show the

peculiar characteristic of exhibiting fluorescence.

1.2 Fluorescent organic chromophores

Fluorophores, *i.e.* molecular entities (often organic) that emit fluorescence,[49] show a wide range of applications from technology to chemical and biological analysis. This is due to the properties of the fluorescence emission, which are strongly influenced by structural modifications and surrounding media, thus allowing a precise and selective tuning and monitoring. The usually observed properties are spectrum shape, peak position, quantum yield and lifetime; more specific techniques make use of other properties, such as quenching, fluorescence anisotropy and excimer formation.[50] Especially the dependence of the fluorescence emission from the micro-environment around the fluorophore (type of solution, presence of other interacting species, polymer surfaces, crystalline structures) and any possible interaction of the excited species therewith is largely employed to get information on local parameters: physical, structural or chemical. In this context it is used the term fluorescent probe (or indicator in the case of chemical parameters like pH and the concentration of a species). When the fluorophore is covalently bound to a target molecule, and the aim is to visualize or localize such species, the term fluorescent label or tracer is used. Fluorescent probes and tracers provide a wealth of information on various fields: polymers, solid surfaces, surfactant solutions, biological membranes, vesicles, proteins, nucleic acids and living cells.[49] Some of the most typical applications of fluorescent probes and tracers are summarized below, while selected fluorescent compounds used as probes are depicted in **Scheme 1**.
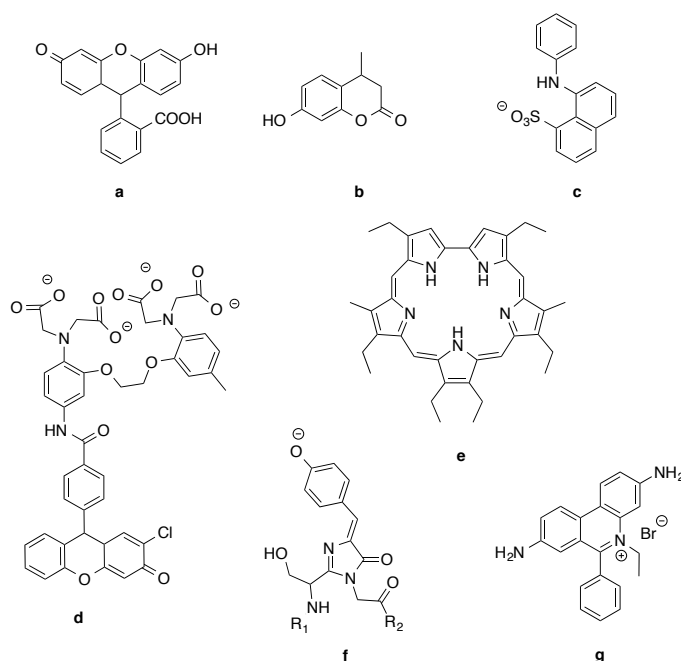
Scheme 1: Some representative fluorescent probes.

pH Indicators. Offer much better sensitivity than the classical dyes based on color change, and thus are widely used in analytical chemistry, bio-analytical chemistry, cellular biology and medicine. Two of the most known examples are fluorescein (**a**), with an exceptionally broad range of pH response, and 4-methylumbelliferone or 4-MU (**b**), a derivative of coumarin.

Polarity probes. Fluorescence emission is affected by the polarity of the medium, giving the possibility to employ polarity-dependent probes. An example is 1-anilino-8-naphthalenesulfonate or ANS (**c**), which is non- fluorescent in aqueous solution and highly uorescent in solvents of low polarity, allowing the selective visualization of hydrophobic regions in biological systems.

Molecular thermometers. They are based on the temperature dependence of some photophysical properties: fluorescence spectrum, quantum yield, excited-state lifetime. Typical of either organic or organometallic compounds; in all cases the intensity and lifetime decreases with a temperature increase.

Pressure sensitive paints. Also known as PSP, these are fluorescent paints sensitive to air pressure, used for the aerodynamic characterization of aircraft and car models in wind tunnels. They are oxygen-sensitive, containing fluorophores whose fluorescence is quenched by oxygen; therefore, the larger the air pressure, the larger the partial pressure of oxygen and the higher the efficiency of quenching.

Molecular sensors for ion and molecule recognition. They consist of a fluorophore (signaling unit) linked to a receptor (recognition moiety); the recognition event (*i.e.* analyte binding) is converted into an optical signal expressed as the changes in the characteristics of fluorescence. Many aspects are taken into account in the design of such sensors. They are used for the recognition of a variety of species: (i) cations, like the Calcium Green (**d**), for Ca^{2+} ions; (ii) anions, like diprotonated form of hexadecyltetramethylsapphyrin (**e**) for F^- ions; (iii) neutral molecules (based for example on cyclodestrins or porphyrins).

Auto fluorescence and fluorescent labels in biology. Used in tracing and imaging biological objects by means of their fluorescence, intrinsic or acquired with specific labels. Several detection techniques, based on a presence/absence answer, rely on specific fluorescence. Cases of intrinsic fluorescence are found in diverse biomolecules, the most famous example being the green fluorescent protein or GFP, with an aminoacid-derived fluorophore (**f**). Some coenzymes and porphyrins are other examples. Small molecules are used more as labels, like the DNA-intercalating compound ethidium bromide (**g**), non-fluorescent in solution but highly fluorescent and bright when bound to

the nucleic acid.

1.3 Push pull organic chromophores in energetic devices and smart materials

In the field of dye-sensitized solar cells (DSSCs) *push-pull* systems find wide application. A DSSC is a system with three components: a semiconductor, a chromophore (or dye or sensitizer, in many cases a fluorophore) and an electrolyte brought together to generate electric power from light without suffering from any permanent chemical transformation.[51] A monolayer of the dye is attached to the surface of the semiconductor; its photoexcitation results in the injection of an electron into the conducting band of the semiconductor (**Figure 3**).
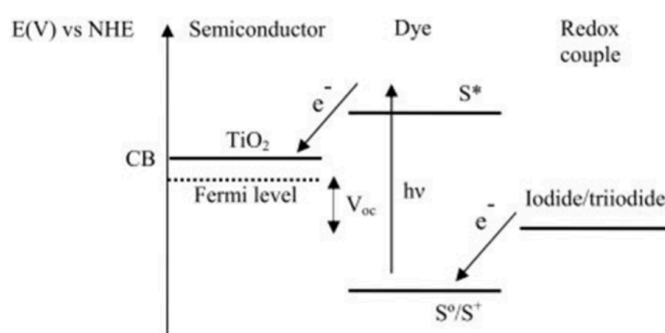
Figure 3: Schematic representation of a DSSC.

The dye is regenerated by an electrolyte, usually an organic solvent containing a redox couple, such as iodide/triiodide. This electron donation is compensated by the reduction of triiodide at the counter electrode, closing the circuit.

The performance of DSSCs strongly depends on the nature of the sensitizer and its combination with electrodes and electrolytes. It is necessary to employ chromophores that possess broad absorption spectra in order to absorb more photons for energy conversion. Ruthenium complexes are a well-studied class of sensitizers, one of the most widespread is the complex $[Ru(bipy)_3]^{2+}$, with good results in terms of light to electricity conversion. However, ruthenium is a noble and expensive metal and other metals used share this characteristic (rhenium, osmium and iridium), thus research has been directed towards the development of metal-free sensitizers, especially organic sensitizers.[52] These systems have a number of advantages, such as high molar extinction coefficients, high efficiency and low cost.[52, 53]

Other applications range from laser emission to mechanical properties. For example, under specific conditions, some *push-pull* fluorophores can show lasing emission, being able to convert the emission of a cheap and easily available IR laser into a more useful visible laser emission through a two-photon absorption induced fluorescence phenomenon.[40, 54, 55] Some systems instead show

piezochromism: their optical properties depend on applied external pressure in the solid state. These systems are of interest in the fields of piezochromic materials, security papers, data storage, opto-electronic devices,[56, 57] and can also be incorporated in polymeric matrices.[58, 59]

The combination of an organic dye with polymeric matrices can lead to the formation of the so-called "smart" materials.[59] These materials offer a particular optical response to external stimuli (mechanical, thermical and others) thanks to the presence of the incorporated organic dye. Besides these applications, very interesting devices that can be achieved through the combination of organic fluorophores with polymers are Luminescent Solar Concentrators (LSCs).[11, 12]

The LSC[60] is a unique nonimaging optical device that can be used to concentrate sunlight onto a small area of solar cells. A typical design consists of a polymer plate doped with a luminescent material, such as a fluorescent organic dye, with solar cells optically matched to the plate edges. **Figure 4**[61] shows a cross sectional diagram of an LSC and illustrates the operation of the device.
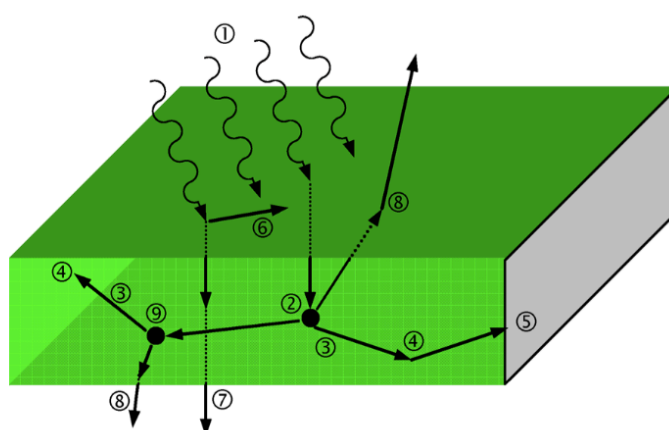
Figure 4: Cross sectional diagram of a LSC. Ideally sunlight (1) incident on the front surface of the LSC is absorbed by a fluorescent organic dye molecule (2). Light is subsequently re-emitted at a longer wavelength at a high fluorescent quantum yield (3) and is transported to the edge by means of total internal reflection (4). Solar cells (5) mounted to the perimeter of the LSC convert the concentrated luminescence to electricity. Common loss mechanisms include front surface reflection (6), transparency to long-wavelength incident light (7), and escape cone losses for light emitted within the Brewster angle (8). Additionally, luminescence may be reabsorbed by dye molecules that have an overlapping absorption and emission spectra (9), which can again result in luminescence being emitted (3) and transported to the edge (4) or passing out the front or rear escape cones (8). Some loss mechanisms are not illustrated here such as parasitic absorption in the host matrix, and scattering of light from within the bulk and at surfaces.

The main reason for implementing an LSC is to replace the large area of expensive solar cells required in a standard flat-plate photovoltaic panel, with an inexpensive polymeric collector, thereby, reducing the cost of the module (in dollars per watt) and also of the solar power (in dollars per kilowatthour). A main advantage of LSC technology compared to other concentrating systems is that it can collect both direct and diffuse solar radiation. This means that tracking of the sun is not required,

thus enhancing further potential cost reductions and making LSCs excellent candidates for building integrated photovoltaics, as well as making them the ideal PV technology for cloudier northern European climates. Similarly to electricity conversion, LSCs also have applications in daylighting,[62] thermal conversion, and hybrid thermal–photovoltaic systems that could generate electricity and extract the heat generated by the LSC plate.[63] The first publications on LSCs first appeared in the late 1970s,[60,63] and the technology was studied intensely through the early 1980s.[64] The highest conversion efficiency achieved for a large-area LSC (40 cm × 40 cm × 0.3 cm) was η (LSC) = 4.0% with a two-stack system consisting of a shorter wavelength emitting plate coupled to gallium arsenide (GaAs) solar cells and below that, a longer wavelength emitting plate coupled to silicon (Si) solar cells.[65] Multilayered mixed-dye thin-film LSCs of smaller dimensions (14 cm× 14 cm × 0.3 cm) achieved η (LSC) = 3.2% using Si solar cells and η (LSC) = 4.5% using GaAs devices.[66] It was estimated that the maximum achievable conversion efficiency of LSCs that collected sunlight in the range 300–900 nm was η (LSC) = 8–12%.[66] However, to the best of our knowledge the best efficiency for LSC devices was reported by Sloff *et al*.[67], with a power conversion efficiency of 7.1%. This result was affordable through the combination of two organic dyes (Lumogen Red 305 and Fluorescence Yellow CRS040) dispersed in PMMA.

Recently, there has been a renewed interest in LSCs due to the availability of new luminescent materials. There are four main criteria that should be met in order for LSCs of high efficiency to be achieved with Si solar cells.

- Absorption of all wavelengths λ < 950 nm with high absorption coefficients
- Minimum reabsorption losses due to overlap of absorption   and emission spectra
- Near-unity fluorescence quantum yield (FQY)
- Long-term outdoor stability (more than ten years)

Typically, organic and inorganic materials possess unique characteristics, both satisfying some but not all of the aforementioned criteria. However organic materials can display several advantages compared to the inorganic ones: they are affordable with cheaper and simpler synthetic procedure, and avoid the precence of heavy metals in the environment. The implement of chromophoric organic entities with promising features for LSC devices is thus a challenging subject and is going to be one of the main aim of this dissertation.

1.4 Heteroaromatic push-pull chromophores

Recently, it was also recognized that push–pull systems applicable as organic materials should possess high chemical and thermal robustness, good solubility in common organic solvents, and should be available in reasonable quantities. Hence, various five- and six-membered heteroaromatics were utilized as suitable π-conjugated chromophore backbones. Moreover, heteroatoms may act as auxiliary donors or acceptors and improve the overall polarizability of the chromophore. In this respect, five-membered azoles seem to be particularly suitable as π-conjugated backbones.

It is worth mentioning how the presence of heteroaromatic rings can affect aromaticity and therefore the HOMO-LUMO band gap. As an example we can analyze the result of a study, reported by Kulhánec *et al.*,[34] on different derivatives bearing, as unsaturated linker, 1,4-phenylene and 2,5-thienylene spacers (**Scheme 2**).
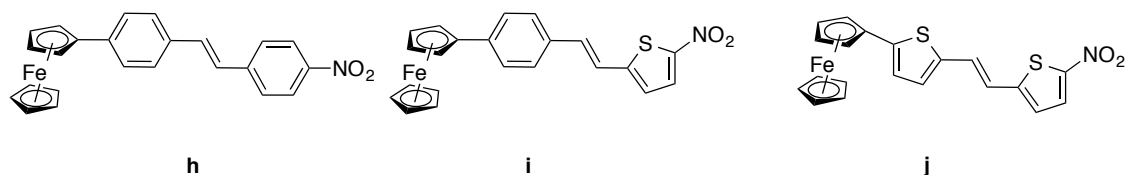
Scheme 2: Ferrocene-π-NO$_2$ push-pull molecules

In this case it is clear how the change from a pure aromatic core to an heteroaromatic one can modify the electronic properties of the whole sistem. Gradual replacement of 1,4 phenylene moieties with 2,5-thienylene ones mainly results in lowered LUMO energetic levels. Hence, the replacement of one 1,4-phenylene unit resulted in a decrease of energy gap from 1.51 to 1.34 eV. Conversely, the replacement of the second phenylene unit poorly affected the band gap. This phenomenon can be due to the lower aromaticity of the heteroaromatic cores, due to the fact that heteroaromatic rings display a poorer aromatic character when compared to benzene.[68] Moreover, in the series **h-j** the absorption spectra showed a gradual red-shift, this can also be due to the overall lower aromaticity of the system. The phenomenon shown by this example is only one of the reasons why heteroaromatic compounds can afford peculiar optical feautures.

The main advantages of employing heteroaromatics lie in their high chemical and thermal robustness, good solubility in common organic solvents and availability. Furthermore, heteroatoms can enhance the donor/acceptor character of the groups (playing the role of auxiliary donors or acceptors) and improve the overall polarizability of the chromophore.

Among azoles, imidazole has been studied as part of π-conjugated backbones. The role of imidazole in π-backbones and synthetic routes towards these systems have been recently reviewed

by Bureš and Kulhánek.[40] It possesses two nitrogen atoms of different electronic nature, has good characteristics of stability and can be easily synthesized and further functionalized at positions N1, C2, C4 and C5. Other azoles, like oxazole and thiazole, have similar properties and could thus be substitutes of imidazole.
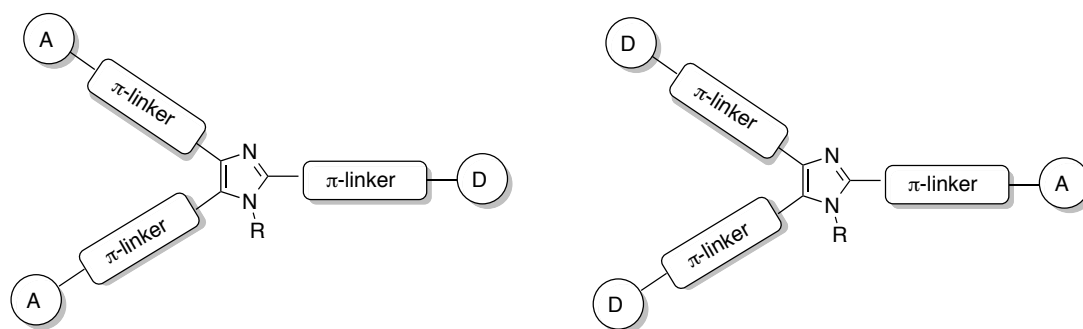
Scheme 3: Orientations of substituents in imidazole-derived CT-chromophores. A and D are respectively the acceptor and donor group, while the linker is a -conjugated linker.

Triarylimidazoles and derivatives with larger π-linkers represent a typical D-π-IM-(π-A)$_2$ and A-π-IM-(π- D)$_2$ push–pull systems. In these kind of chromophores two orientations of the substituents on an imidazole ring are possible, giving the molecule an overall Y-shape (**Scheme 3**). D-π-IM-(π-A)$_2$ systems generate the first class of chromophores, where every D/A group is linked at the imidazole through and additional π-linker; at the same way A-π-IM-(π-D)$_2$ systems generate the second class of chromophores. A non-symmetrical orientation of donors and acceptors is rare, most likely due to complications in the synthetic pathway.

The most employed method for the construction of these imidazole-based chromophores is the Debus-Radziszewski synthesis, based on the condensation of α-diketones and aldehydes in the presence of ammonia or ammonium salts (**Scheme 4**). Various substituted 2,4,5-triarylimidazole-derived chromophores (lophines) have been synthesized with this method.[40] Similar strategies are used for diimidazole-derived compounds, bearing two imidazole rings as donor and acceptor moieties, and benzimidazole-derived compounds, which can be obtained also with the condensation of arylenediamines or *o*-nitroanilines with an aldehyde or carboxylic acid.[40] A typical and well-studied acceptor moiety is the 4,5- dicyanoimidazole, firstly synthesized in 1950 by Woodward.[40]
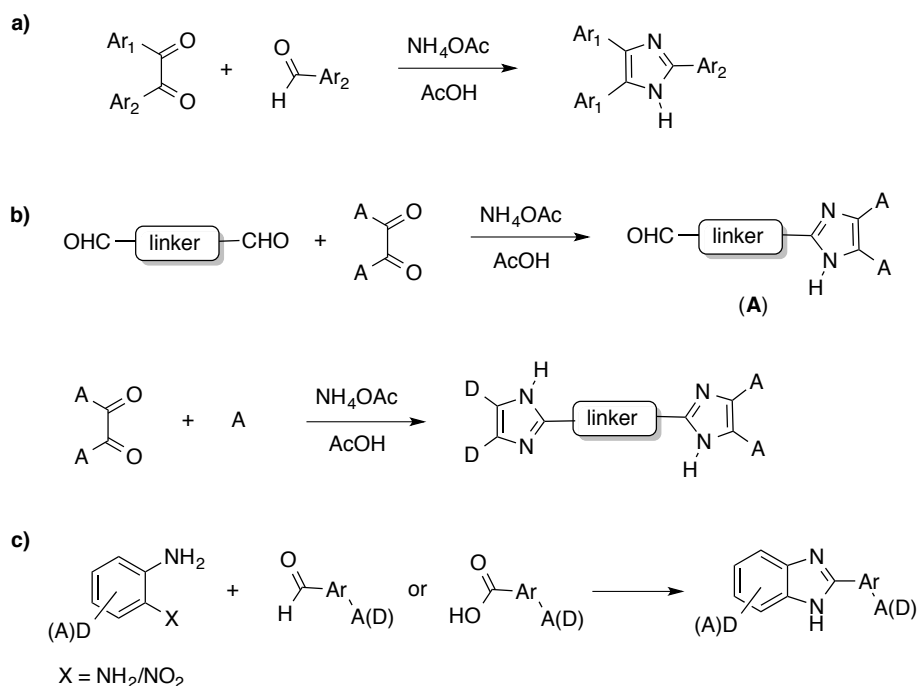
Scheme 4: Debus-Radziszewski synthesis as a common approach towards various chromophores: (a) general procedure towards triarylimidazole derivatives; (b) general two-step procedure towards diimidazole derivatives; (c) general procedure towards benzimidazole derivatives.

In **Scheme 5** are summarized some derivatives of this compound recently used as precursors for the construction of various CT chromophores. Y-shaped aryl-substituted azole-based chromophores have been intensively studied since the first efforts by Moylan, Miller and coworkers;[40, 69 70] they synthesized and compared the optical properties of a series of D/A triarylazoles (imidazoles, oxazoles and thiazoles) of the A-π-IM-(π-D)$_2$ class, as reported in **Scheme 6**. These systems showed exceptional thermal stabilities, respectable dipole moments and significant nonlinearities, showing a major dependence of properties from the D/A substituents rather than the conjugating heterocyclic ring.
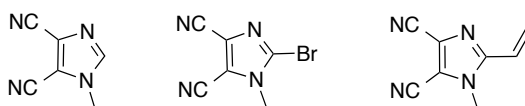
Scheme 5: Important dicyanoimidazole derivatives.

X = NH, O, S
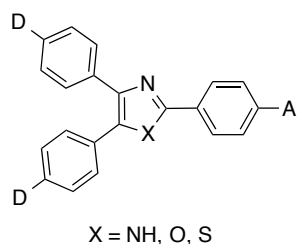
Scheme 6: Moylan and Miller's model of azole-based Y-shaped chromophore.

A very simple but less studied motif is the 1,4-phenylene linker; in this domain the synthetic methods leading to 1,4-phenylene linked bis-heterocyclic compounds have been recently reviewed by Shaker.[71] These studies concerning different azoles focus on the formation on mainly symmetric derivatives, we report two significant examples in **Scheme 7**.

a)

CHO + 2 (phenyl, O, OH) →(2 NH$_4$OAc, 10 mol% CAN)→ product

b)

CHO + 2 (R$_1$, R$_2$, R$_3$, NH$_2$, NH$_2$) →(PEG-400 (0.1 mL), 140 °C)→ product (R$_1$, R$_2$, R$_3$)
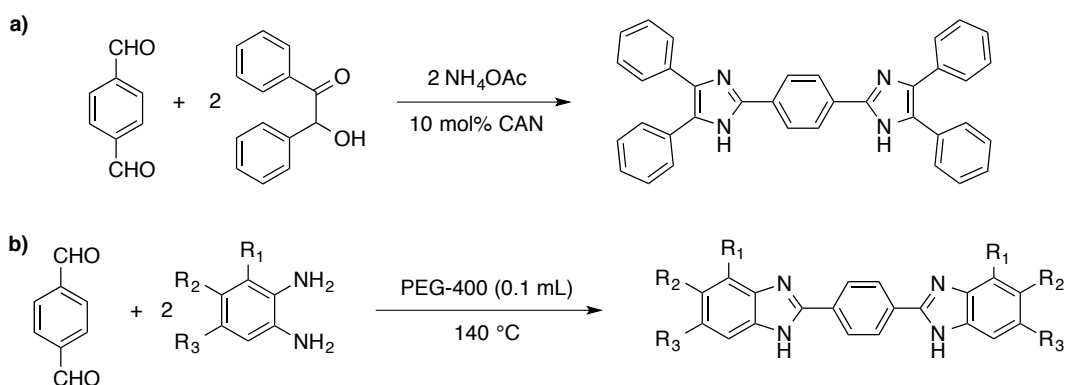
Scheme 7: Two synthesis of 1,4-phenylene spaced bis-azoles and benzoazoles reviewed by Shaker.

The major part deals with imidazole compounds, but also oxazole, isoxazole and thiazole derivatives can be found in this review. The typical method of synthesis involves a cyclization generating the desired heterocycles, often with a condensation step like the above-mentioned Debus-Radziszewski synthesis. Large use have been made of this class of compounds due to their unique optical properties and the possibility to use them in two-photon fluorescence and as pH probes.[72] In 1975 Mahadik and Sunthankar[73] reported the synthesis of a series of *N,N'*-disubstituted phenylene-linked bis-imidazoles with yields of 50-60%, but without any optical properties. Since then only in 2008 Jadhav and coworkers[74] described the synthesis of 2,2'-(1,4-phenylene)bis(5-phenyl-1*H*-imidazole) (along with tetrasubsituted similar compounds), again without reporting any optical properties. The synthesis was accomplished as a condensation between terephthalic aldehyde and phenylglyoxal in the presence of ammonium acetate and catalysis by phosphomolybdic acid in aqueous acetonitrile (**Scheme 8**). In 2010 Song and coworkers[75] reported the synthesis of several symmetrical disubstituted bis-imidazole derivatives with a 1,4-phenylene as linker.

The reaction consisted in a condensation between benzene-1,4-dicarboximidamidium dichloride and different 1-aryl-bromoethanones in solventless conditions through microwave irradiation (**Scheme 9**). The obtained compounds showed interesting fluorescence properties, with little dependence on functional substituents, and good quantum yields. These compounds also showed solvatochromism (dependence of the wavelength of emission on the nature of the solvent). In 2013 other compounds of this kind were synthesized again by Song and coworkers[76] with their own methodology, along with fluorescence spectra and crystal and electronic structure determination.

Moving on to thiazoles, in 1944 Erlenmeyer and coworkers[77] obtained diverse thiazole derivatives, including 2,2'-(1,4-phenylene)bis(5-phenylthiazole) through condensation reactions. In 1955 a patent by Trosken[78] described the preparation of the 2,2'-(1,4-phenylene)bis(5-phenylthiazole), an analogue containing oxazole in place of thiazole, and their sulfonated derivatives. The latter derivatives were employed in whitening cotton owing to their blue fluorescence. In 1986 the synthesis of some brominated phenylene bis-oxazoles, bis-benzothiazoles and bis-thiazoles was reported, along with their fluorescence spectra. [79] In 2009 and 2010 Noei and Khosropour[80, 81] reported the synthesis of a series 2,2'-(1,3- phenylene)bis(5-arylthiazoles). They employed two different *green* protocols based on a high yieald an ultrasound assisted condensation reaction, using as reaction *green* medium 1-*n*-butyl-3-methylimidazolium tetrafluoroborate ([bmim]BF4) or PEG-400 (**Scheme 10**). However this work is more biologically than technologically oriented. It can be observed that in each of these cases the employed synthetic protocols consisted in condensation reactions by which the heteroaromatic nuclei are created. Simple and characterized by high yields, these protocols are however able to provide only symmetrical derivatives due to poor selectivity. Furthermore, the required precursors are often not readily available, thus limiting the structural variety of synthesized compounds.
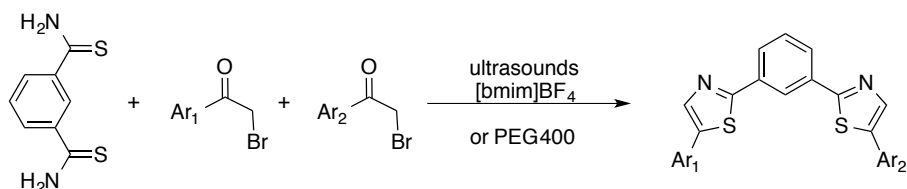
Scheme 10: Noei and Khosropour's synthesis of some 1,3-phenylene bis-thiazoles.

In 2014 Bellina and coworkers[23] published the first synthesis of unsymmetrically substituted 1,4-phenylene linked bis-imidazoles **1**, employing a totally different approach: instead of condensations, two sequential regioselective palladium-catalyzed direct C-H arylation reactions were the key steps of the whole procedure. In contrast with the traditional transition metal-catalyzed cross-coupling reactions involving stoichiometric amounts of organometallic reagents and (pseudo)halides, transition metal-catalyzed direct arylation reactions allow the formation of (hetero)aromatic C-C bonds without the need of activation of both coupling partners.[82-84] The unsymmetrical derivatives obtained in this way show interesting optical properties such as large Stokes shifts, high fluorescence quantum yields and fluorescence retaining in the solid state, as similar compounds (like oxazole-containing derivatives) already described in the literature.[85] The procedure is summarized in **Scheme 11**, but it will be further discussed in the next sections.
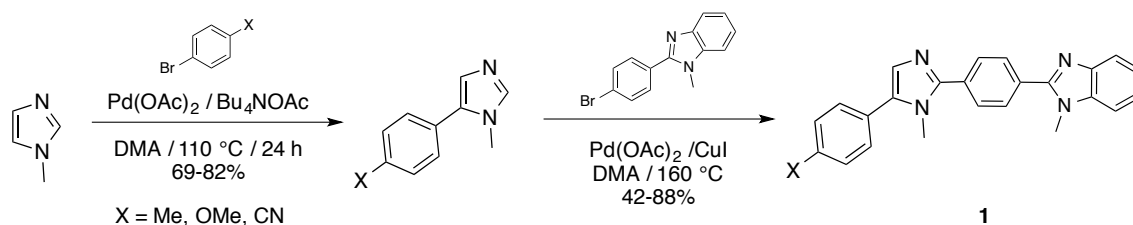
Scheme 11: Bellina's synthesis of unsymmetrically substituted 1,4-phenylene linked bis-imidazoles.

In continuation with these recent results, in this thesis two new series of fluorophores of general structure **2 and 3** (**Scheme 12**) will be synthesized, and their optical properties will be evaluated. Furthermore we will take into account a computational approach to evaluate possible molecular modification in order to obtain more interesting spectroscopic features.
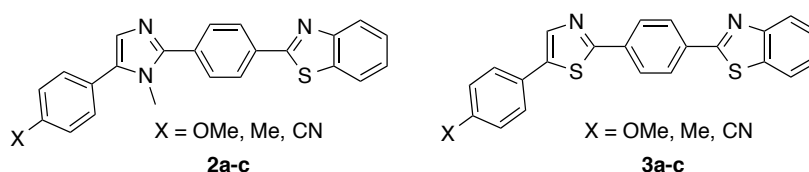
Scheme 12: Target compounds **2a-c** and **3a-c**.

These novel compounds structurally resemble bis-imidazoles **1**, but differ from them in the

replacement of 1-methylbenzimidazole with benzothiazole and, for compounds **2 and 3**, also for the presence of thiazole in place of 1-methylimidazole. These structural modifications have been planned with the aim of evaluating the influence of the replacement with sulphur of one or both the nitrogen atoms on the physical and spectroscopic properties of the fluorophores. We focus on *p*-substituted derivatives to avoid synthetic complications due to steric hindrance while keeping conjugation between the X group and the π-skeleton. The three groups are chosen as typical examples of electron-releasing, electron-neutral and electron-withdrawing groups, respectively OMe, Me and CN (Hammet's constants[33] (**Table 1**): OMe -0.27; Me -0.17; CN +0.66). Thus they are likely to be representative of other similar substituents concerning synthetic difficulties and spectroscopic properties. In the compounds of the series **2a-c**, we deal with *N*-methylated derivatives to obtain a better solubility in organic solvents and, upon substitution of the methyl group with longer alkyl chains, to achieve good affinity with polymeric matrices. Furthermore, the protection of the N1 position allows the use of a wider spectrum of synthetic techniques.[82] Compounds **3a-c** were addressed also under a computational point of view, in order to understand and explain the different spectroscopic behaviour caused by the insertion of different heteroatoms in the molecular backbone.

Another interesting set of chromophores, derived from a functionalization of the imidazole ring, is represented by compounds **4** (**Scheme 13**). In this case *N*-methylimidazole was arylated at C2 and alkynylated at C5. This modifications allowed the formation of a novel family of chromogenic molecules, through our recently reported synthetic procedure, figuring a two step protocol that will be discussed in detail in the next chapters.[86]
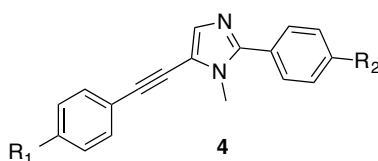
Scheme 13: Target compounds **4**.

We devoted our efforts in studying the optical behaviour of compounds **4** in solution and in a polymeric matrix, trying to find the best computational model to describe the experimental result, and to design a new and promising fluorescent dye. Both family of compounds **2**-**3** and **4** derived from an unsymmetrical functionalization of *N*-methylimidazole. It is possibile however to give very interesting compounds also from a symmetrical dervatization of azoles: in this insight the new class of compounds **5** and compound **6** (**Scheme 14**) represent a significant example. In the next sections we will address the C2 and C5 double direct arylation procedure to allow the formation of promising

fluorohores (compounds **5**) for luminescent solar concentrators applications. In this case we will also exploit computational tools to rationalize experimental results. In particular we will focus on the structural characteristics that lead to a powerful optical response in such small molecules.
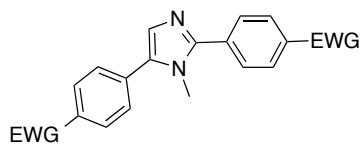
Scheme 13:Target compounds **5**.

2. Heteroaromatic chromophores for Luminescent Solar Concentrators

As stated in the previous chapter, Luminescent Solar Concentrators are basically constituted by a thin slab of polymer doped with a luminescent material, mainly an organic dye. Upon solar radiation the light is absorbed by this dye and then re-emitted and concentrated on small photovoltaic cells placed on the edges of the device. Given the structural features of Luminescent Solar Concentrators, the characteristic of the luminescent species within contained, are of primary interest in improving this technology. The ideal chromophore for this application should provide:

- High quantum yield, in order to maximize the fraction of light that is concentrated on the PV cells.
- Wide Stokes shift, to minimize re-absorption of the emitted light.
- Thermal and photochemical stability.
- Effective and scalable synthetic approach.

In this insight push-pull organic chromophores, containing heteroaromatic rings, result particularly appealing. Such compounds are, in fact, attainable through simple and scalable synthetic procedures and their optical features can be tuned according to light modifications on the molecular backbone or functionalities. Even the insertion of a different heteroatom can result in a dramatic difference in the optical behaviour, as we will show in the next section.

Here we report the synthesis, optical study and computational analysis of three different classes of heteroaromatic dyes, that were prepared and designed to give interesting performances in LSCs technology. All the three sets of compounds are the result of the functionalization of imidazole (and thiazole, for compounds **3**) on its C2 and C5 position, this is a brief overview on their main structural aspects:

- *1,4-Phenylene-spaced azole-benzothiazole chromophores of general structure **2** and **3*** (**Scheme 15a**)
  This dyes were designed in continuation with a recent work by our research group,[23] to study the effect of the insertion of one and then two atoms of sulfur in replacement of nitrogen, on the spectroscopic behaviour of these compounds.
- *5-Phenylethynyl-4-phenylimidazole push-pull fluorophores of general structure **4*** (**Scheme 15b**)
  Through a novel and efficient synthetic protocol, developed by our research group,[86] we were able to synthesize these class of organic dyes that features as key aspect a triple carbon-carbon bond as part of the π-backbone.
- *2,5-Diarylimidazole dyes of general structure **5*** (**Scheme 15c**)

This last set of compounds is the simplest among the three: imidazole was functionalised with a double direct arylation reaction to give chromophores **5**. Eventhough these latest compounds are small-sized they showed very interesting optical features.
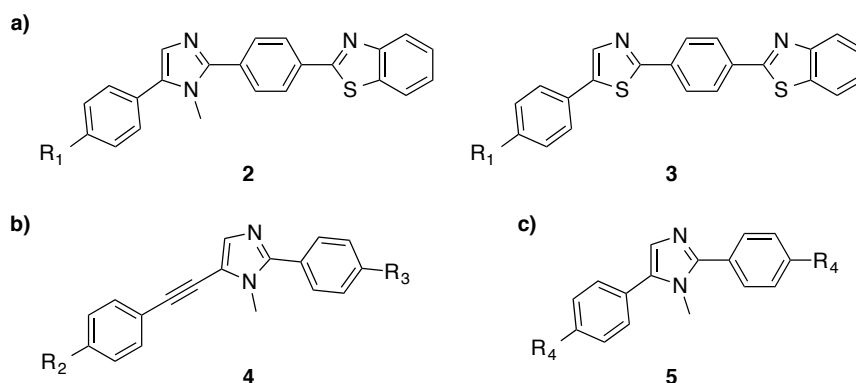
Scheme 15: Target compounds **2-5**.

2.1 1,4-Phenylene-spaced azole-benzothiazole chromophores of general structure 2 and 3

As stated above, we exploited the potentiality offered by the new 1,4-phenylene-spaced azoles as near-UV absorbing fluorophores characterized by large Stokes shifts (SS) and green emission to be used in colorless LSC with optical efficiencies close to 6. Mixed imidazole-benzimidazole analogues were already proposed by us[23] as fluorophores with SS near 100 nm, very high F, and with a bright blue-green emission well retained in the solid state. Notwithstanding their excellent emission features, their fluorescence peaked at λ < 430 nm did not match the working window of a Si-based PV cell (λ ≥ 500 nm),[87] thus impeding their application in LSCs technology.[23] Therefore, new push-pull imidazole-benzothiazole and thiazole-benzothiazole fluorophores, **2a-c** and **3a-c** (**Scheme 16**), were efficiently synthesized aimed at retaining the features of imidazole-benzimidazole analogues (**1a-c**), while shifting their emission to longer wavelengths.

2.1.1 Synthetic approach

Due to the structural analogies between bis-imidazoles **1** and compounds **2**, and taking into account that *N*-methylimidazole and thiazole usually display very similar reactivities when involved in direct C-H arylations,[83] a synthetic strategy, very similar to the one adopted for the synthesis of structure **1** was devised[23] (**Scheme 16**). This two-step sequence involve at first the regioselective direct C-5 arylation of 1-methyl-1*H*-imidazole (**10a**) for compounds **2a-c** or thiazole (**10b**) for compounds **3a-c** with commercial aryl bromides **9a-c**. The resulting 5-aryl-1-methyl-1*H*-imidazoles **7a-c** or 5-arylthiazoles **7d-f** were then involved in a direct C-2 arylation with 2-(4-bromophenyl)benzo[*d*]thiazole (**8**), which represents a common precursor of both classes of

derivatives.
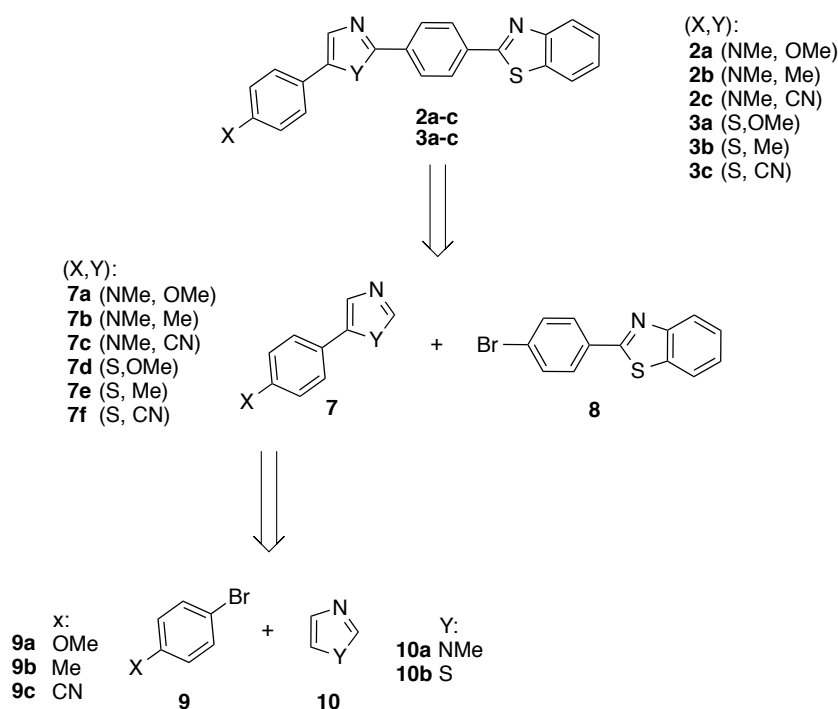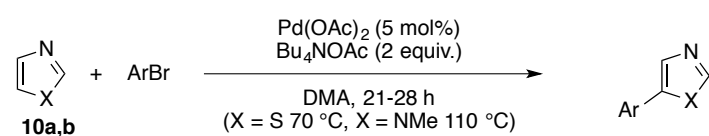
Scheme 16: Retrosynthetic approach to compounds **2** and **3**.

2.1.2 Synthesis of 5-arylazoles

In 2013 Bellina and coworkers[83] published a protocol for the direct C5 arylation of various azoles with aryl bromides. Starting from a study on 1-methyl-1*H*-pyrazole as model substrate, they found that the use of tetrabutylammonium acetate (TBAA) as base under ligand-free conditions provides good yields at an unusually low temperature for this kind of reactions. In particular, the coupling was carried out at 70 °C with 1-methylpyrazole, **10b** and oxazole, and at 110 °C with **10a**. A scheme and a selection of results for both *N*-methylimidazole (**10a**) and thazole (**10b**) are summarized in **Table 2**. Good C5 regioselectivity was observed irrespective of the nature of the *para* substituent on the aryl bromide, probably because the possibility of lowering the reaction temperature to 70 °C due to the successful use of TBAA enhanced the kinetic discrimination among the C-H bonds of the azoles, which possess different dissociation energies. Thanks to its mild conditions, efficiency and very high regioselectivity this protocol has been chosen as the most suitable for the synthesis of the required 5-arylazoles **7**. According to the method reported by Bellina and coworkers[83] (**Table 2**), azoles **10a** and **10b** were reacted with 1.5 equiv. of the required bromide **9a-c** in the presence of 5 mol% Pd(OAc)$_2$ as precatalyst, 2 equiv. of TBAA as base in DMA for 24-72 h (**Table 3**). The reaction temperature was 70 °C when employing **10b** and 110 °C when employing **10a**. Isolated yields were generally good, except for compounds **7b** and **7c** probably due to the use of a not very well dried lot of TBAA

(which is a highly hygroscopic solid). In fact, the crude reaction mixture of the direct arylation involving **10a** and **9c** was contaminated by *p*-bromobenzamide, deriving from the hydrolysis of **9c**.

Table 2: Bellina's C5 arylation of thiazole and 1-methylimidazole with TBAA.[83]

Pd(OAc)$_2$ (5 mol%)
Bu$_4$NOAc (2 equiv.)

DMA, 21-28 h
(X = S 70 °C, X = NMe 110 °C)

10a,b + ArBr →

X/Ar	Reaction time [h]	Isolated Yield [%]
S / 4-MeC$_6$H$_4$	21	65
S / 4-MeOC$_6$H$_4$	48	67
S / 4-O$_2$NC$_6$H$_4$	48	70
S / 2-MeOC$_6$H$_4$	29	59
NMe / 4-MeC$_6$H$_4$	22	81
NMe / 4-MeOC$_6$H$_4$	24	82
NMe / 4-O$_2$NC$_6$H$_4$	24	45
NMe / 2-MeC$_6$H$_4$	24	68
NMe / 4-NCC$_6$H$_4$	24	69
NMe / C$_6$H$_5$	23	75

Remarkably, the observed C5 regioselectivity was higher than 95%. The products were characterized by NMR spectroscopy and mass spectrometry and had generally high GLC purities.

Table 3: Synthesis of 5-arylazoles **7a-f**.

Pd(OAc)$_2$ (0.05 mol%)
Bu$_4$NOAc (2 equiv.)

DMA (5 mL/mmol)
Y = NMe: 110 °C
Y = S: 70 °C

10a,b + **9a-c** (1.5 equiv.) → **7a-f**

Arylbromide	5-arylazole	Reaction time [h]	Isolated yield [%]
9a	7a	24	82
9b	7b	26	26
9c	7c	72	34
9d	7d	56	53
9e	7e	24	65
9f	7f	56	61

2.1.3 Mechanism of the C5 Pd-catalyzed direct arylation of azoles

The first mechanistic hypothesis by Miura[88] is that direct arylation of azoles (and more generally of five-member heteroaromatics) takes place as an electrophilic aromatic substitution (S$_E$Ar). The C5 position is preferred for an electrophilic substitution according both to resonance theory and quantum-mechanical computations.[89] The catalytic cycle involving a S$_E$Ar mechanism for a generic 1,3-azole is reported in **Scheme 17**. The first step is the oxidative addition of the nucleophilic Pd^0 to the aryl halide. When a Pd^{II} catalyst is used, preliminary reduction occurs by other species present in the reaction medium. The Pd^{II} complex resulting from the addition displays electrophilic nature and can therefore substitute through a common S$_E$Ar mechanism a hydrogen atom on the heteroaromatic ring. After the formation of the *cis* complex, the cycle ends through the reductive elimination step giving the 5-arylazole and restoring the Pd^0 catalytic species. Several experimental data support this hypothesis, particularly those reported by Bellina in 2005:[90] no reaction is observed with 1-arylimidazoles when a strong electron withdrawing group is present on the aryl moiety (the electron availability of the heterocycles is reduced); electron-poor aryl halides react better with 1-

arylimidazoles than electron-rich ones, while those extremely electron-rich do not react at all; the observed order of reactivity of *N*-substituted imidazoles[90, 91] follows the trends of Hammet's constants (σ_p) and of the ionization constants of protonated imidazoles:

$$NMe > NBn > NAr$$

$$\sigma_p:^{[41]}\ NPh\ (-0.01) > NBn\ (-0.09) > NMe\ (-0.17)$$

$$pK(BH^+):^{[92]}\ NPh\ (5.10) > NBn\ (6.09) > NMe\ (7.12)$$
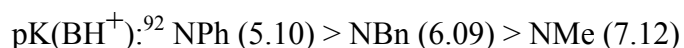
In 2006 Fagnou and coworkers[93] used pivalic acid as a co-catalyst in Pd-catalyzed direct arylation of aromatic systems. In particular, they carried out the arylation of benzene with 4-bromotoluene as a first screening of the carboxylic acids (co-catalysts), and with other bromoarenes using pivalic acid with good yields. A competition study showed that 4-bromotoluene reacts more easily with benzene over the electron-rich anisole in a ratio of 2:1, and that the electron-poor fluorobenzene reacts faster than benzene in a ratio of 11:1. The reaction with anisole produces a mixture 22:53:25 of *o*/*m*/*p* isomers, indicating that there is no directing effect by the methoxy substituent, no electronic preference and a minor steric bias resulting in a small statistical preference for the *m* and *p* positions. Whereas, the reaction with fluorobenzene gives a mixture 22:3:1 of *o*/*m*/*p* isomers, pointing out the importance of C-H bond acidity in regioselectivity and reactivity.
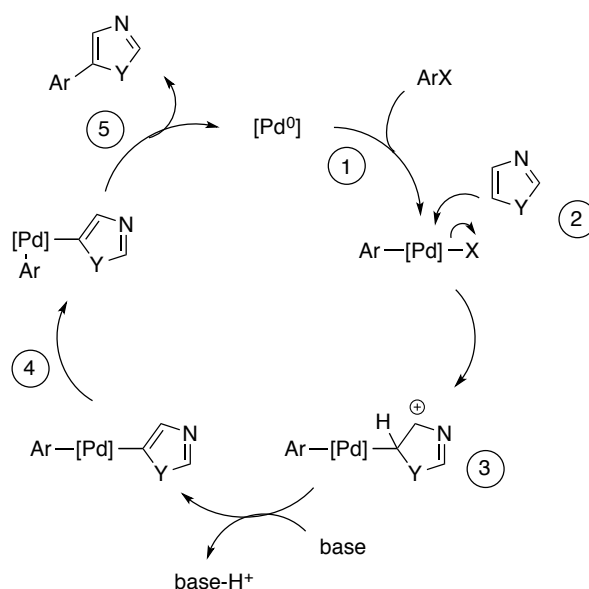
Scheme 17 Proposed S_EAr mechanism for the Pd-catalyzed direct arylation of azoles. Highlighted steps: (1) oxidative addition; (2) electrophilic aromatic substitution; (3) Wheland intermediate, stabilized by delocalization of the positive charge; (4) *cis-trans* isomerization of the Pd complex; (5) reductive elimination.

These results are incompatible with a S_EAr mechanism, but can be correlated to a proton-transfer

pathway. The mechanism proposed to explain these results is a Concerted Metalation-Deprotonation (CMD) type mechanism, reported in **Scheme 18** for a generic azole (it is the same process initially proposed for benzene[93]). After the usual oxidative addition, an anion exchange on the complex takes place and the complexed pivalate ion (generated *in situ* from pivalic acid and an inorganic base) assists the simultaneous metalation and deprotonation step on the azole, permitting the C-H bond cleavage; this is maintained coordinated to palladium without a Wheland intermediate. The efficiency of pivalate in respect of other carboxylate ions (acetate for example) is due to its good solubility in organic solvents. Recent theoretical investigations revealed that a CMD mechanism is of relevance for the Pd-catalyzed direct arylation of azoles.[94-96] In particular, the C-H bond at the C5 site is more reactive than the other two C-H bonds due to the stronger interaction between the Pd[II]-carboxylate catalyst and the azole at the C5 site.[96]

Despite the good results with benzene, it has already been pointed out that Fagnou's protocol[97] varies in efficiency (in terms of yield and selectivity) when azoles are employed; in particular the poor results with **10a** should be noted. An improvement came with the protocol by Bellina in 2013[83] with the use of TBAA as a promoter of the C5 regioselective direct arylation of various azoles.
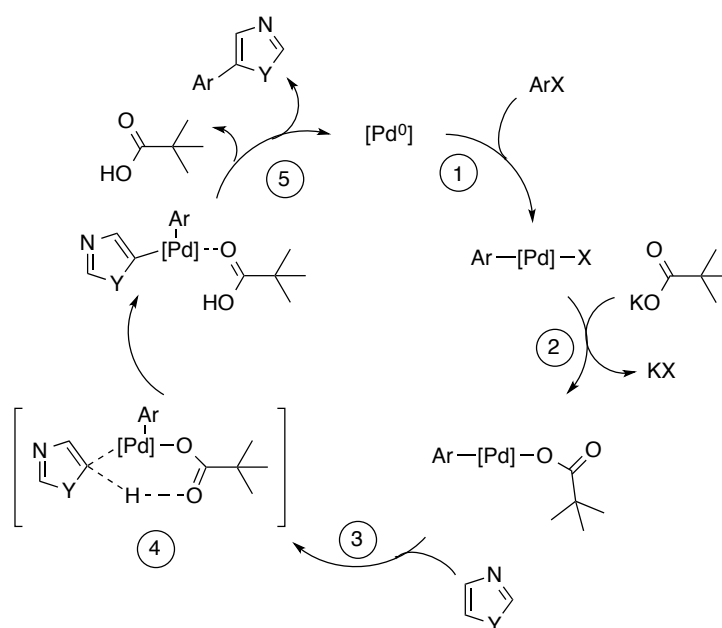
Scheme 18: Proposed CMD mechanism for the C5 arylation of azoles using pivalic acid as co-catalyst (Fagnou[93]). The same mechanism can be hypothesized for the C5 arylation with TBAA developed by Bellina.[83] Highlighted steps: (1) oxidative addition; (2) anion exchange with pivalate; (3) complexation of the azole; (4) transition state: the pivalate permit deprotonation with simultaneous metalation of the azole in position 5; (5) reductive elimination.

In this case it was found that the experimental order of reactivity for the three 1,3-azoles agrees with the calculated Gibbs free energies for the cleavage of the C5-H bond for a CMD mechanism:

oxazole > thiazole > 1-methylimidazole

ΔG at 298 K [Kcal/mol]:[94] oxazole (23.5) < thiazole (23.7) < 1-methyilimidazole (25.0)

This order of reactivity is different from that reported for common electrophilic substitution reactions in non-acidic media:[98]

1-methylimidazole > oxazole > thiazole

These experimental results suggest that a S_EAr pathway in these conditions can be excluded, while a CMD mechanism, supported by theoretical investigations,[94, 96] can be reasonably taken into account.

2.1.4 Synthesis of bis-azoles **2**

Regarding 2-(4-bromophenyl)benzo[*d*]thiazole (**4**), which represents, as already stated, the common precursor to compounds **2**, Qin and Yang in 2007[99] and Ji in 2010[100] reported two efficient protocols for its preparation through a condensation of *o*-aminothiophenol with *p*-bromobenzaldehyde in DMSO (reflux at 190 °C) (**Scheme 19**). The two reaction conditions differ for concentration and reaction time. We chose to follow the method used and by Ji[100] for its simplicity and efficacy. The condensation was carried out with 5 mmol of reactants (*p*-bromobenzaldehyde and *o*-aminothiophenol) and 10 mL of DMSO (2 mL/mmol as used by Ji), at 190 °C for 2h, with a 81% isolated yield of **8** (**Scheme 20**). The product was characterized by NMR spectroscopy and mass spectrometry.
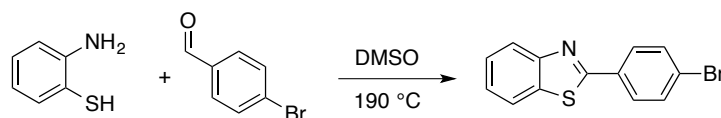
Scheme 19: Synthesis of compound **7**. Reaction conditions: concentration 2 mL/mmol, under Ar, 30', yield 92% (Qin, Yang); concentration 30 mL/mmol, 2 h, yield 88% (Ji).
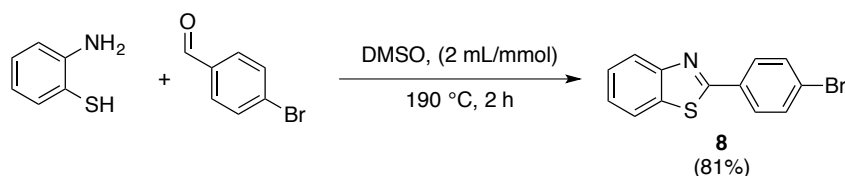
Scheme 20: Synthesis of 2-(4-bromophenyl)benzo[*d*]thiazole (**7**).

For the C2 arylation of 5-arylazoles **7a-f**, obtained as described in a previuos section, we chose to employ the procedure developed by Bellina for imidazole[101] and 1-benzylimidazole,[90] later applied with success to the synthesis of chromophores of structure **1**.[23] Hence, 5-arylazoles **7a-f** were reacted with 1.5 equiv. of **8** in the presence of 5 mol% Pd(OAc)$_2$ as the precatalyst and 1.5 equiv. of CuI in

DMA at 160 °C for 72 h (**Table 4**). The required bis-azole derivatives **2** and **3** were isolated in good to excellent yields except for compound **3b**, which was recovered in 25% isolated yield. This low yield was attributed partly to the formation of byproducts and partly to a difficult separation of **3b** from these same byproducts. In fact in the crude reaction mixtures of the preparation of compounds **2c** and **3a-c** a detectable amount (around 10%) of byproducts was formed.

The main byproduct recognized by GC-MS analysis was the dimerization product of the azole (**Scheme 21**). It was probably formed by Cu-catalyzed oxidative coupling of the azole in the presence of oxygen (from residual air in the reaction environment). This class of reactions is well known, and oxidative dimerization reactions catalyzed by copper at high temperatures in the presence of air have already been employed. Selected examples for the dimerization of azoles are reported in **Scheme 22** with references.[102-104]

Table 4: Synthesis of target compounds **2a-c** and **3a-c**.

5-arylazole	2,5-diarylazole	Isolated yield (%)
7a	2a	66
7b	2b	66
7c	2c	83
7d	3a	72
7e	3b	25
7f	3c	53
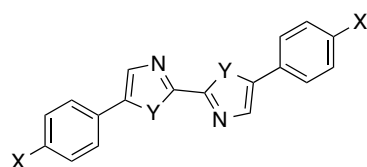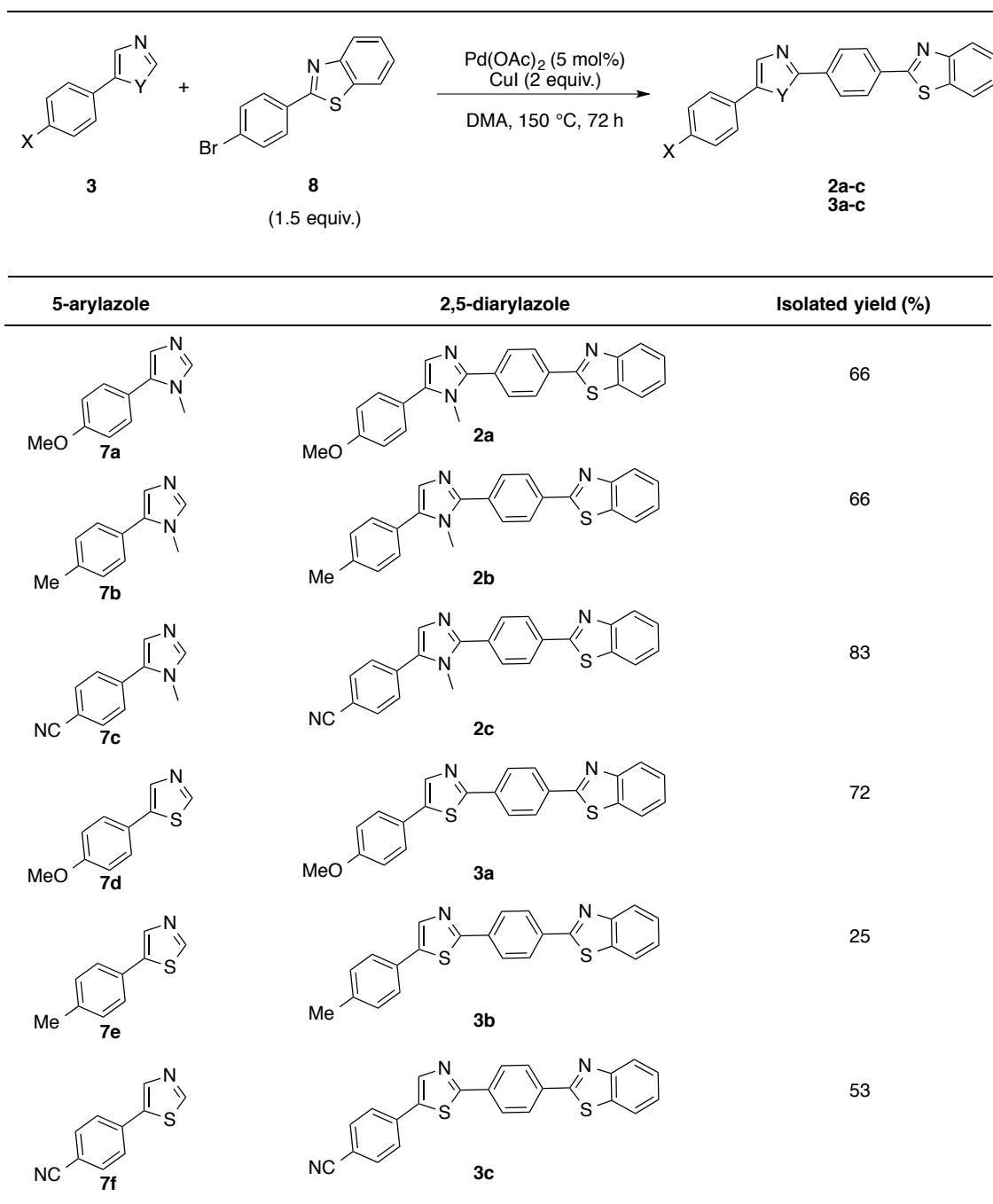
Scheme 21: Observed byproduct from the dimerization of the employed 5-arylazole.
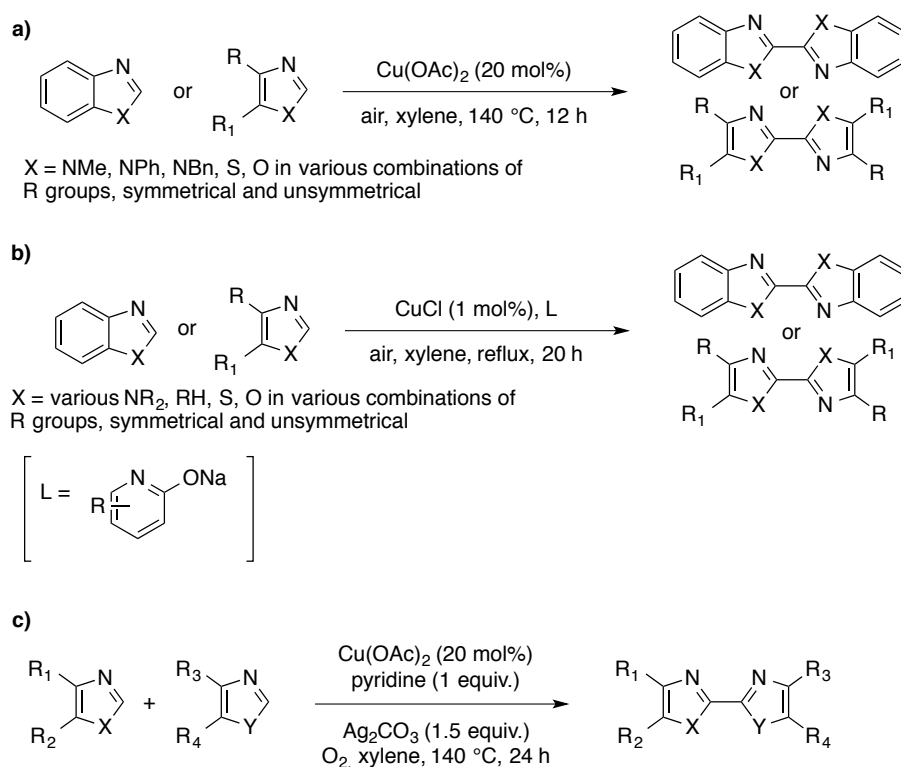
Scheme 22: Selected examples of Cu-catalyzed dimerization reactions of azoles: (a) Bao 2010;[102] (b) Yamaguchi 2011;[103] (c) You 2012.[104]

2.1.5 Mechanism of the C2 Pd,Cu-mediated direct arylation of azoles

The central role of Cu^I in the change from C5 to C2 regioselectivity was clear since the first studies in this field by Miura.[88] The C2 hydrogen atom is the most acidic site of *N*-substituted imidazoles, thiazoles and oxazoles due to the inductive effect of the two heteroatoms. Copper was thus supposed to assist the deprotonation of the azole, driving the regioselectivity towards the most acidic site. In their copper-catalyzed direct arylation of benzothiazole with aryl iodides Chodowska-Palicka and Nilsson[105] hypothesized two different intermediates: an azole-organocopper compound and a copper-complexed nucleophilic carbene (**Scheme 23**). In fact, their reaction gave better results with electron-poor aryl iodides.
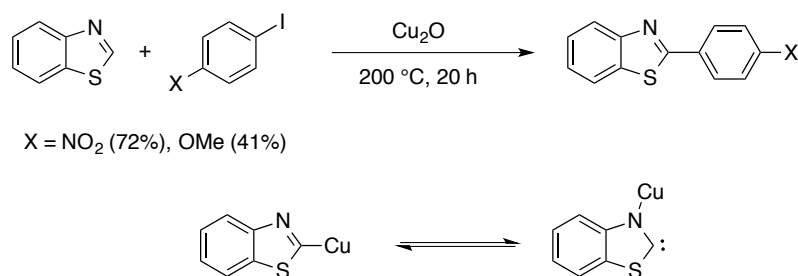
Scheme 23: Chodowska-Palicka and Nilsson's C2 arylation of benzothiazole with aryl iodides. Under the reaction scheme, the possible intermediates.

A mechanism proposed for the Pd-catalyzed and Cu-mediated C2 arylation of azoles resembles that of the classical Sonogashira reaction,[106] where, similarly to alkyne coordination, the pre-coordination of the substrate to Cu^I takes place. The aspects concerning this mechanistic hypothesis can be found in a recent review by Fairlamb, on the function of copper in direct arylation reactions.[107] In particular, the complex Cu-azole is likely to take part in an equilibrium with an organocuprate species (**Scheme 24**), which could undergo transmetallation with the arylpalladium complex generated from oxidative addition, with loss of CuX. The C2-arylation product is finally formed by reductive elimination, with simultaneous regeneration of the active palladium catalyst. Several experimental data support this mechanistic hypothesis.
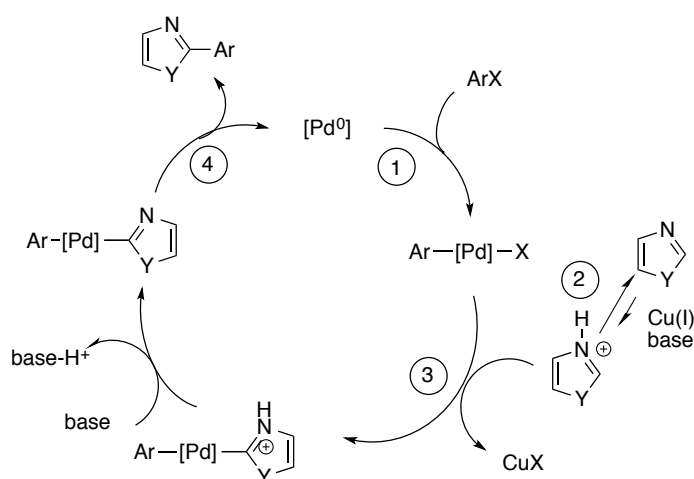
Scheme 24: Proposed mechanism for the Pd,Cu-mediated C2 arylation of azoles. Highlighted steps: (1) oxidative addition; (2) formation of the organocopper compound; (3) transmetallation; (4) reductive elimination.

For example, better results have been obtained when electron-withdrawing groups, which enhance the acidity of the C2-H proton and subsequently the rate of cuprate formation, are linked to the substituent aryl groups of 1-arylimidazoles[108] (**Scheme 25**).

X = MeO (86%), H (76%), MeSO$_2$ (84%)

Scheme 25: Influence of the aryl substituent in the C2 direct arylation between 1-arylimidazoles and *p*-iodoanisole.

A reduction in C2 selectivity was also observed with an increase of Pd loading when the reaction was performed in the presence of an inorganic base, because in this case the competitive copper-free direct C5 arylation may be present. The C5 direct arylation occurs also when sub-stoichiometric amount of CuI was employed. The fact that more than 1 equiv. of CuI have to be used, while, according to the mechanistic hypothesis, only catalytic amounts could be sufficient for the reaction

to succeed, can be explained with an equilibrium between the cuprate species and the free copper iodide. These phenomena involving copper species are probably the key factors to the reaction progress. As a further confirmation, the formation of the organocopper azole may be supported by a mildly basic solvent like DMF and DMA (**Scheme 26**).
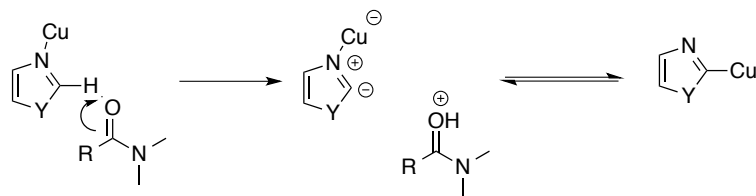
Scheme 26: Role of the mildly basic solvent in the formation of the organocopper species.

In fact Bellina and coworkers[109] observed that base-free and ligandless conditions give good results only when the reaction is performed in a solvent with a mildly basic character while reaction media such as toluene, xylene, dioxane, diglyme, acetonitrile or DMSO are ineffective. Recently a work by Gorelsky[94, 96] showed through calculations that a Concerted Metalation-Deprotonation (CMD) mechanism is possible for the C2 direct arylation of azoles catalyzed by Pd carboxylates in the presence of Cu^I. In the CMD transition state proton abstraction from a C-H bond by the carboxylate ligand occurs concurrently to the formation of the Pd-C bond. To understand how copper can tune reactivity Gorelsky applied the Cu^I-azole coordination. The CMD barriers for cleavage of different C-H bonds using a palladium-acetate catalyst have been evaluated by DFT (Density Functional Theory). A distortion analysis for every C-H bond was then performed. There are two contributions to the CMD barrier: the energetic cost associated with the distortion of the Pd complex and the arene from their ground-state structures to their geometries in the transition state (TS) and the energy gain resulting from the electronic interaction of the two species to form the TS (**Scheme 27**). When an azole is coordinated to copper all C sites become activated for the CMD process, but cleavage of the C2-H bond becomes the lowest-energy process due to a decrease of the arene distortion energy and an increase in the interaction energy between the catalyst and the substrate. The significant decrease in the distortion energy may be explained by the increase of azole C-H bond acidities after charge donation from the azole ligand to the copper ion that occurs with coordination. In this hypothesis only copper coordination is included; the formation of Cu^I carbenes as proposed before[105] is not taken into consideration. However, Gorelsky's study does not rule out the existence of an organo-copper intermediate and does not fully explain some experimental results, so this remains an open question.
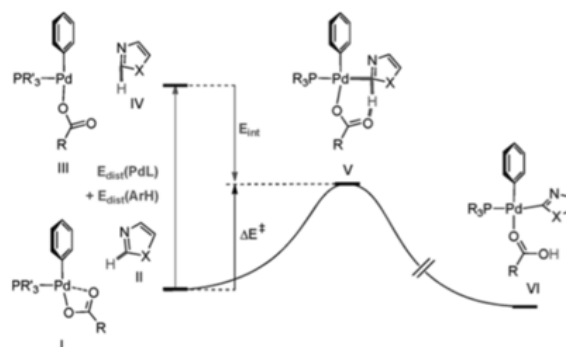
Scheme 27: Schematic representation of the two contributions to the CMD barrier: distortion energy (E_{dist}) and interaction energy (E_{int}). I and II: Pd-complex and arene in their ground-state structures; III and IV: Pd-complex and arene in the geometries of the TS; V: TS; VI: product after CMD (reproduced from reference 96).

2.1.6 Optical properties of 1,4-phenylene-spaced azole-benzothiazole chromophores in CHCl$_3$ solutions

As stated in the introduction, we were interested in determining the optical properties of compounds of structure **2** and **3** (**Figure 5**), which were promising as fluorescent dyes.

1a: R$_1$ = OMe
1b: R$_1$ = Me
1c: R$_1$ = CN

2a: R$_1$ = OMe
2b: R$_1$ = Me
2c: R$_1$ = CN

3a: R$_1$ = OMe
3b: R$_1$ = Me
3c: R$_1$ = CN
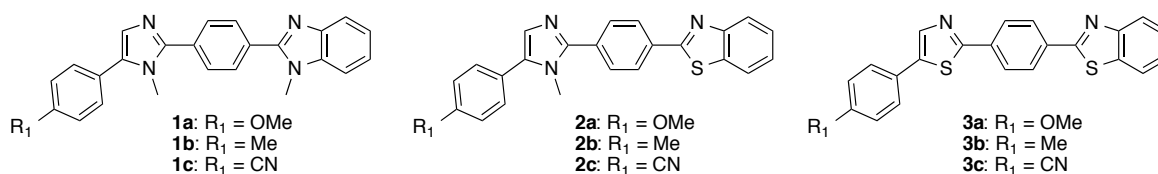
Figure 5: Synthesized azole-benzazole chromophores **1a-c**, **2a-c** and **3a-c**.

Absorption and emission spectra were thus measured in CHCl$_3$ (**Figure 6**). We will discuss them on the basis of the two series of compounds **2a-c** containing *N*-methylimidazole in their structure, and **3a-c**, based on the thiazole nucleus. It is also important to make a comparison between these results and the spectroscopic behaviour of *N*-methylimidazole-benzimidazole based chromophores of general structure **1**, reported in a recent publication by our research group.[23]

The optical features displayed by compounds **2** and **3** are summarized in **Table 5**. Notably, there is little difference between the absorption spectra within the same series of compounds, while there is a big difference in the position of the peak of absorbance between the two series. Among the absorption values of compounds **2a-c**, there is not much divergence: all bands are peaked around 342-345 nm. Howevere in this series compound **2c** displays a higher extinction coefficient as well as it is reported for the analogous compounds **1a-c**. This feature was also mirrored by fluorescence, in that case the spectrum becomes increasingly red-shifted in the order **2c**, **2b**, **2a**, and thus the Stokes shift grows in the same direction.

Table 5: Spectroscopic properties of fluorophores **2** and **3** dissolved in CHCl$_3$.

Chromophore	λ^{max}_{abs} [nm][a]	ε [M^{-1}cm^{-1}]	λ^{max}_{em} [nm] [a]	S [nm]	Φ_f[b]
1a	320	36000	427	107	0.90
1b	316	31000	415	100	0.88
1c	328	39000	416	87	0.93
2a	345	32000	457	112	0.90
2b	342	32000	442	100	0.81
2c	343	42000	426	83	0.80
3a	372	38800	460	88	0.61
3b	367	43000	443	76	0.59
3c	372	47500	436	64	0.55

[a]Measured for a 10^{-5} M solution in CHCl$_3$, **3a-c**: $\lambda_{exc.}$ = 330 nm, **2a-c**: $\lambda_{exc.}$ = 355 nm, **3a-c**: $\lambda_{exc.}$ = 330 nm.
[b]Fluorescence quantum yield (Φ) was determined relative to quinine sulphate in 0.1 M H$_2$SO$_4$ (Φ = 0.54).

To get a quantitative idea of the intensity of emission, fluorescence quantum yields (Φ) were calculated: all the three compounds resulted strong emitters, with quantum yields (Φ) comprised between 0.8 and 0.9. Compounds **2c** exhibits the lowest value of Φ, probably caused by the significant overlapping between absorption and emission bands. A similar behaviour was observed for compounds **3a-c**. These 1,4-phenylene-linked thiazole-benzothiazole derivatives were synthesized with the primary aim of pushing the maximum emission wavelenght towards higher values. Remarkably the thiazole ring contributed to increase the absorption maxima of more then 25 nm for all the three compounds **3a-c**, however a lower shift was observed in emission. This phenomenon caused a decreased in the Stokes shift to less then 80 nm, with a consequent decrease in quantum yields, that attest around half-unity. Remarkably a common trend can be observed in the two series on the positions of the emission maximum: **2a** and **3a** with the methoxy group on the phenyl substituent show the greater shift, decreasing passing to **2b** and **3b** with the methyl group and then to **2c** and **3c** with the nitrile functional group. The electronic effect of these substituents on the Stokes shift is thus clear; a similar effect was also observed on compounds **1**.[23]In the emission spectra of **2c**, **3b** and, more clearly, **3c** a vibronic structure can be observed, while absorption spectra don't show vibronic structure in all cases. The mirror image rule, which states that absorption and emission spectra are symmetric in shape, is thus not followed by these compounds. This phenomenon has already been observed for various species; the most studied case is *p*-terphenyl,[53] on which also computational studies have been carried out.[110] It seems that symmetry breakdown is due to the rearrangement of the nuclei in the excited state; since the excited state lifetime is relatively long, the individual rings become more coplanar in the excited state.[53] For compounds **2c**,**3b** and **3c** a similar explanation may be given.

In order to rationalize the optical properties found in compounds **2** and **3** we carried out a computational study on these series of cromophores as well as it is reported for compounds **1** in a recent work by our research group.[23]
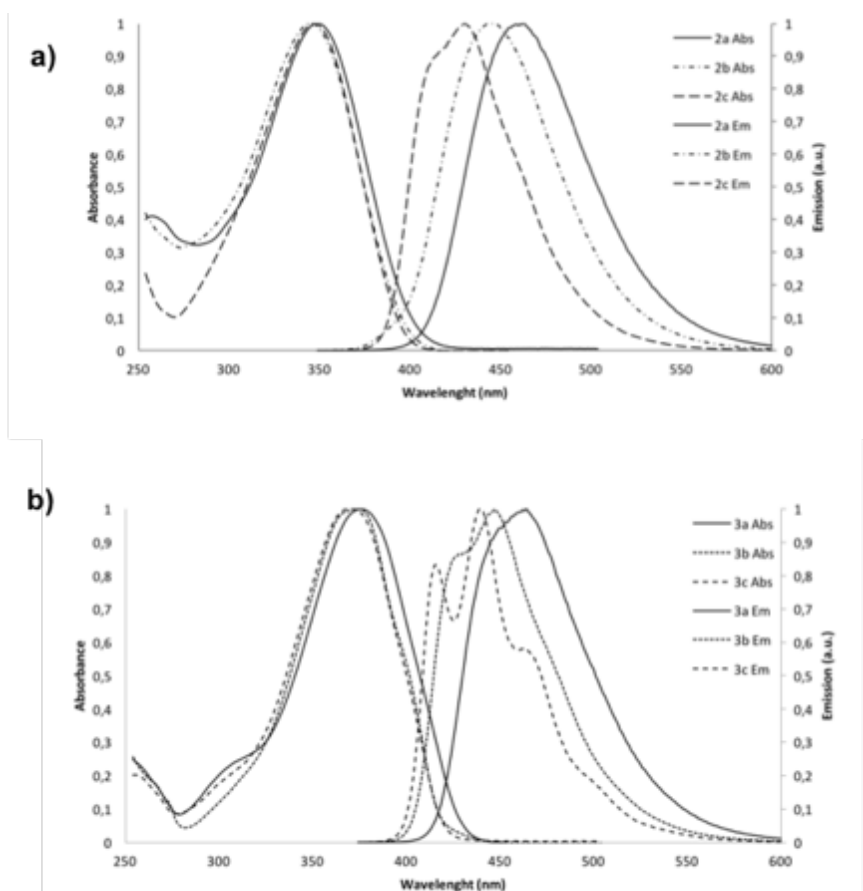
Figure 6: Normalized absorption and emission spectra of 10^{-5} M $CHCl_3$ of compounds **2a-c** ((a) λ_{exc} = 330 nm) and **3a-c** ((b) λ_{exc} = 355 nm).

2.1.7 Computational analysis of 1,4-phenylene-spaced azole-benzothiazole chromophores

A computational investigation was conducted with the aim of understanding how changing the heteroaromatic scaffold, by moving from *N*-methylimidazole to thiazole, could affect the optical behaviour of the chromophores. Moreover we also wanted to address the effect of the functional group on the terminal phenyl ring, in order to provide a comprehensive picture and to design molecular modification to improve the observed spectroscopic features. Quantum mechanical (QM) calculations on fluorophores **2a-c** and **3a-c** (**Figure 7**) have been performed at the density functional theory (DFT) and its time-dependent extension (TD-DFT) levels of theory.[111-114] Owing to the likely presence of long-distance charge transfers, the CAM-B3LYP functional[115] has been chosen, in conjunction with the SNSD basis set,[116] which was developed for spectroscopic studies of medium-to-large molecular systems.
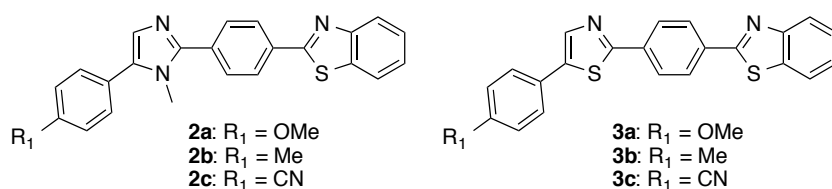
Figure 7: Studied azole-benzazole chromophores **2a-c** and **3a-c**.

This basis set allows cost-effective predictions for a broad range of spectroscopic properties, including electronic absorption and emission spectra.[24, 117]

Compounds **2** and **3** were optimized employing the tight criterion, using the CAM-B3LYP functional and the SNSD basis set. The optimized geometries of all species were characterized as true minima on the potential energy surfaces using vibration frequency calculations. To compute the optical properties, TD-DFT has been employed on the optimized geometries. Solvent effects (here, $CHCl_3$) have been simulated using the PCM model.

Since two possible conformers can be envisaged for structures **2** and **3** (reported in **Figure 8** for derivatives **2b** and **3b** as examples). Computational optimization of the ground states for the two conformations were performed in the case of compounds **2b** and **3b**, showing an energetic difference of around 0.01 eV in both cases, and therefore practically isoenergetic.
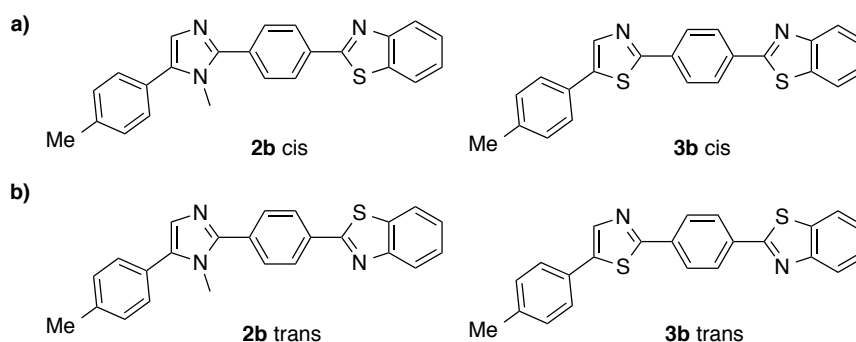
Figure 8: The two possible conformers of compounds **2** and **3**, reported as example for derivatives **2b** and **3b**: a) cis b) trans.

Moreover, through geometry optimization of the excited electronic state we could observe how the transition results in an increased planarization of the individual rings in all cases (computed dihedral angles for compounds **2b** and **3b** as examples in **Figure 9**). As shown in **Figure 9**, switching from *N*-methylimidazole to thiazole in the heretoarometic scaffold, significantly alters the molecular geometry. The steric hindrance caused by the presence of the methyl group on *N*-methylimidazole is responsible for a higher distrortion between the rings and consequently a more significant planarization upon transition to the first excited state. Such a remarkable degree of planarization upon excitation has been observed in both sets of chromophores (**Table 6**).
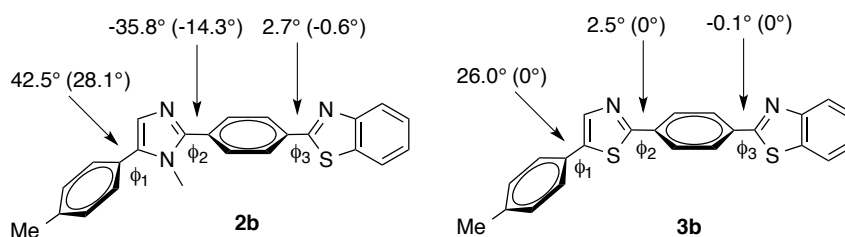
Figure 9: Computed diehedral angles for compounds **2b** and **3b** as examples. The values reported in parentheses are relative to the first excited state optimized geometry, while the others are relative to the ground state optimized geometry.

Computed diehedral angles ϕ_1, ϕ_2, ϕ_3 (**Figure 9**) are reported in **Table 6** for both ground electronic state (S0) and first excited electronic state (S1).

Table 6: Computed diedral angles for compounds **2** and **3** in both ground (S0) and excited (S1) electronic states.

Chromophore	ϕ_1 S0/S1	ϕ_2 S0/S1	ϕ_3 S0/S1
2a	44/27	-36/-14	4/-0.5
2b	43/28	-36/-14	3/-0.6
2c	39/22	-36/-14	4/-0.2
3a	28/0	2/0	0.2/0
3b	26/0	3/0	-0.1/0
3c	21/0.8	3/-0.1	0.7/-0.3

The data reported in **Table 6** illustrate how the replacement of *N*-methylimidazole with thiazole results in an overall planarization of the three diedral angles, giving a significant discrepancy between the two sets of compounds. However along each series it is not possible to observe any noteworthy difference caused by the different electronic nature of the peripherical functionality (OMe, Me or CN). A very important phenomenon is the planarization that occurs moving from the ground state to the first excited state, that is more dramatic in the case of compounds of structure **2**, given their higher degree of distortion in the ground state. The notable planarization of the molecule in the equilibrium structure of the excited electronic state is a consistent explanation of the high Stokes shifts observed, as already reported in literature for analogous POPOP-type dyes.[118]

As afore-mentioned theoretical calculations at the (TD)-DFT/CAM-B3LYP/SNSD/PCM level of theory were performed to gain a better understanding of the optical properties, therefore we computed the values for maximum absortption and emission wavelenghts for chromophores **2** and **3**. The computational data are compared to the experimental ones in **Table 7**.

Table 7: Computed (calc.) and experimental (exp.) absorption and emission wavelenghts (respectively λ_{abs} and λ_{em}), ans the Stokes shifts (S, in nm) for compounds of structure **2** and **3**. Calculated oscillator strenghts (F) and fluorescence quantum yield (Φ) are also reported.

Chromophore	λ^{max}_{abs}[nm] calc.	λ^{max}_{abs}[nm][a] exp.	λ^{max}_{em}[nm] calc.	λ^{max}_{em}[nm][a] exp.	F_{abs}	F_{fluo}	Φ_f^b	S [nm] calc./exp.
2a	326	345	451	457	1.61	2.02	0.90	125/112
2b	325	342	445	442	1.61	2.00	0.81	120/100
2c	332	343	444	426	2.01	2.21	0.80	113/83
3a	357	372	488	460	1.73	1.85	0.61	132/88
3b	353	367	478	443	1.72	1.82	0.59	125/76
3c	363	372	477	436	2.01	2.01	0.55	114/64

[a]Measured for a 10^{-5} M solution in $CHCl_3$.
[b]Fluorescence quantum yield (Φ) was determined relative to quinine sulphate in 0.1 M H_2SO_4 ($\Phi = 0.54$).

It has been shown[119-121] that TD-DFT calculations almost systematically overestimate excited states energies, thus underestimating absorption wavelengths. In the case of compounds **2** and **3** the Stokes shift are therefore overestimated (**Table 7**). However it is possible to see how the experimental trend is well reproduced: calculated data gave confirmation that Stokes shifts increase with the electron-releasing capability of substituents on the terminal phenyl ring, and between calculated and experimental values of Stokes shift there is a good linearity in both sets of compounds (**Figure 10**).
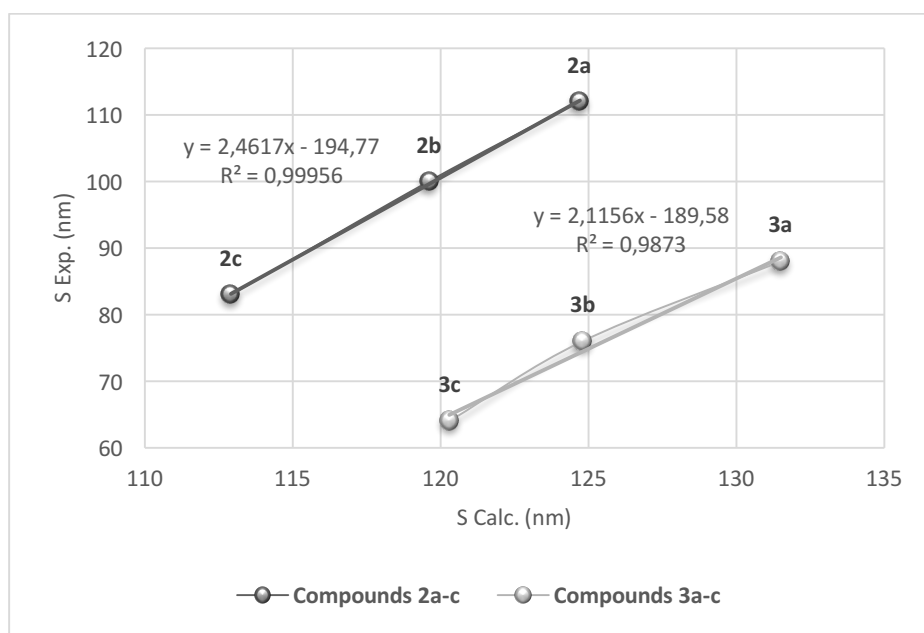
Figure 10: Correlations between calculated and experimental Stokes shifts values for compounds **2** and **3**.

The effect of presence of an electron donating functional group is to enhance both the Stokes shift and the quantum yield in both cases of compound sets **2** and **3** (**Table 7**), this may be explained by inspection of frontier molecular orbital (MO) graphical representations, since the observed band is almost entirely due to HOMO-LUMO transition. We can take as examples the MO isosurfaces of compounds **2b** and **2c**, *i.e.* those bearing respectively the electron-donating (OMe) and electron-

withdrawing (CN) functional groups, are reported in **Figure 11**.
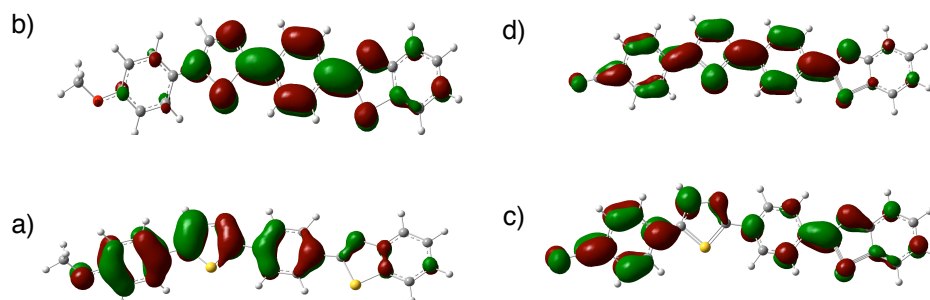
Figure 11: a) HOMO and b) LUMO for **2a**, b) HOMO and c) LUMO for **2c**.

Though, in both cases the HOMO is almost equally spread allover the molecule, the LUMO significantly varies between the two compounds. For **2a** there is a charge transfer from the methoxy-substituted phenyl ring towards the benzothiazole nucleus; while for **2c** the charge transfer takes place exactly in the opposite direction: from the benzimidazole moiety to the CN-substituted phenyl ring. However as is patent from **Figure 8** the charge transfer is not really effective in the case of **2c**, and this phenomenon can be responsible for the difference in the optical properties observed for the two compounds. **2a** displays a larger stokes shift and a consequent higher fluorescence quantum yield if compared to **2c** (**Table 7**). These better features can be ascribed to the more efficient ICT, allowed by the presence of an electron donating functionality on the peripherical phenyl ring.

Quantum mechanical calculations at the DFT level confirmed the evidence of experimental data: the best luminescent properties are attainable by the combination of an electron-releasing substituent on a general structure of compound **2**, *i.e. N*-methylimidazole-benzothiazole heteroaromatic scaffold. These good performances are likely due to the more planar structure of the chromophoric unit in the excited state geometry.

Given these results we designed two new derivatives, **2d** and **2e**, **(Figure 12)** based on the *N*-methylimidazole-benzothiazole scaffold.
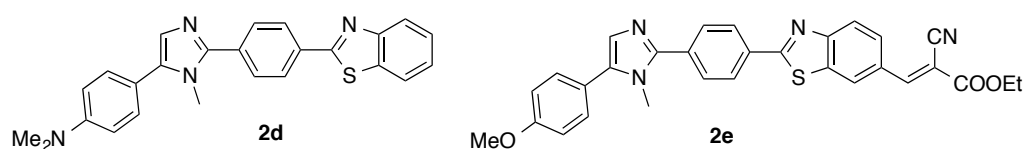
Figure 22: Designed chromophores **2d-e**.

Compounds **2d** and **2e** feature respectively a powerful electron-releasing functionality on the terminal phenyl ring and a strong electron-withdrawing group on the benzothiazole moiety. Both modifications were designed in order to improve the ICT along the molecule and therefore to enhance

the optical features of the chromophores, in particular with the increase of the emission maximum wavelenght, thus mantaining a wide Stokes shift and a high fluorescence quantum yield. Predicted spectroscopic data for compounds **2d-e** are reported in **Table 8**.

Table 8: Predicted spectroscopic data for chromophores **2d** and **2e**.

Chromophore	λ^{max}_{abs}[nm] calc.	λ^{max}_{em}[nm] calc.	F_{abs}	F_{fluo}	S [nm] calc.
2d	334.6	478.9	1.62	2.04	144,3
2e	376,0	500,3	2,11	2,49	124,3

These calculation were performed after geometry optimization, at a (TD)-DFT/CAM-B3LYP/SNSD/PCM level of theory, and the chemical environment (here CHCl$_3$) was taken into account by means of PCM.

Given the interesting predicted spectroscopic data for compounds **2d** and **2e**, these two derivatives were synthesized and studied to find the best candidate to be employed in a Luminescent Solar Concentrator prototype.[122]

2.2 Synthesis and Optical properties of 1,4-phenylene spaced imidazole benzothiazole chromophores 2d and 2e

2.2.1 Synthetic strategy

Chromophores **2d** and **2e** (**Figure 12**) were synthesized according to the procedure already reported for analogous compounds **2a-c** (section **2.1**) with some slight modifications. Two sequential C5 and C2 arylation reactions on *N*-methylimidazole (**10a**) are the key steps of the process (**Scheme 28**). The base-free protocol, employed for chromophores **2a-c**, proved to be unsuitable for compounds **2d** and **2f**, bacause of the high reaction temperature. The two derivatives were thus obtained in good yields adding 2 equivalents of TBAA, which allowed the reaction to succeed at a temperature of 110 °C instead of 160 °C. Following this procedure **2d** and **2f** were prepared in 46 and 68% yields by Pd/Cu co-mediated C2-arylation of *N*-methylimidazole. Compound **2e** was finally obtained in 90% yield by a Knoevenagel condensation of **2f** with ethyl cyanoacetate.[123]
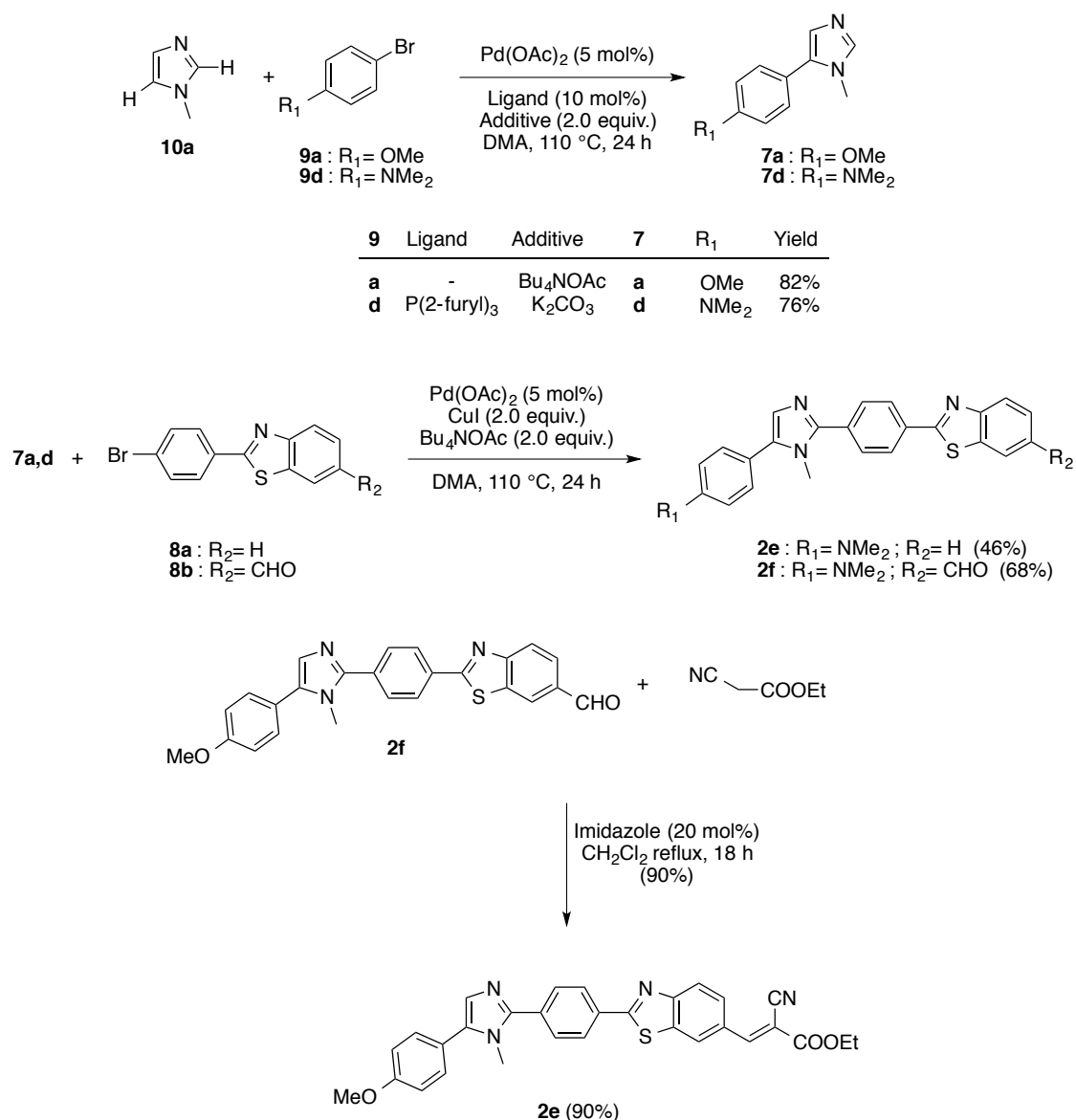
Scheme 28: Synthetic strategy for compounds **2d** and **2e**.

2.2.2 Optical properties and LSC performance

Compounds **2d** and **2e** (**Figure 12**) were designed and studied with the aim to red-shift their fluorescent emission above 500 nm. Optical properties for derivatives **2d** and **2e** in 10^{-5} M CHCl$_3$ solution are reported in **Table 9**.

Table 9: Experimental spectroscopic data for chromophores **2d** and **2e** dissolved in CHCl$_3$.

Chromophore	λ^{max}_{abs}[nm]	λ^{max}_{em}[nm]	ε [M^{-1}cm^{-1}]	Φ_f^a	S [nm]
2d	351	518	32700	0.42	165
2e	385	532	38000	0.11	147

^{a}Fluorescence quantum yield (Φ) was determined relative to quinuine sulphate in 0.1 M H$_2$SO$_4$ (Φ = 0.54), $\lambda_{exc.}$ = 363 nm.

Both derivatives **2d** and **2e** exhibit very interesting maximum absorption and emission wavelenghts (higher then 500 nm): notably the insertion of an electron-withdrawing functional group

red-shifted the emission maximum, while mantaining the absorption maximum under 390 nm. This phenomenon increased the Stokes shift to 147 nm, but had a negative effect on quantum yield, which resulted to be only 0.11 for compound **2e**. The situation appears different in the case of chromophore **2d**: the data in **Table 9** show a very wide Stokes shift (165 nm) and an average quantum yield (0.42). The combination of these optical properties, *i.e.* no significant absorption above 400 nm, largest Stokes shift, emission maximum wavelenght higher then 500 nm and satisfactory quantum yield of 0.42, allowed **2d** to be studied in polymer films (using poly(methyl methacrylate)) for application in colourless LSC.

Fluorophore **2d** was studied in PMMA films, prepared with drop casting, with a thickness of 25 ± 5 μm. The optical preperties of **2d**/PMMA system were recorded at a 0.5 wt% concentrated film and display absorption and emission bands peaked at 359 nm and 500 nm, respectively, exhibiting a Stokes shift of 141 nm.
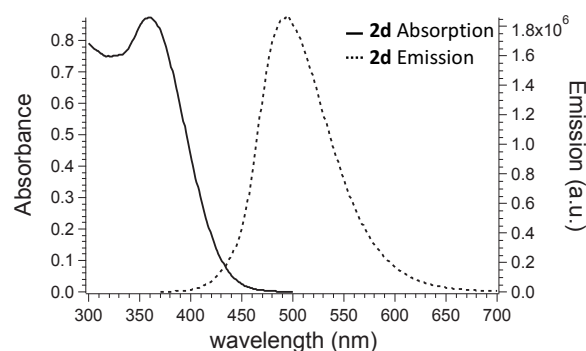
Figure 13: Absorption and emission ($\lambda_{exc.}$ = 360 nm) spectra of **2d**/PMMA 0.5 wt% film with a thickness of 25 ± 5 μm.

Stokes shift of **2d** in PMMA was thus smaller than that recorded in $CHCl_3$ solution (165 nm), likely owing to the blue-shifted emission caused by the different dielectric constant of the medium (for PMMA = 2.6-2.8; for $CHCl_3$ = 4.81). However, a Stokes shift wider than 135 nm significantly limited any self-absorption occurrence. The absolute fluorescent quantum yield (QY) of **2d** in PMMA reached an average value of 28%, but slightly decreased to 22% when the highest concentration of 1.8 wt% was employed. Even the highest value of QY in PMMA (28%) is lower than that of $CHCl_3$ solution (42%), this may be due to the self-quenching that usually characterize fluorophores in the solid state,[50] nonetheless it still remains interesting and promising for optical applications in polymers.

The performances of **2d**/PMMA films as LSC were evaluated on optically pure 50 × 50 × 3 mm glass. Photocurrent measurements (**Figure 14**) were recorded with a home-built apparatus[124] by using

a set of three 1 × 1 cm photodiodes assembled in parallel fashion. Photodiodes turn the optical power into an electrical current, thus allowing for a fast, precise and reproducible response even with different sets of samples, and are therefore ideal for measuring light sources in LSC emission range. The **2d**/PMMA films with the highest photocurrent, *i.e.* those containing 1.4 and 1.8 wt% of **2d**, were analysed by using a Si-based PV cell attached to one edge of the concentrator.
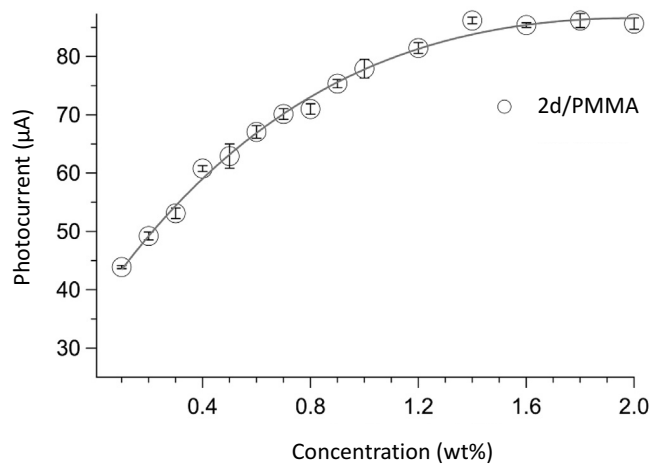
Figure 14: Photocurrent of **2d**/PMMA films of a thickness of 25 ± 5 μm with increasing dye concentration (wt%).

The optical efficiency η_{opt} (**Table 10**) was calculated from the concentration factor C, which is the ratio between the short circuit current measured in the case of the cell over the LSC edge (I_{LSC}) and short circuit current of the bare cell when perpendicular to the light source (I_{SC}) (eq. (1)):

$$\eta_{opt} = \frac{I_{LSC}}{I_{SC} \cdot G}$$

G is the geometrical factor (in our case, G = 13.3), which is the ratio between the area exposed to the light source and the collecting area. In **Tabe 10** the optical efficiency for the **2d**/PMMA system is compared to the Lumogen Red dispersed in poly(methyl methacrylate) (LR/PMMA), which, to the best of our knowledge, exhibits the best currently known performances in LSC.

Table 10: Optical efficiencies (η_{opt}) calculated for **2d**/PMMA LSC and compared to those of LR/PMMA LSC with similar geometrical factor.[124, 125]

	wt%	η_{opt} (%)
2d/PMMA	1.4	5.2
	1.8	5.9
LR/PMMA	1.5-1.8	~8.0

The **2d**/PMMA system shows an optical efficiency lower then that collected from the LR based

LSC in the same range of concentration and geometrical factor. The difference of about 2% between optical efficiencies is likely due to the poor visible light absorption by **2d** compared to the state-of-the-art LR. Remarkably η_{opt} for compound **2d** reached values as high as 6%, possibly owing to the beneficial combination of large Stokes shift (*i.e.*, 137 nm for **2d**/PMMA and 23 nm for LR/PMMA[126]) and satisfactory QY (about 0.3) that strongly contributed in fluorescence trapping, thus enhancing its concentration efficiency.

2.2.3 Conclusions

We have shown that the dispersion of a near-UV absorbing imidazole-benzothiazole fluorophore with brilliant green emission in PMMA allowed the preparation of thin film LSCs with a faint colored tinting and optical efficiencies close to 6. Different fluorophores characterized by imidazole-benzothiazole and thiazole-benzothiazole backbones were synthesized aimed at obtaining the best combination of optical properties in terms of near-UV absorption, Stokes shift larger than 150 nm and a fluorescence quantum yield higher than 0.4. Among them, the 1,4-phenylene-spaced imidazole-benzothiazole bearing an electron-donating dimethylamino group was found the best candidate and was selected as fluorescent dopant in PMMA thin films together with an analogue azole-based fluorophore with emission higher than 500 nm. Photocurrent experiments of the derived LSC revealed optical efficiencies not surprisingly lower than those evaluated by the state-of-the-art systems due to the limited absorption in the visible region. Moreover, the trapping efficiency was maximized for fluorophores having the highest achievable QY, rather than very large SS. Nevertheless, η_{opt} values as high as 6 flanked by significant light transmittance in the visible region consistently support the use of the prepared device as colourless LSC.

2.3 Alkynylimidazole based fluorophores of general structure 4

Alkynyl-substituted azoles represent important structural cores of several biologically active molecules[127] and organic functional materials.[70, 128, 129] We devoted our efforts to the design and synthesis of novel alkynylimidazole based fluorophores **4a-d** (**Scheme 29**) to evaluate their potential performance in luminescent solar concentrators devices. These chromophores feature a triple carbon-carbon bond connecting (hetero)aromatic moieties as key aspect. The presence of this type of π-linker can give the overall structure good rigidity and robustness, without any problem related to stereo-mutation, which would otherwise take place in the case of double C-C bonds that consitute other largely used π-spacers.

2.3.1 Synthetic approach

An efficient and scalable synthetic route to 5-alkynyl-2-arylimidazoles was recently developed in our research group.[86] This synthetic protocol was followed for the synthesis of chromophores of general structure **4** (**Scheme 29**). This synthetic procedure involves as the key step a one-pot sequential regioselective C5 bromination and Sonogashira alkynylation reaction described in a recent work by our research group (**Scheme 29**).[86] In detail, 2-arylimidazoles **11a,b** were efficiently prepared by a base-free and ligandless palladium/copper co-catalyzed direct C2-H arylation reaction, involving 1-methylimidazole (**10a**) and bromoarenes **9e,f**. The 2-arylimidazoles **11a,b** thus obtained were then regioselectively brominated at C5 position through reaction with NBS in DMF at room temperature. The resulting 2-aryl-5-bromoimidazoles **12a,b** was not isolated, instead it was directly reacted with an arylalkyne (**13a,b**) (1.1 equiv.) in the presence of PdCl$_2$(PPh$_3$)$_2$ (2 mol%) and CuI (4 mol%). The reaction mixture was then warmed up to 80 °C and stirred for 3 h. Through this procedure fluorophores **4a-d** were isolated in 72–90% yield (**Scheme 29**).

11	R$_1$	Yield (%)
a	NO$_2$	82
b	COOEt	74

4	R$_1$	R$_2$	Yield (%)
a	NO$_2$	H	81
b	NO$_2$	OMe	72
c	COOEt	H	74
d	COOEt	OMe	90
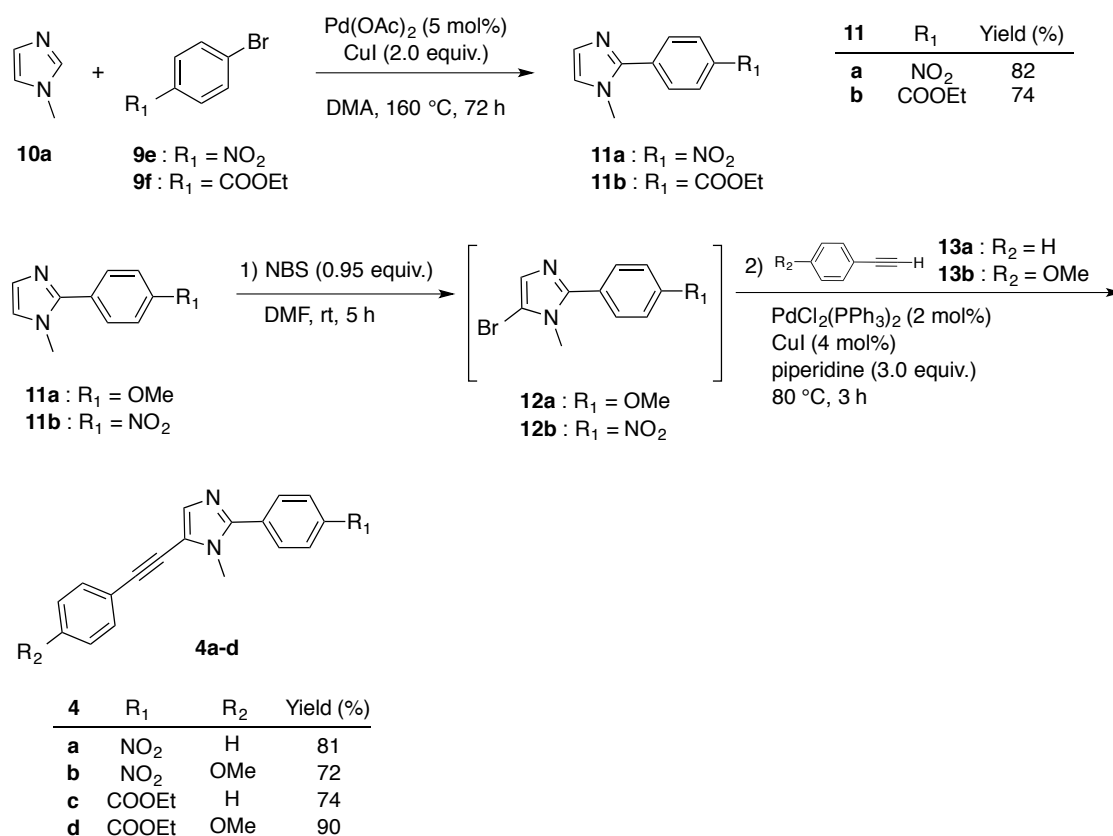
Scheme 29: Synthetic route to fluorophores **4a-d**.

2.3.2 Optical properties of 5-alkynyl-2-arylimidazoles *4a-d*

The optical features of the prepared fluorophores **4a-d** dissolved in THF solutions are reported in **Table 11** and represented in **Figure 15**.

Table 11: Experimental spectroscopic data for chromophores **4a-d** in 5×10^{-6} M THF solution.

Chromophore	λ^{max}_{abs}[nm]	λ^{max}_{em}[nm]	ε [M^{-1}cm^{-1}]	Φ^a_f	S [nm]	B [M^{-1} cm^{-1}]
4a	367	517	17000	0.10	150	1700
4b	373	538	15000	0.10	165	1500
4c	329	408	36000	0.61	79	21960
4d	331	422	27000	0.51	91	13770

[a]Fluorescence quantum yield (Φ) was determined relative to quinuine sulphate in 0.1 M H$_2$SO$_4$ ($\Phi = 0.54$), $\lambda_{exc.} = 366$ nm.

Absorption bands are comprised in the interval between 330 and 370 nm for all four derivatives, closely associated to the near UV range of the electromagnetic spectrum of light. In the investigated range of concentration, *i.e.* between 10^{-6} and 5×10^{-5} M, no absorption bands attributed to dyes aggregates were observed. As expectable from empirical intuituion, **4a** and **4b** show red-shifted absorpion and emission wavelenghts if compared to compounds **4c** and **4d** and this shift is likely due to the presence of a stronger electron-withdrawing functionality (NO$_2$) in the case of the former fluorophores. The same behaviour can be observed in the case of emission spectra, where the effect of the nitro group is amplified (**Figure 15**): **4a** and **4b** emit in the interval 500-600 nm with Stokes shift 70 nm larger than that of **4c** and **4d** fluorophores. Remarkably, the presence of the electron-donating methoxy groups red-shifts the emission maximum wavelenght of 21 nm, in the case of **4a**/**4b** and 14 nm in the case of **4c**/**4d** (**Table 11**).
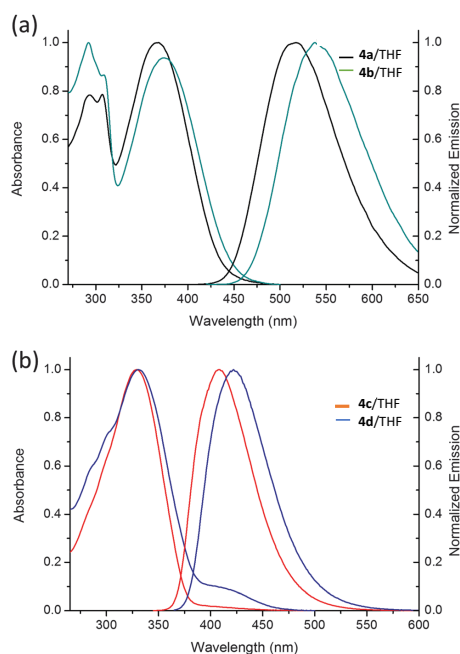
Figure 15: Absorption and emission spectra of fluorophores **4a-d** in 10^{-6} M THF solution.

In order to make an effective comparison among the different fluorophores, we chose to employ a very useful parameter which is the brightness (B) of the dye. The brightness is directly proportional to the product of the extinction coefficient (ε) and the quantum yield (QY) and accounts for both the

amount of absorbed light and the quantum efficiency of the fluorophore. From the data reported in **Table 11**, it is clear that the insertion of the nitro functionality heavily affects both extinction coefficient and QY, thus leading to modest B values for compounds **4a,b**. This finding is however not so surprising as the nitro group is, in fact, believed to be a general quencher of fluorescence due to donor-excited photoinduced electron transfer (d-PeT) originating from the excited fluorophore moiety showing strong electron-withdrawing effect.[130] On the other hand, the emission properties of the **4c** and **4d** fluorophores are comparable to those of the common bright fluorophores (B over 10^4 $M^{-1} cm^{-1}$), such as fluorescein,[131] even though they are characterized by smaller Stokes shift than nitro **4a,b** derivatives.

2.3.3 Fluorescent properties of poly(methyl methacrylate) (PMMA): toward luminescent solar concentrators

Thanks to the abovementioned properties of compounds **4a,b**, that is Stokes shift larger than 150 nm and emission maxima shifted to the yellow-red portion of the electromagnetic spectrum of light, these fluorophores were investigated when dispersed in a transparent and totally amorphous polymer matrix such as PMMA. Through this approach our goal was the determination of the optical properties of the chromophore/PMMA thin films, to explore the possibility of employing them in luminescent solar concentrators. As stated in the introduction, LSCs contain PV cells as photovoltaic elements placed on the edges of the device. It is worth mentioning that PV cell efficiencies can be further increased by matching the dye emission with the cell responsivity.[13] This is an efficient approach to solar PV since the intrinsic red-shifting that accompanies fluorescent emission, in **4a** and **4b**, allows to combine the maximum solar emission intensity (at about 500 nm) and the highest PV cell responsivity, i.e. between 500 and 1000 nm.[13]

Fluorophore **4a,b** were studied in PMMA thin films, prepared by drop casting, with a thickness of 25 ± 5 μm. The optical preperties of **4a**/PMMA and **4b**/PMMA system were recorded at a 1 wt% concentrated film and are reported in **Figure 16** and summarized in **Table 12**. **4a** and **4b** fluorophores in PMMA displayed absorption and emission features in agreement to their respective behaviour in THF solution, thus showing that the polymer matrix well interact with the guest molecules avoiding their aggregation. Moreover, no decrease in quantum efficiency is observed on passing from THF solutions to polymeric thin films.

This phenomenon can be attributed to the increased rigidity of the fluorophore when dispersed in the polymer matrix which allows to reduce the loss of efficiency often observed upon dispersion in a solid matrix.
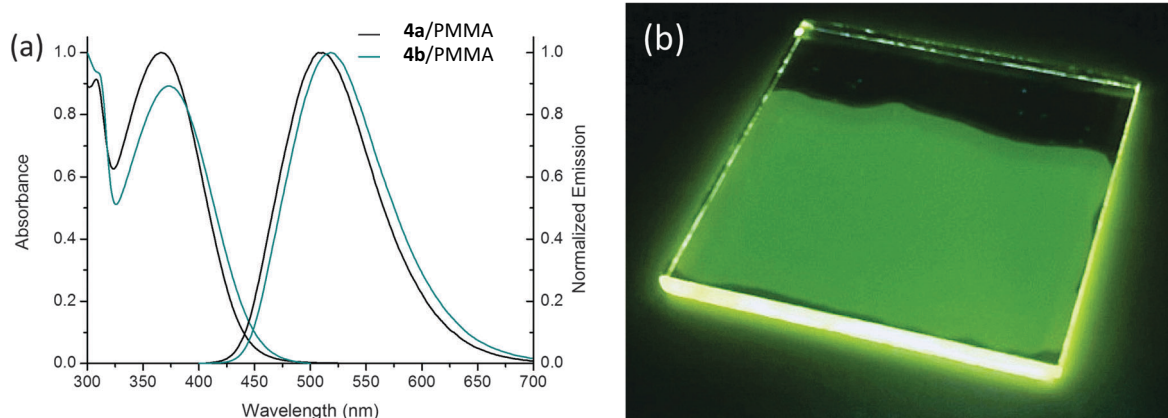
Figure 16: (a) Absorbance (left) and emission (right) spectra of 1 wt% **4a**/PMMA and **4b**/PMMA thin films (25 ± 5 μm); (b) an optically pure 50 × 50 × 3 mm glass coated with 25 ± 5 μm thick **4b**/PMMA film.

Table 22: Spectroscopic properties of **4a**/PMMa and **4b**/PMMA thin films.

Chromophore	λ^{max}_{abs}[nm]	λ^{max}_{em}[nm]	Φ^a_f	S [nm]
4a	367	517	0.10	150
4b	373	538	0.10	165

[a]Fluorescence quantum yield (Φ) was determined relative to 9,10-diphenylantracene in PMMA ($\Phi^s_f = 0.83$).

Remarkably, both films display emissions maxima between 450 and 650 nm (**Figure 16**), very large Stokes shift values (i.e., around 150 nm), thus making them suitable for LSC applications. In order to assess the performances as LSC, an optically pure 50 × 50 × 3 mm glass was coated with PMMA films with a thickness of 25 ± 5 μm. Photocurrent measurements were accomplished with a home-built apparatus[124] by using a set of three 1 × 1 cm photodiodes assembled in parallel fashion. As stated in the previous section, photodiodes are ideal for measuring light sources in LSC emission range, since they turn the optical power into an electrical current, thus allowing for a fast, precise and reproducible response even with different sets of samples.

The maximum photocurrents measured with our setup were 44.5 ± 0.1 mA for 1 wt% **4b**/PMMA and 37.0 ± 0.1 mA for 1 wt% **4a**/PMMA systems. The higher value of photocurrent generated by the system **4b**/PMMA can be due to the more red shifted emission maximum (of about 20 nm) if compared to **4a**/PMMA. Notably, no significant variation of the photocurrent values was observed when increasing fluorophores concentration in PMMA up to 2 wt%. The LSC with the highest photocurrent, i.e. the **4b**/PMMA system, was analyzed by using a Si-based PV cell attached to one edge of the concentrator, as described in the Experimental section. The optical efficiency η_opt was calculated from the concentration factor C, which is the ratio between the short circuit current measured in the case of the cell over the LSC edge (I_LSC) and short circuit current of the bare cell

Phys. Chem. Chem. Phys., 2015, **17**, 26710–26723 | **26721**

50

when perpendicular to the light source (I_{SC}) (eq. (1), **Section 2.2**). The calculated η_{opt} for the **4b**/PMMA system was lower than 5% and it agrees well with the optical efficiencies of LSC made of PMMA and containing fluorophores with similar characteristics in terms of emission maxima and QY values.[132]

2.3.4 Theoretical characterization of 4 derivatives in THF solution and in PMMA

In order to rationalize the spectroscopic properties of the studied chromophores we firstly set up an appropriate computational strategy, in particular we focus on the choice of the method to be applied to compute molecular structures, properties, and spectra. In addition to the **4**-derivatives we will also consider two model systems: **4b'**, an analogue of **4b** with OMe replaced by OH and **4d'**, an analogue of **4d** with OMe and COOEt replaced by OH and COOH.
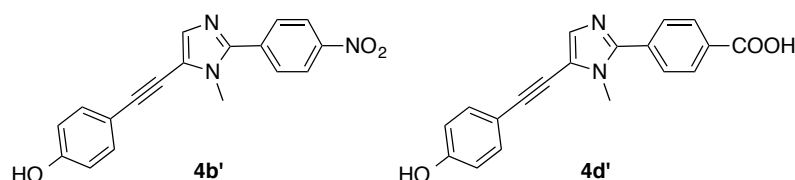
It has been already shown[22] that lateral methoxy groups can be effectively substituted in computational studies by OH groups, to avoid the problem of methyl rotation with the electronic transition, while in experiment, the methoxy group is preferred over OH, due to the undesired reactivity of the latter. Geometry optimizations and TD-DFT VE calculations have been performed at B3LYP/SNSD, B3LYP/SNSD/PCM(THF) and CAM-B3LYP/SNSD/PCM(THF) levels of theory, in order to assess the most adequate computational approach to be used in the following studies. The vertical excitation energies of the first bright electronic transition computed with the above mentioned methods at the fully optimized ground-state geometries are listed in **Table 13**.

Table 13: Vertical absorption energies (in nm) of the first bright electronic transition computed with B3LYP, B3LYP/PCM(THF) and CAM-B3LYP/ PCM(THF) for **4** derivatives. In all cases computations are performed in conjunction with the SNSD basis set, and are compared to the experimental values in 5×10^{-6} M THF solution.

Chromophore	B3LYP	B3LYP/PCM(THF)	CAM-B3LYP/PCM(THF)	Exp. λ_{max}
4a	449	494	349	367
4b	476	530	357	373
4b'			356	
4c	374	385	315	329
4d	387	401	319	331
4d'			321	

Comparison with experimental absorption maxima shows that the vertical excitation energies are strongly underestimated using the B3LYP and B3LYP/PCM(THF) methods, while a much better

agreement is obtained with CAM-B3LYP/PCM(THF). The B3LYP gas phase results are also closer to experiment than the ones including solvent effects, while for CAM-B3LYP/PCM(THF), the VE results agree with experimental λ_{max} within 20 nm for all compounds. The TD-CAM-B3LYP/SNSD computations in conjunction with the C-PCM model show also that VE of **4b'** and **4d'** match well their methoxy counterparts (**4b** and **4d**).

Considering the equilibrium structures in the ground electronic state, as optimized in THF solution, contrary to what suggests the skeletal formula, the planar configurations (C_s symmetry) are first-order saddle points (one imaginary frequency), while the minima show a slight distortion of the molecule around the C2-phenyl moiety (**Figure 17**). Indeed, the planar configuration is a transition state (TS) between the two equivalent distorted ground state geometries. The energy difference between the planar and distorted configurations is of about 4-5.5 kJ mol^{-1}. For example, the energy differences between the planar and the distorted (minimum) configuration in the ground state are 4.3 kJ mol^{-1} for **4b'** and 5.2 kJ mol^{-1} for **4d'**, with a 361 and 381 distortion of the dihedral angle between the imidazole and the phenyl–pull moiety, respectively.
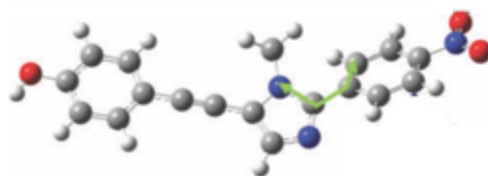
Figure 17: Distorsion around the C2-phenyl bon in **4b'**.

The situation is quite different in the first excited state (S_1), where for all chromophores unconstrained geometry optimizations in THF have led to nearly planar configurations (the dihedral angles between the imidazole and the phenyl–pull moiety in the ground state and in the excited state are reported in **Table 14**). This behavior may be explained based on the features of the molecular orbitals. In particular, during the HOMO–LUMO transition a charge transfer from the phenyl-ethynyl–imidazole moiety to the C2-phenyl one occurs, causing the planarization of the molecules.

Table 14: Dihedral angles (in degrees) between the imidazole and the phenyl–pull moiety in the ground state (S_0) and in the excited state (S_1) for **4** derivatives.

Chromophore	S0	S1
4a	-36	-6
4b	-36	-10
4b'	-36	-10
4c	-39	-8
4d	-39	-10
4d'	-38	-8

A detailed analysis of molecular orbitals shows that the gap between the HOMO and the LUMO is lower for chromophores with **4a,b** than with **4c,d**. This behavior is explained by the stabilization of the LUMO when the nitro moiety is the pull group (**Figure 18**). Furthermore, when a push group (OMe, OH) is present, the HOMO is destabilized, resulting in a decrease of the HOMO–LUMO gap.
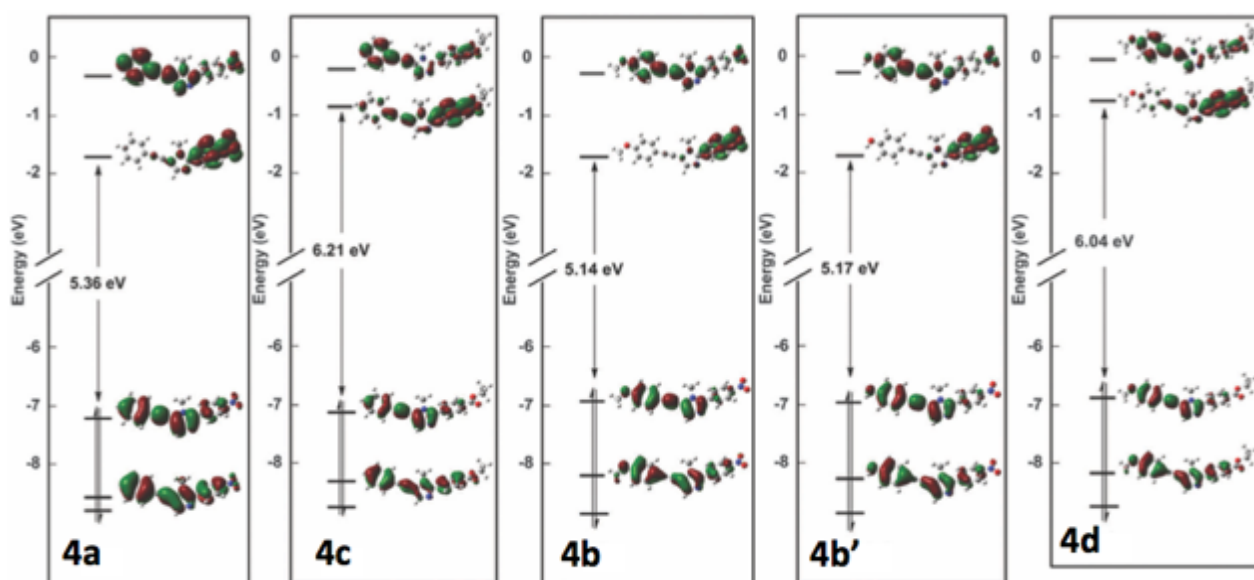
Figure 18: MOs diagrams of **4**-derivatives obtained at CAM-B3LYP/PCM(THF) level of theory.

To test the impact of using OH instead of OMe, both substitutions have been considered in conjunction with NO_2 functionality (**4b** and **4b'**). As shown in the molecular orbital diagrams (**Figure 18**), the HOMO is mainly localized on the phenylethynyl–imidazole moiety for all molecules, while the LUMO is mostly localized on the phenyl–pull moiety. However, with COOEt functional group, the LUMO is more delocalized than in the case of NO_2. This can be related to the antibonding character of the delocalized LUMO, which explains why this orbital is more destabilized than for chromophores bearing NO_2 (**4a,b**). Moreover, the first bright electronic transition, can be mainly described as HOMO–LUMO, which suggests a charge transfer from the phenylethynyl–imidazole moiety to the C2-phenyl ring, clearly visible from the plot of the electron density difference (ELD) between the ground and the first excited electronic states shown in **Figure 19**.
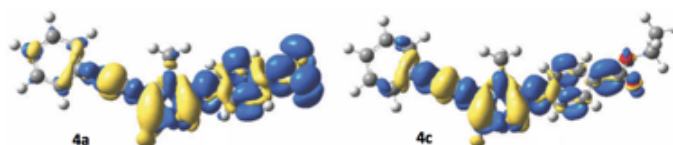
Figure 19: Plots of the difference in electron density (ELD) between the ground state and the first excited electronic state both in the equilibrium geometry of the ground state for the **4a** and **4c** chromophores computed at CAM-B3LYP/PCM(THF) level of theory. The regions that have lost electron density as a result of transition are shown in yellow, whereas the blue regions have gained electron density. ELD densities were plotted with an isovalue threshold of 0.001.

Such a plot points out a significant redistribution of the charge during the electron transition, especially in the case of the chromophore with the NO_2 pull group (**4a**). The strong electron-withdrawing effect of the nitro group can be quantified by the analysis of atomic NBO charges presented in **Figure 20**, showing a significantly larger increase of electron density upon the electronic excitation on the NO_2 (Δ = -0.08) in comparison to the COOEt (Δ = -0.02).
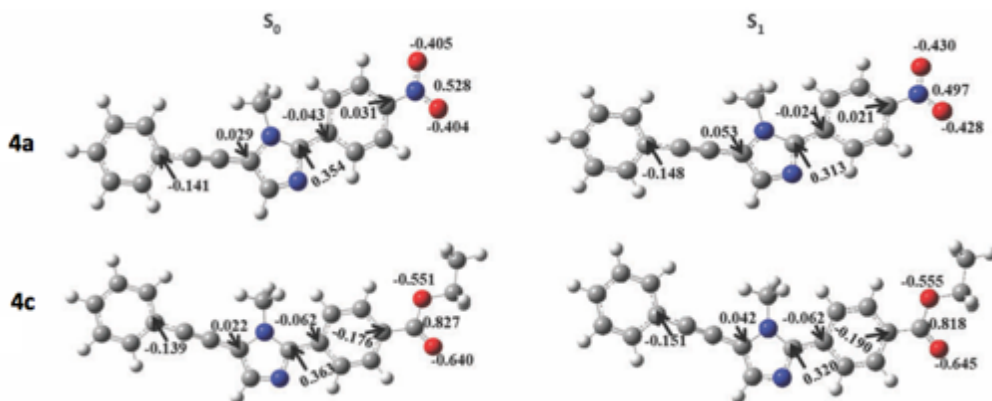
Figure 20: Selected atomic charges from natural bond orbital analysis for the **4a** and **4c** chromophores. Values computed at CAM-B3LYP/SNSD/ PCM(THF) and TD-CAM-B3LYP/SNSD/PCM(THF) levels of theory for the ground and excited states, respectively.

The TD-DFT vertical absorption and emission electronic transitions, computed within the non-equilibrium solvent regime are reported in **Table 15**. In order to study emission properties, the excited-state geometry (S_1) of each system has been optimized at the TD-DFT level. Concerning the absorption spectra a good agreement between TD-CAM-B3LYP/SNSD/C-PCM(THF) computed excitations and the reference experimental data has been already pointed out.

Table 15: Vertical absorption and emission wavelengths and relative oscillator strengths for **4** derivatives calculated at TD-CAM-B3LYP/SNSD level, in THF solution and PMMA matrix.

Chromophore/THF	λ^{max}_{abs}[nm] calc.	λ^{max}_{em}[nm] calc.	F_{abs}	F_{fluo}	S [nm] calc.
4a	349	449	1.11	1.52	100
4b	357	465	1.11	1.56	108
4b'	356	462	1.08	1.52	106
4c	314	402	1.57	1.80	88
4d	319	410	1.67	1.88	91
4d'	321	412	1.53	1.77	91
Chromophore/PMMA					
4a	346	426	1.19	1.37	80
4b'	353	438	1.16	1.35	85

The situation is more challenging for the comparison between the computed and observed fluorescence wavelengths. For compounds **4c** and **4d**, *i.e.* when the pull group is COOEt, the observed and computed values are very close (discrepancies lower than 15 nm). On the other hand, for **4a,b**,

i.e. with NO$_2$ as the pull moiety, there is a systematic underestimation of about 70 nm. This behavior cannot be ascribed to structural effects since the geometry distortion from the ground state to the excited state seems to be independent of the pull group as shown in **Table 14**. This larger discrepancy seems to be a purely electronic effect related to intrinsic limits of the TD-DFT model. However, we note that the TD-DFT computations lead to a correct trend as far as the relative positions of absorption and emission maxima, and also the Stokes shifts are concerned.

The VE theoretical absorption spectra, convoluted using Gaussian functions with a half-width at half-maximum of 2500 cm^{-1} are shown in **Figure 21** for all chromophores. Although those TD-DFT calculations clearly show two bands in the 250-500 nm range for **4a** and **4b**, our study has been focused on the lower-energy ones for all chromophores. The latters, indeed match rather well the band positions and shapes of the experimental spectra with an average error between calculated and experimental values of the absorption maxima of about 15 nm. Moreover, as already discussed based on the data from **Table 15**, the experimental trend moving from one chromophore to the other is computationally well reproduced. In fact, it can be noted that the strong sensitivity of the absorption maximum wavelength on the nature of the push/pull substituents is correctly simulated, showing shifts towards different spectral regions depending on the specific push/pull groups.
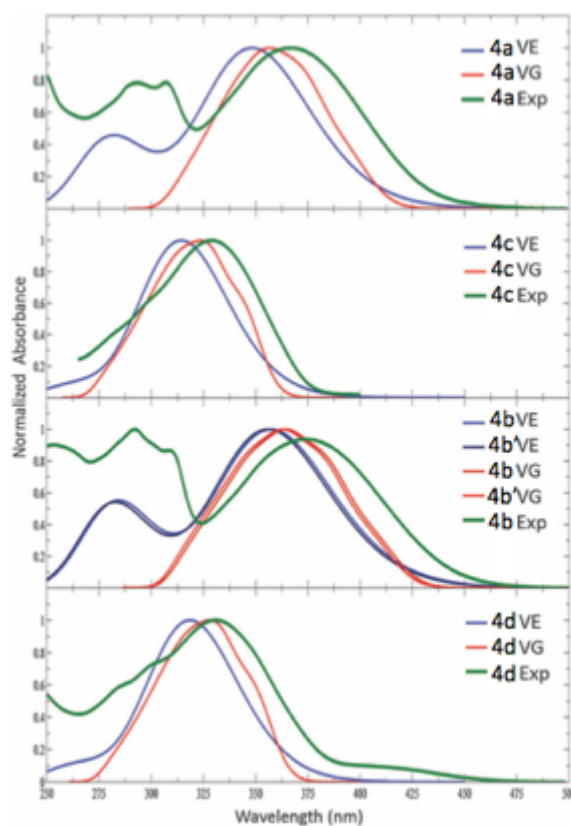
Figure 21: Normalized simulated electronic (VE approach) and vibronic (VG approach) absorption spectra for the 1- and 2-derivatives, compared with the experimental absorption spectra. The theoretical spectra line-shapes have been convoluted using Gaussian functions with a half-width at half- maximum (HWHM) of 2500 cm^{-1} for the electronic spectra and 750 cm^{-1} for the vibronic ones.

A significant improvement to the computed electronic spectra can be achieved by taking into proper account the vibrational effects, with vibronic calculations, which will be considered within the Vertical Gradient approach. The FC|VG model is computationally inexpensive and well suited to the study of low-resolution absorption spectra of strongly allowed transitions. The absorption FC|VG spectra shown in **Figure 21** point out the increased agreement with experiments. In particular, FC|VG maximum absorption wavelengths agree within about 6 nm with experiment (improvement of about 10 nm with respect to VE) and describe much better the experimental line shapes. In fact, contrary to the VE spectra, the asymmetry of the band shape is now clearly visible.

For the chromophores under study it is noteworthy that, contrary to the ground state, the excited-state equilibrium geometry is nearly-planar, which implies a marked distortion associated to the electronic transition. As a consequence, the case of emission is more challenging since the initial state is the excited one, and the considered time-scales involve relaxation to its nearly-planar equilibrium geometry. The adiabatic shift model take into account directly PESs of the initial and final states computed about their respective minima, at the same time avoiding expensive excited state frequency computations. Nevertheless, the large changes in the equilibrium geometries upon excitation from S_0 to S_1 (as shown in **Figure 22** for the specific case of **4a**) results, of course, in a strongly reduced overlap integrals between the corresponding vibrational ground states.
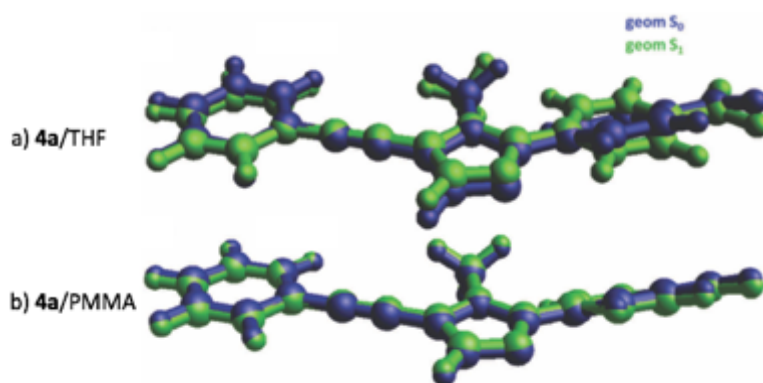
Figure 22: Superposition of the ground (blue) and excited state (green) equilibrium structures of the **4a** (a) in THF solution and (b) in the PMMA.

This leads to a rather low intensity of the simulated emission spectra for all chromophores, as shown in **Figure 23** for the model systems **4b'** and **4d'**.
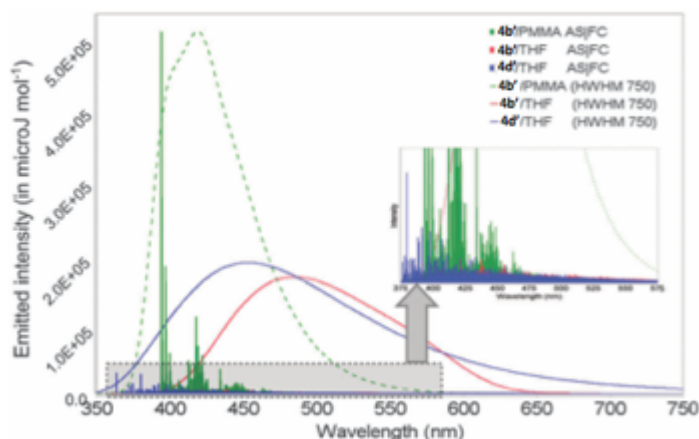
Figure 23: Simulated vibronic (AS approach) emission spectra for **4b'** and **4d'** chromophores in THF and in PMMA. The theoretical stick-spectra have been convoluted using Gaussian functions with a half-width at half- maximum (HWHM) of 750 cm^{-1}.

However, for the **4a** and **4c** chromophores, showing the most promising properties due to the largest Stokes shift, intensity is further decreased most likely due to some non-radiative processes *i.e.* quenching effects *via* a donor-excited photoinduced electron transfer.[64] Indeed the LUMOs of compounds **4a** and **4b** are less unstable than those of compounds **4c** and **4d**, and this is accompanied by a much larger electron transfer toward the nitro group.

The computational studies carried out on **4a,b** in THF solution suggest that the quantum yields of these promising chromophores are affected by the large geometry changes between the ground and excited electronic structures and the corresponding low FC overlaps.[13] Such geometrical distortions involving rather large functional groups are less likely to take place in a rigid polymeric matrix.[31] According to this assumption we set up a simplified computational model that allows us to mimick spectroscopic behaviour in polymers. In detail, during the excited state optimisation the dihedral angle between the imidazole and the phenyl–pull moieties has been fixed to its ground-state value, while all other nuclear degrees of freedom have been relaxed. As a result the S_1 equilibrium structure presented in **Figure 22** displays a large overlap respectively to its ground state structure. In order to take into account the electrostatic effects of the polymer, PCM in its Conductor-like (C-PCM) variant was employed, with the dielectric costant corresponding to PMMA($\varepsilon = 3.3$). Vibronic calculations were employed using time dependent Franck Condon Abiabatic-Shift (FC|AS) model. Fluorescence spectra, calculated in PMMA, are significantly more intense with respect to their counterparts in THF solution, where full geometry relaxation of the chromophores is allowed. This increase in intensity acts as a counter-balance to the intrinsic quenching effects of the polymer matrix, which would otherwise further reduce the observed QY.

Eventually **4a** and **4b'** emission spectra in PMMA are presented in **Figure 24**. A more detailed

analysis of **4a** and **4b'** excited-state properties in THF and PMMA can be seen through the electron density difference (ELD) plots (**Figure 25**) and confirms that the expected favourable fluorescence properties in polymeric matrix should be due to geometrical/steric rather than to electronic effects of the S_1-S_0 transition. Following the current theoretical analysis we propose that an effective *in silico* pre-screening can be performed assuming directly increased rigidity of chromophores in the polymeric matrix, instead of modelling the isolated flexible chromophores in solution. However, we note that the scheme is still under development and further improvements are necessary including proper account of non-radiative processes affecting emission quantum yields as well as more reliable modeling of polymer matrices.[29-32]
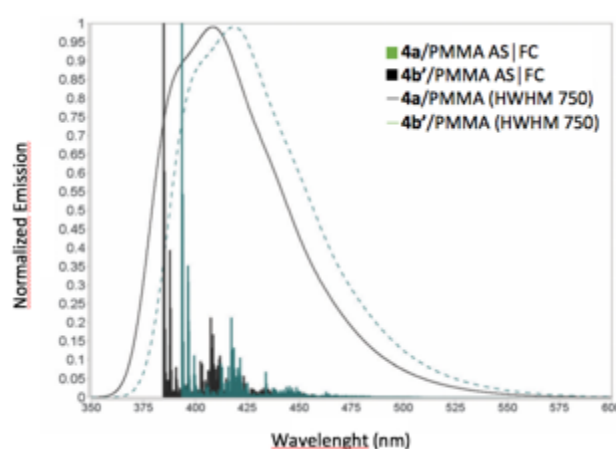

Figure 19: Normalized simulated vibronic (AS approach) emission spectra for **4a** and **4b'** chromophores in PMMA. The theoretical stick-spectra have been convoluted using Gaussian functions with a half-width at half-maximum(HWHM) of 750 cm^{-1}.
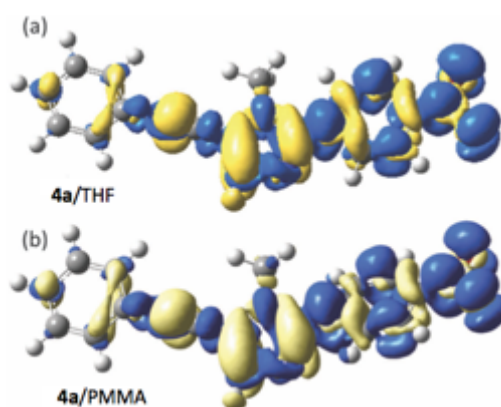
Figure 25: Plots of the difference in electron density (ELD) between the ground state and the first excited electronic state of the **4a** at the excited state equilibrium geometry (a) in THF and (b) in PMMA computed at CAM- B3LYP/PCM(THF) level of theory. The regions that have lost electron density as a result of transition are shown in yellow, whereas the blue regions have gained electron density. ELD densities were plotted with an isovalue threshold of 0.001.

2.3.5 Conclusions

This contribution focused on the evaluation of stereo-electronic and spectroscopic properties of a new family of chromophores characterized by a alkynylimidazole backbone and different push and pull groups. The fluorophores were obtained in good yields (72–90%) and showed optical features in

THF, in the visible region, mostly influenced by the nature the electron-withdrawing group. Firstly, our results indicate that the CAM-B3LYP/PCM(THF) method is the most appropriate to compute vertical excitation energies and simulate absorption spectra, taking into proper account solvation, which represents an important environmental effect strongly affecting the spectral features. Then, the basic VE approach has been used to simulate electronic spectra, providing good predictions for vertical excitation energies and correctly reproducing the strong sensitivity of the absorption maximum wavelength to the nature of the push/pull substituents. However, a significant improvement has been achieved by computation of the vibrationally-resolved electronic spectra by means of the VG approach, which can be confidently applied to simulate the broad absorption spectral features observed experimentally. With respect to the emission spectra, simulated through adiabatic AS model, it has been found that large changes between equilibrium structures of ground and excited electronic states in solution lead to low fluorescence intensities, with further fluorescence quenching observed for nitro derivatives. However, considering that our final target is the chromophore dissolved in the polymeric matrix, we have proposed a cost-effective computational protocol to simulate one-photon absorption and emission spectra in the polymer environment.

2.4 2,5-Disubstituted 1-methylimidazoles of general structure 5

Aryl-substituted imidazoles including 2,5-diarylimidazoles are important structures due to their biological properties. For example, Fenflumizol and Trifenagrel are platelet aggregation inhibitors.

Fenflumizol   Trifenagrel
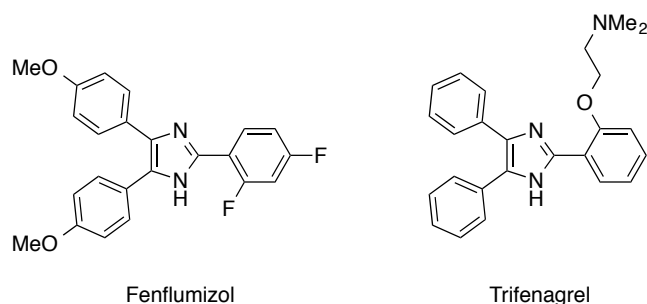
In recent years our research group studied 2,5-disubstituted imidazoles as potential analogues of resveratrol.[133] However, as far as 2,5-diarylimidazoles are concerned, their potential performance in terms of material science are poorly investigated, thus triggering the study of 2,5-disubstituted 1-methylimidazoles. Although having a very simple structure and being accessible through a straightforward one-pot synthesis, these compounds show very interesting fluorescent properties and can be easily functionalized, thus tuning their optical features.

Suzuki, Stille or Negishi palladium-catalysed cross-coupling reactions are among the most efficient methods to prepare 2,5-diarylimidazoles.[134] These methods require, however, the *in situ*

presence of an organometallic derivative. In 1990, Ohta et al. reported the direct arylation of heteroaromatics with aryl halides via a C-H bond activation with moderate to good yields using Pd(PPh$_3$)$_4$ as the catalyst.[135]

From these findings on, the Pd-catalysed direct arylation of heteroaryls promoted by aryl halides as coupling partners has proved to be a very powerful tool for a simpler and greener access to a wide variety of arylated heterocycles, as the major by-products of the reaction are a base associated to HX, instead of metallic salts produced under more classical cross-coupling procedures.[136, 137] Moreover, the method avoids the preliminary preparation of an organometallic reactant. However, so far, the direct arylation of imidazoles has attracted less attention than the arylation of thiophenes or thiazoles, and most times only mono-arylations procedures have been taken into consideration.[138] Again, Ohta and co-workers in 1992, reported the first example of direct 5-arylation of imidazoles employing chloropyrazines as coupling partners and 5 mol % Pd(PPh$_3$)$_4$ as catalyst.[138] Since these results, several groups described reaction conditions allowing the intermolecular Pd-catalysed direct 2- or 5-arylation of imidazoles.[83, 91, 108, 109, 139-144]

To the best of our knowledge only a few examples of Pd-catalysed arylations at both C2 and C5 carbons of imidazoles in one pot have been described.[90, 91, 145-148] In 1998, Miura *et al*. reported the regioselectivity of the arylation of 1-methylimidazole using various reaction conditions.[149] In the presence of bromobenzene, they observed the formation of a mixture of 5-arylation and 2,5-diarylation products in a 54:24 ratio (**Scheme 30a**). They also reported that the addition of 2 equiv of CuI to the reaction mixture, using iodobenzene as coupling partner, significantly alters the selectivity of the reaction, since a mixture of C2 and C2, C5 arylation products in a 37:40 ratio was obtained. It should be noted that CuI itself is able to promote the C2 arylation of imidazole. Bellina, Rossi and co-workers also studied the influence of several parameters for the arylation of imidazoles, and succeeded in a few cases to obtain directly the 2,5-diarylated imidazoles although in moderate yields(**Scheme 30b**).[91] A few 2,5-diarylimidazoles have also been prepared by Shibahara, Murai *et al*. using a 1,10-phenanthroline containing Pd catalyst and aryl iodides as coupling partners (**Scheme 30c**).[147, 148]
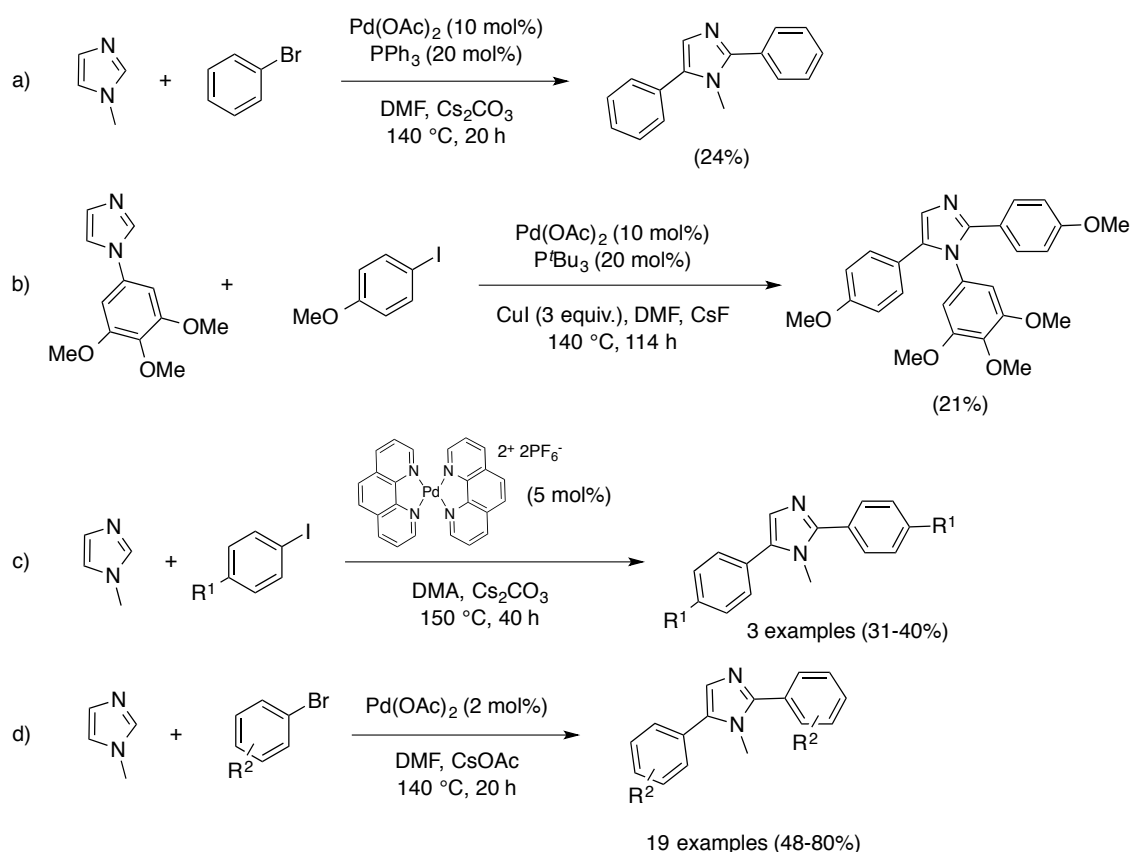
Scheme 30: Reported examples of Pd-catalysed one pot access to 2,5-diarylimidazoles.

More recently, in 2014, Doucet *et al*. reported the synthesis of various 2,5-diarylated N-methylimidazoles bearing both electron-withdrawing and electron-donating functionalities.[150] In this recent work the authors report the employment of Pd(OAc)$_2$ as catalyst without the need for ligands or the presence of metallic co-catalysts (**Scheme 30d**), however the competitive formation of the monoarylated C5 by-product becomes a serious issue. The selection of the base appears crucial in the reaction pattern, since the use of CsOAc leads to the formation of mainly the C2-C5 diarylated products, allowing for moderate to good yields.

Overall, we can state that, so far, sequential Pd-catalysed direct arylation remains the most reliable method to prepare 2,5-diarylimidazoles in good yields. Therefore, the employment of effective conditions, for the direct coupling of aryl halides at both C2 and C5 positions of imidazole derivatives in one pot, constitutes a considerable advantage allowing a simpler access to 2,5-diarylimidazoles.

Our study began with a serendipitous finding during the synthesis of an alkynylimidazole derivative. While performing a C2 direct arylation on 1-methylimidazole (**10a**) with 4-bromobenzaldehyde (**9g**) we got a significant amount of the 2,5-diarylated 1-methylimidazole **5a** as by-product (**Scheme 31**).
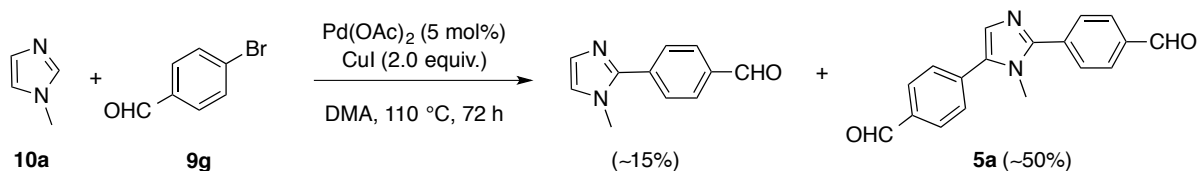
Scheme 31: C2 direct arylation on 1-methylimidazole (**10a**) with 4-bromobenzaldehyde (**9g**).

Diarylimidazole **5a** showed a very bright yellow-green fluorescence, which is retained even in the solid state (**Figure 26**).
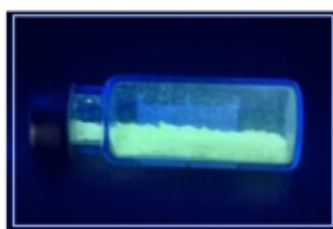
Figure 26: Bright fluorescent powder of compound **5a** under the excitation at 366 nm.

Being the fluorescent properties of **5a** interesting, we decided to carry out a brief reaction conditions screening to find the most efficient synthetic route for our target compound. Moreover we studied the effect of stronger electron-withdrawing functionalities than formyl group, to improve the fluorescent features of this dye.

2.4.1 Reaction condition screening

We took into account the direct arylation of 1-methylimidazole (**10a**) with 3 equiv. of 4-bromobemzaldehyde (**9g**) to force the double arylation and obtain the 2,5-diarylated derivative **5a**.
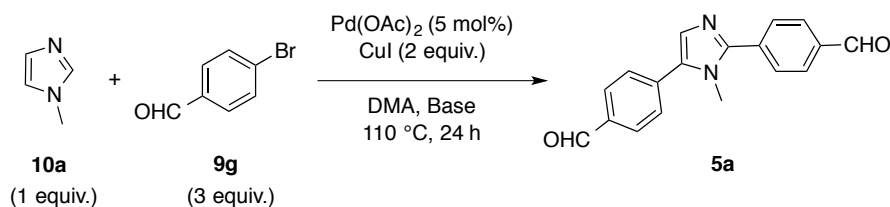
Scheme 32: Synthesis of compound **5a**.

Based on our knoledege we chose DMA as solvent, performing the reaction at 110 °C in the presence of 5 mol% Pd(OAc)$_2$ and 2 equiv. of CuI as co-catalyst (**Scheme 32** and **Table 13**). Under this conditions the reaction outcome proved to be strictly related to the nature of the base (**Table 13**),

with CsOAc scoring the best results were obtained using CsOAc as base (entry 4 **Table 13**), according to what reported by Doucet *et al.* in a recent work concerning the 2,5-diarylation of 1-methylimidazole.[150] The presence of 2 equiv. of CsOAc allowed the formation of the diarylated product **5a** in 55% isolated yield. Starting from this result, we then examined the influence of the amount of catalyst, of copper promoter and the employement of P^tBu_3 as ligand (**Table 14**). The presence of 10 mol% of P^tBu_3 seems to have a slight negative efect on reaction yield if compared with ligandless conditions (entries 1 and 2, **Table 14**), whereas the decrease of CuI and $Pd(OAc)_2$ catalytic load resulted in a more serious decrease on the reaction outcome (entry 3 and 4 **Table 14**). Hence the best catalytic performance appeared in the presence of 5 mol% of $Pd(OAc)_2$ and 2 equiv. of CuI (entry 1, **Table 14**).

Table 13: Different bases employed in the direct arylation of *N*-methylimidazole with 4-bromobenzaldehyde.

Entry	Base (2 equiv.)	Yield[a] in 5a (%)
1	TBAA	46 (44)
2	K_2CO_3	50
3	Cs_2CO_3	56
4	CsOAc	58 (55)
5	KOAc	56

Reaction conditions: 1 mmol *N*-methylimidazole, 3 equivalents of 4-bromobenzaldehyde, $Pd(OAc)_2$ (5 mol%), CuI (2 equiv.), DMA (5 mL), 110°C, 24h, under Argon atmosphere.
[a]GC yield using naphtalene as internal standard, isolated yields are repported in parentheses.

Table 14: Screening of the catalytic loading in the direct arylation of *N*-methylimidazole with 4-bromobenzaldehyde.

Entry	$Pd(OAc)_2$	CuI	Yield[c] in 5a (%)
1[a]	5 mol%	2 equiv.	58
2[b]	5 mol%	2 equiv.	46
3[a]	5 mol%	1 equiv.	32
4[a]	2 mol%	2 equiv.	22

[a]Reaction conditions: 1 mmol *N*-methylimidazole, 3 equivalents of 4-bromobenzaldehyde, DMA (5 mL), 110°C, 24h, under Argon atmosphere.
[b]Reaction conditions: 1 mmol *N*-methylimidazole, 3 equivalents of 4-bromobenzaldehyde, 10 mol% P^tBu_3 DMA (5 mL), 110°C, 24h, under Argon atmosphere.
[c]GC yield using naphtalene as internal standard.

To further improve the yield of **5a**, we studied the effect of the reaction temperature on the formation of **5a**. As reported in **Table 15** no formation of the desired product is observed at reaction temperature of 70 °C (entry 1). A progressive raise of the temperature from 90 °C to 110 °C increased the yield of **5a** from 28% to 58% (entries 2 and 3, **Table 15**), while a further increment from 110 °C to 140 °C resulted in only 8% of improvement. Given these results we decided to test the potential benefit of increasing reaction time from 24 to 48 h (entry 5, **Table 15**). However, this last attempt left the reaction yield practically unaltered. Finally, we succeeded in enhancing the formation of **5a** by stirring the reaction at 110 °C for 24 h in the absence of CuI, then going on for another 24 h at 140 °C after the addition of 2 equiv of CuI (entry 6, **Table 15**). With this last modification of the reaction procedure we were able to isolate **5a** in a 77% yield.

Table 15: Screening of the reaction time and temperature in the direct arylation of *N*-methylimidazole with 4-bromobenzaldehyde.

Entry	Reaction time	T(°C)	Yield[c] in 5a (%)
1	24 h	70[a]	n.d.
2	24 h	90[a]	28
3	24 h	110[a]	58
4	24 h	140[a]	64
5	48 h	110[a]	59
6	48 h	110 to 140[b]	82 (77)

[a]Reaction conditions: 1 mmol *N*-methylimidazole, 3 equivalents of 4-bromobenzaldehyde, Pd(OAc)$_2$ (5 mol%), CuI (2 equiv.), DMA (5 mL), under Argon atmosphere.
[b]Reaction conditions: 1 mmol *N*-methylimidazole, 3 equivalents of 4-bromobenzaldehyde, Pd(OAc)$_2$ (5 mol%), DMA (5 mL), 110°C, 24h, then addition of CuI (2 equiv.), 140 °C, 24 h, the process is performed under Argon atmosphere.
[c]GC yield using naphtalene as internal standard, isolated yields are repported in parentheses.

This last amelioration can be explained taking into account the results previously reported by us[151] on the direct Pd- and Cu-mediated arylation of 1,2- and 1,5-diarylimidazoles. In those studies, we found that the rate of the C2 arylation of a typical 1,5-diaryl-1*H*-imidazole is higher than that of the C5 arylation involving the corresponding 1,2-diaryl-1*H*-imidazole, and that the Pd- and Cu-mediated direct C2 arylation of 1-arylimidazoles is faster than the corresponding Pd-catalyzed direct C5 arylation. Hence, when the reaction involving 1-methylimidazole (**10a**) is carried out in the presence of Pd and Cu, the diarylated imidazole **5a** has to come mainly from the C5 arylation of the intermediate 2-aryl-1-methylimidazole, because the formation of this last compound is faster than the formation of the C5 monoarylated regioisomer. But, as stated before, the C5 arylation of a 2-arylated imidazole is slower than the C2 arylation of a 5-arylated imidazole. As a consequence, starting from 1-methylimidazole we thought it right to promote first the regioselective formation of the C5 monoarylated imidazole **7g** working with palladium alone, and to subsequently add the copper salt to push the reaction to completion by C2 arylation of the C5 arylated intermediate (**Scheme 33**).[90]
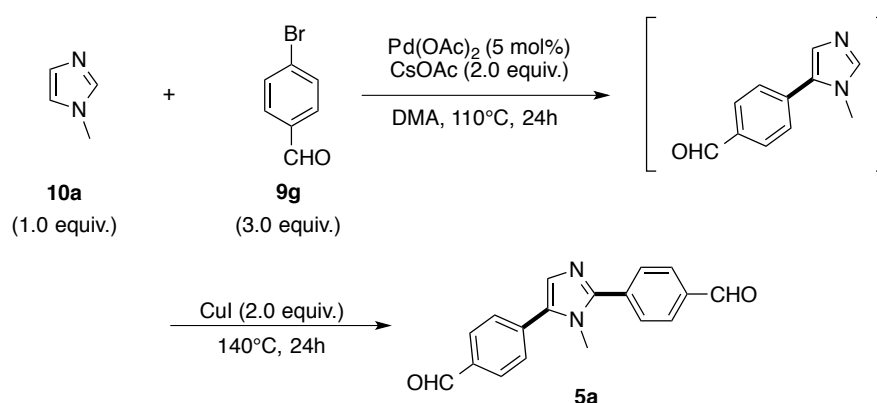
Scheme 33: Two step 2,5-diarylation process on 1-methylimidazole with 4-bromobenzaldehyde.

Thanks to this modification we were also able to get a better yield in **5a** then what reported in the recent work of Doucet and co-workers.[150] Given this interesting result we decided to synthesize compound **5a** and another analogue bearing a stronger electron withdrawing functional group (NO$_2$,

compound **5b**) to evaluate the effect on the spectroscopic feature of these systems.
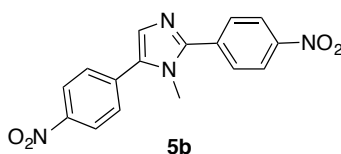
2.4.2 Synthetic approach

Accroding to the experimental conditions reported for entry 6 in Table 15, compounds **5a,b** were synthesized. In detail, *N*-methylimidazole (**10a**) was reacted with 3.0 equiv of aryl bromides **9e** and **9g** employing only palladium acetate as the catalyst precursor. As mentioned in the previous section, this first step allowed the selective formation of the C5 monoarylated imidazoles **5a,b**.[90] After 24 h at 110 °C, to the reaction mixture were added 2.0 equiv. of CuI and the reaction temperature was raised to 140 °C in order to promote the activation of the C2-H bond by formation of an *in situ* organocopper complex, and to drive the reaction to completion. Compounds **5a** and **5b** were obtained respectively in 77% and 35% isolated yield (**Scheme 34**).
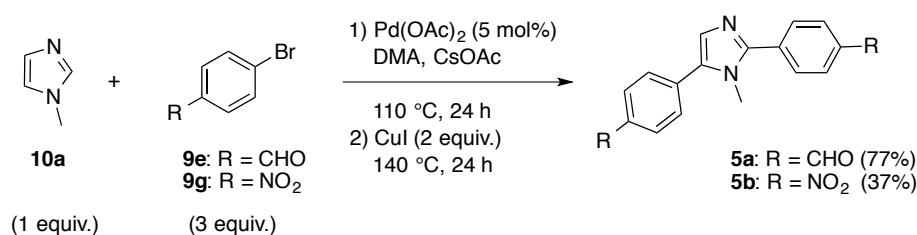
Scheme 34: Synthesis of target compounds **5a,b**.

2.4.3 Fluorescent properties of chromophores 5a,b

Imidazoles **5a** and **5b** exhibited fluorescence not only in THF solution, but also in the solid state, being compound **5a** a yellow fluorescent powder, while compound **5b** was a brilliant orange solid.

Figure 22: Solid appearance of chromophore **5a** (right) and **5b** (left) under the excitation at 366 nm.

This finding was quite relevant given the small size of these dyes. The optical features for compounds **5a,b** in 10^{-5} THF solution are reported in **Figure 23** and summerized in **Table 16**. As evidenced by these data, we found maximum emission wavelenght for compound **5b** around 500 nm but, despite this interesting red-shifted emission, other optical properties of **5b** resulted affected by

the well-known issues of the nitro functionality, *i.e.* quenching of fluorescence quantum yield and poor extinction coefficient.[152]

Table 15: Experimental spectroscopic data for chromophores **5a,b** in 10^{-5} M THF solution.

Chromophore	λ^{max}_{abs}[nm]	λ^{max}_{em}[nm]	Φ^a_f	ε	S [nm]
5a	351	448	0.20	32400	97
5b	377	503	0.10	23000	126

[a]Fluorescence quantum yield (Φ) was determined relative to quinuine sulphate in 0.1 M H_2SO_4 (Φ = 0.54), λ_{exc} (**5a**) = 363 nm, λ_{exc} (**5b**) = 373 nm.
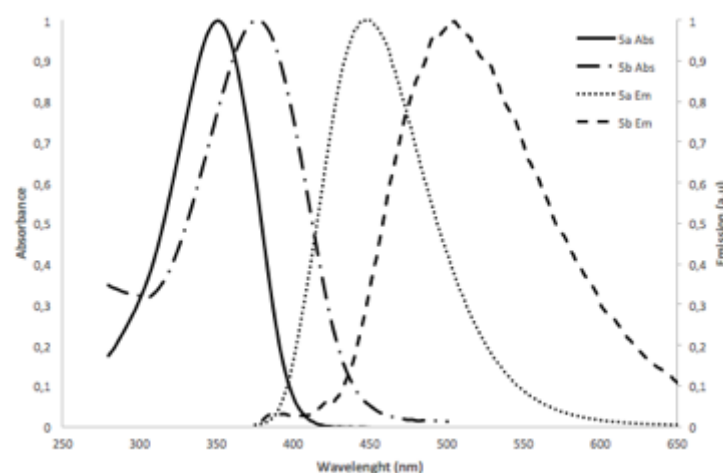
Figure 23: Experimental oprical properties for chromophores **5a,b** dissolved in 10^{-5} M THF solution.

*2.4.4 Derivatization of compound **5a** by insertion of stronger electron-withdrawing functional groups*

Due to the interesting, but not interely satisfactory, optical features of imidazoles **5a,b**, we decided to further investigate the nature of the EWG group, i.e. maintaining the push imidazole moiety and the two arylic π-bridges. Hence, we employed the bis-formyl substituted imidazole **5a** as a reactant in Knoevenagel condensations to obtain in good chemical yields three unprecedented imidazoles, compounds **5c-e**, bearing dicyanovinyl, cyanoacryl, and indandione, respectively, as stronger electron-withdrawing functional groups (**Scheme 35**).
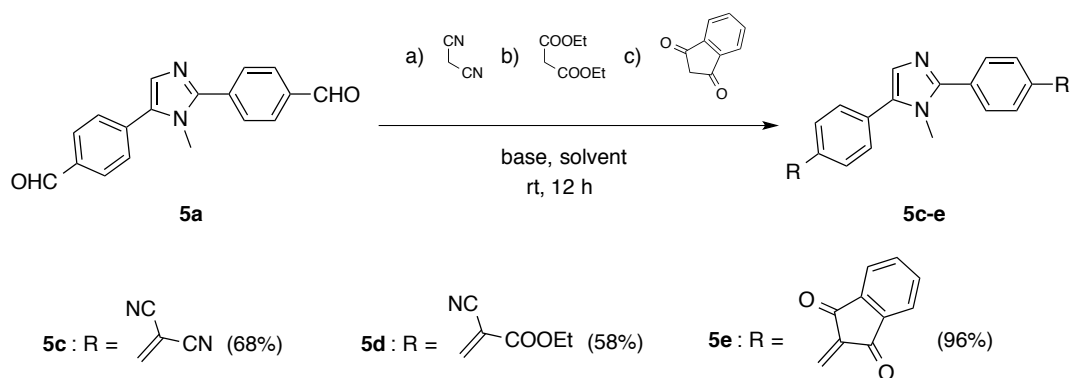
Scheme 35: Synthesis of derivatives **5c-e** by Knoevenagel condensation of **5a** with a) malonitrile, b) diethyl malonate, c) 1,3-indanedione

2.4.5 Optical features of chromophores 5c-e in THF solution

As stated above, our main aim in the synthesis of compounds **5c-e** was the improvement of the optical features already found for compounds **5a** and 5b. In particular, a batochromic shifted emission, a large Stokes shift, and a good quantum yield were our main goals. **Figure 24** and **Table 16** report the optical features for compounds **5c-e**. The introduction of more powerful electron-withdrawing groups also able to widen the π-conjugation, resulted in a shift of the fluorescence emission towards the red region of the UV-Vis spectrum in respect to chromophores **5a** and **5b**, preserving Stokes shifts around 120 nm (**Table 16**).

Table 16: Experimental spectroscopic data for chromophores **5a,b** in 10^{-5} M THF solution.

Chromophore	λ^{max}_{abs}[nm]	λ^{max}_{em}[nm]	Φ^a_f	ε [M^{-1}cm^{-1}]	S [nm]
5c	420	536	0.15	15000	125
5d	403	518	0.25	39800	115
5e	448	576	0.04	30100	128

[a]Fluorescence quantum yield (Φ) was determined relative to quinuine sulphate in 0.1 M H_2SO_4 (Φ = 0.54), λ_{exc} = 373 nm.
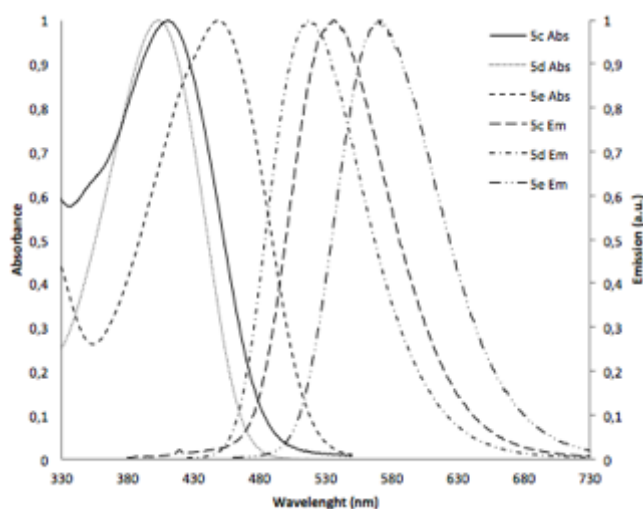
Figure 24: Experimental oprical properties for chromophores **5c-e** dissolved in 10^{-5} M THF solution.

On the other hand, the fluorescence quantum yield resulted inversely proportional to the fluorescent wavelenght, as it is well evidenced in **Figure 25** where the different emission for compounds **5c-e** are plotted against their relative quantum yield. In particular, it is possible to see that the best quantum efficiency is observed for compound **5d**, followed by **5c**. In the case of **5e** the dramatic decrease in quantum yield can reasonably be ascribed to its red shifted emission. In fact it is well known that a batochromic shift can result in a parallel decrement of the fluorescence quantum yield.

*2.4.6 Optical features of chromophores **5d** dispersed in PMMA*

The hearth of a simple LSC device is made by a plate of optical glass coated with a thin polymeric film,[11] usually poly(methyl methacrylate) (PMMA), in which the active dye is dispersed. With the aim of developing an effective imidazole-based dye to be used in LSCs, the 2,5-diarylimidazole **5d**, which displayed the best UV-Vis features in solution, was dispersed in PMMA thin films, prepared with drop casting, with a thickness of 25 ± 5 μm.
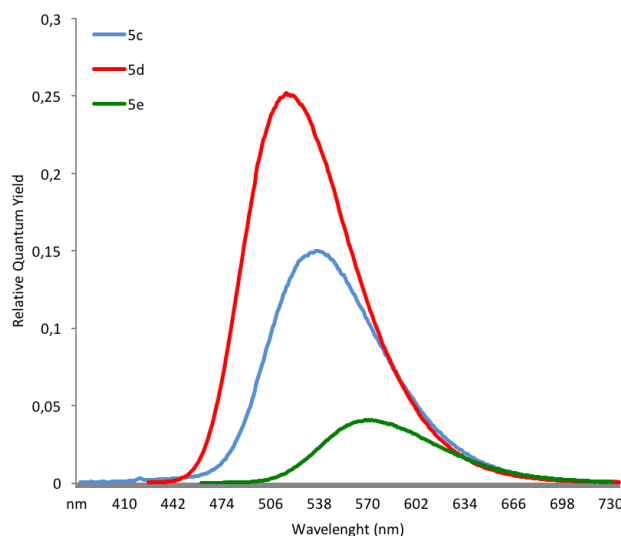
Figure 25: Emission bands of chromophores **5c-e**, plotted against the value of their relative quantum yield.

It is worth nothing that the optical properties of **5d** observed in THF solution were fully preserved after its dispersion in the polymeric matrix (**Table 17**).

Table 17: Spectroscopic properties of **5d**/PMMA thin films at 0.6 wt% concentration and in 10^{-5} M THF solution.

Chromophore	λ^{max}_{abs}[nm]	λ^{max}_{em}[nm]	S [nm]
5d/PMMA	404	519	115
5d/THF	403	518	115

This last result allowed us to plan the verification of the efficiency of **5d** in a real LSC device (**Fig. 26**).
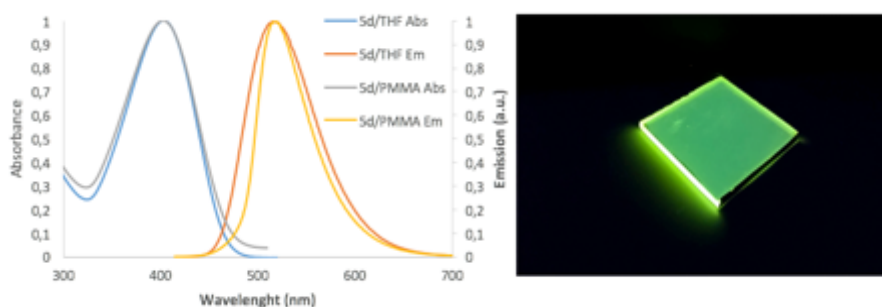
Figure 26: (left) Absorbance and emission spectra of 1 wt% **5d**/PMMA thin films (25 ± 5 μm); (right) an optically pure 50 × 50 × 3 mm glass coated with 25 ± 5 μm thick **5d**/PMMA film under the excitation at 366 nm.

The LSC prototype containing **5d**/PMMA system, was analyzed by using a Si-based PV cell attached to one edge of the concentrator, as described in the Experimental section. The optical efficiency η_{opt} was calculated from the concentration factor C, which is the ratio between the short circuit current measured in the case of the cell over the LSC edge (I_{LSC}) and short circuit current of the bare cell when perpendicular to the light source (I_{SC}) (eq. (1), **Section 2.2**). The calculated η_{opt} for the **5d**/PMMA system was lower than 7% and it well agrees with the optical efficiencies of LSC made of PMMA and containing fluorophores with similar characteristics in terms of emission maxima.[132] In **Tabe 18** the optical efficiency for the **5d**/PMMA system is compared to the Lumogen Red dispersed in poly(methyl methacrylate) (LR/PMMA), which, to the best of our knowledge, exhibits the best currently known performances in LSC.

Table 18: Optical efficiencies (η_{opt}) calculated for **5d**/PMMA LSC and compared to those of LR/PMMA LSC with similar geometrical factor.[124, 125]

	wt%	η_{opt} **(%)**
5d/PMMA	0.7	6.2
	1	6.9
LR/PMMA	1.5-1.8	~8.0

2.4.7 A theoretical explanation of the optical features of 5 derivatives

2,5-Diarylimidazoles of general structure **5** display a significant fluorescence despite their small size. This aspect could be due to a ICT phenomenon upon excitation. To elucidate this aspect, we conducted QM calculations to analize the difference in the molecular orbital distribution in HOMOs and LUMOs. In these calculations compound **5a** and **5d** were taken into account, and in the case of chromphore **5d** the perypheral ethyl chains were neglected and replaced with hydrogen atoms to simplify the structure, and its analogue **5d'** was considered in the calculations.
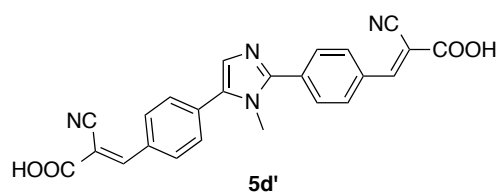
Figure 27, where HOMOs and LUMOs are reported for both **5a** and **5d'** chosen as examples, evidences that the electron density moves from the central electron rich imidazole to the peripheral electron-withdrawing functionalities. HOMOs are alike for **5a** and **5d'**, and the electron density is mainly located on the three central (hetero)aromatic rings. The situation is different for LUMOs: both compounds show a displacement of the electron density toward the electron withdrawing groups, but this behaviour is much more remarkable in the case of **5d'**.
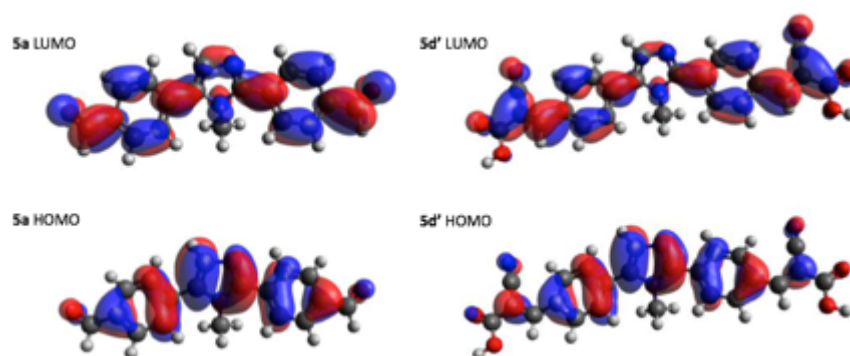
Figure 27: Molecular orbitals HOMO and LUMO for compounds **5a** and **5d'**.

Through the natural bond orbital analysis we can indeed quantify the strenght of the EWG effect, taking **5d'** as example (**Figure 28**). The decrease in the electron density in the heteroaromatic core passing from the ground state (S0) to the first excited state (S1) is mainly highlightened by atomic charge on carbon C4 (in red in **Figure 28**) whereas the increase in the peripheral moiety is well displayed by the terminal alkenyl carbon of the cyanoacrilic functionality (in green in **Figure 28**).
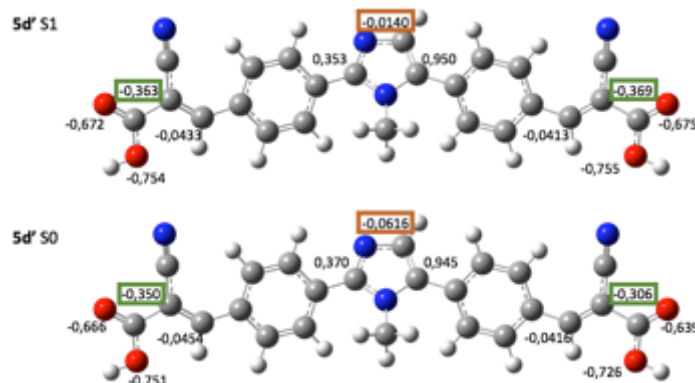
Figure 28: Selected atomic charges from natural bond orbital analysis for **5d'**. Values were computed at CAM-B3LYP/SNSD/PCM(THF) leve lof theory for ground state (S0) and first excited state (S1).

2.4.8 Conclusions

In this last section we present an effective and mild method to approach the synthesis of novel organic dyes. Through very simple procedures we were able to obtain compounds with interesting optical features, and one specific derivative (**5d**) that has suitable properties to be employed in an LSC device. Through means of computational analysis we could rationalize our dyes' spectroscopic behaviour and to quantify the effect of the different electron-withdrawing groups on the overall optical properties.

3 Experimental

3.1 Materials

Melting points were recorded on a hot-stage microscope (Reichert Thermovar). Fluka precoated 60 F254 aluminium silica gel sheets were used for TLC analyses. GLC analyses were performed using two types of capillary columns: an Alltech AT-35 bonded FSOT column (30 m 0.25 mm i.d.) and an Alltech AT-1 bonded FSOT column (30 m 0.25 mm i.d.). Purifications by flash-chromatography were performed using silica gel Merck 60 (particle size 0.040–0.063 mm). EI-MS spectra were measured at 70 eV by GLC/MS. NMR spectra were recorded at room temperature at 200 MHz (^{1}H) and 50.3 MHz (^{13}C) and were referred to TMS or to the residual protons of deuterated solvents. All reactions were performed under argon, by standard syringe, cannula and septa techniques.

3.2 General procedures for the Palladium-catalysed direct 5-arylation of 1-methyl-1H-imidazole (10a) and thiazole (10b) with aryl bromides 9a-d[23, 83]

2-(4-(5-(4-Methoxyphenyl)-1-methyl-1H-imidazol-2-yl)phenyl)-1-methyl-1H-benzo[d]imidazole (**1a**), 1-methyl-2-(4-(1-methyl-5-(p-tolyl)-1H-imidazol-2-yl)phenyl)-1H-benzo [d]imidazole (**1b**), 4-(1-methyl-2-(4-(1-methyl-1H-benzo[d]imidazol-2-yl)phenyl)-1H-imidazol-5-yl)benzonitrile (**1c**) were prepared as previously described by us.[23] All the other commercially available reagents and solvents were used as received.

Pd(OAc)$_2$ (11.2 mg, 0.05 mmol), Bu$_4$NOAc (0.60 g, 2.0 mmol), and aryl bromide **9** (1.5 mmol), if a solid, were placed in a flame-dried reaction vessel. The reaction vessel was fitted with a silicon septum, evacuated, and back-filled with argon. This sequence was repeated twice more. DMA (5 mL), aryl bromide **9** (1.5 mmol), if a liquid, and the appropriate azole **10a** or **10b** (1.0 mmol) were then added successively under a stream of argon by syringe at room temperature. The resulting mixture was stirred under argon for 24 h at 70 °C when thiazole (**10b**) was employed, or at 110 °C when 1-methyl-1H-imidazole (**10a**) was the coupling partner. After cooling to room temperature, the reaction mixture was diluted with AcOEt, filtered through a plug of Celite and eluted with additional AcOEt and CH$_2$Cl$_2$. The filtrate was concentrated under reduced pressure and the residue purified by flash chromatography on silica gel. This procedure was used to prepare compound series **7**.

3.2.1 5-(4-Methoxyphenyl)-1-methyl-1H-imidazole (7a)

The crude reaction product, which was obtained by Pd-catalysed reaction of 1-methyl-1H-imidazole (**10a**) with 4-bromoanisole (**9a**), was purified by flash chromatography on silica gel with a

mixture of CH$_2$Cl$_2$ and MeOH (96:4) as eluent to give **7a** (0.15 g, 82%) as a light-yellow solid, m.p. 106-108 °C. ^{1}H NMR (200 MHz, CDCl$_3$): d 7.48 (s, 1H), 7.30 (m, 2H), 7.02 (s, 1H), 6.96 (m, 2H), 3.83 (s, 3H), 3.61 (s, 3H) ppm. ^{13}C NMR (50.3 MHz, CDCl$_3$): d 159.1, 138.3, 132.3, 129.6 (2C), 127.1, 121.8, 113.9 (2C), 55.1, 32.1 ppm. MS (EI): m/z (%) ¼ 189 (12), 188 (100), 174 (10), 173 (82), 145 (17). The spectral properties of this compound are in agreement with those previously reported.[90]

3.2.2 1-Methyl-5-(p-tolyl)-1H-imidazole (7b)

The crude reaction product, which was obtained by Pd-catalysed reaction of 1-methyl-1H-imidazole (**10a**) with 4-bromotoluene (**9b**), was purified by flash chromatography on silica gel with a mixture of CH$_2$Cl$_2$ and MeOH (96:4) as eluent to give **7b** (0.14 g, 81%) as a yellow oil. ^{1}H NMR (200 MHz, CDCl$_3$): d 7.49 (s, 1H), 7.26 (m, 2H), 7.25 (m, 2H), 7.07 (s, 1H), 3.63 (s, 3H), 2.39 (s, 3H) ppm. ^{13}C NMR (50.3 MHz, CDCl$_3$): d 138.7, 137.6, 133.3, 129.3 (2C), 128.3 (2C), 127.6, 126.7, 32.4, 21.2 ppm. MS (EI): m/z (%) = 173 (13), 172 (100), 171 (17), 144 (14), 130 (16). The spectral properties of this compound are in agreement with those previously reported.[153]

3.2.3 4-(1-Methyl-1H-imidazol-5-yl)benzonitrile (7c)

The crude reaction product, which was obtained by Pd-catalysed reaction of 1-methyl-1H-imidazole (**10a**) with 4-bromobenzonitrile (**9c**), was purified by flash chromatography on silica gel with a mixture of CH$_2$Cl$_2$ and MeOH (96:4) as eluent to give 4c (0.13 g, 69%) as a light-yellow solid, m.p. 148-151 °C. ^{1}H NMR (200 MHz, CDCl$_3$): d 7.73 (m, 2H), 7.59 (s, 1H), 7.53 (m, 2H), 7.22 (s, 1H), 3.75 (s, 3H) ppm. ^{13}C NMR (50.3 MHz, CDCl$_3$): d 140.5, 134.3, 132.5 (2C), 131.6, 129.8, 128.3 (2C), 118.5, 111.2, 33.0 ppm. MS (EI): m/z (%) = 159 (12), 158 (100), 130 (16), 116 (13), 103 (13), 89 (12). The spectral properties of this compound are in agreement with those previously reported.[83]

3.2.4 5-(4-Methoxyphenyl)thiazole (7d)

The crude reaction product, which was obtained by Pd-catalysed reaction of thiazole (**10b**) with 4-bromoanisole (**9a**), was purified by flash chromatography on silica gel with a mixture of toluene and AcOEt (92:8) as eluent to give 5a (0.13 g, 67%) as a bright-yellow solid, m.p. 89-92 °C. ^{1}H NMR (200 MHz, CDCl$_3$): d 8.68 (s, 1H), 7.97 (s, 1H), 7.48 (m, 2H), 6.92 (m, 2H), 3.82 (s, 3H) ppm. ^{13}C NMR (50.3 MHz, CDCl$_3$): d 159.8, 151.2, 139.2, 138.0, 128.2 (2C), 123.6, 114.5 (2C), 55.4 ppm. MS (EI): m/z (%) = 191 (100), 176 (58), 149 (20), 148 (27), 121 (20). The spectral properties of this compound are in agreement with those previously reported.[154]

3.2.5 5-(p-Tolyl)thiazole (7e)

The crude reaction product, which was obtained Pd-catalysed reaction of thiazole (**10b**) with 4-

bromotoluene (**9b**), was purified by flash chromatography on silica gel with a mixture of toluene and AcOEt (90:10 þ 0.1% Et$_3$N) as eluent to give **3b** (0.11 g, 65%) as a pale-yellow solid, m.p. 82-84 °C. ^{1}H NMR (200 MHz, CDCl$_3$): d 8.69 (s, 1H), 8.02 (s, 1H), 7.44 (m, 2H), 7.18 (m, 2H), 2.35 (s, 3H) ppm. ^{13}C NMR (50.3 MHz, CDCl$_3$): d 151.4, 139.3, 138.4, 138.3, 129.6 (2C), 128.1, 126.7 (2C), 21.2 ppm. MS (EI): m/z (%) = 176 (12), 175 (100), 148 (32), 147 (43), 115 (17). The spectral properties of this com- pound are in agreement with those previously reported.[155]

3.2.6 4-(Thiazol-5-yl)benzonitrile (7f)

The crude reaction product, which was obtained by Pd-catalysed reaction of thiazole (**10b**) with 4-bromobenzonitrile (**9c**), was purified by flash chromatography on silica gel with a mixture of toluene and AcOEt (90:10) as eluent to give 5c (0.11 g, 61%) as a yellow solid, m.p. 101-102°C. ^{1}H NMR (200 MHz, CDCl$_3$): d 8.86 (s, 1H), 8.19 (s, 1H), 7.70 (m, 4H) ppm. ^{13}C NMR (50.3 MHz, CDCl$_3$): d 153.7, 140.5, 137.2, 132.7, 135.3, 127.1, 118.2, 111.6 ppm. MS (EI): m/z (%) = 187 (%), 186 (100), 160 (10), 115 (10), 114 (12). The spectral properties of this compound are in agreement with those previously reported.[156]

3.2.7 N,N-Dimethyl-4-(1-methyl-1H-imidazol-5-yl)aniline (7g)

Pd(OAc)$_2$ (11.2 mg, 0.05 mmol), P (2-furyl)$_3$ (23.2 mg, 0.1 mmol), K$_2$CO$_3$ (0.28 g, 2.0 mmol), and 4-bromo-*N.N*-dimethylanyline **9d** (0.30 g, 1.5 mmol) were placed in a flame-dried reaction vessel. The reaction vessel was fitted with a silicon septum, evacuated and back-filled with argon. This sequence was repeated twice more. DMA (5 mL) and 1-methyl-1H-imidazole (**10a**) (80 mL, 82.1 mg, 1.0 mmol) were then added successively under a stream of argon by syringe at room temperature. The resulting mixture was stirred at 110°C under argon for 48 h. After cooling to room temperature, the reaction mixture was diluted with EtOAc, filtered through a plug of Celite, and eluted with additional EtOAc and CH$_2$Cl$_2$. The filtrate was concentrated under reduced pressure, and the crude product was purified by flash chromatography on silica gel with a mixture of CH$_2$Cl$_2$ and MeOH (95:5) as eluent to give **2d** (0.15 g, 76%) as a brown crystalline solid, m.p. 133-137°C. ^{1}H NMR (400 MHz, CDCl$_3$): d 7.49 (s, 1H), 7.28 (m, 2H), 7.02 (s, 1H), 6.79 (m, 2H), 3.65 (s, 3H), 3.02 (s, 6H) ppm. ^{13}C NMR (50.3 MHz, CDCl$_3$): d 150.1, 137.6, 134.0, 129.5 (2C), 124.9, 116.3, 112.1 (2C), 40.3 (2C), 32.6 ppm. MS (EI): m/z (%) = 202 (14), 201 (100), 200 (42), 186 (13), 185 (17). Elemental analysis calcd (%) for C$_{12}$H$_{15}$N$_3$: C 71.61, H 7.51; found: C 71.68, H 7.49.

3.3 2-(4-Bromophenyl)benzo[d]thiazole (8a)[100, 156, 157]

A three-necked 500 mL flask equipped with air condenser and magnetic stirrer was charged with 2-aminothiophenol (0.67 mL, 0.78 g, 6.25 mmol), 4-bromobenzaldehyde **9g** (0.93 g, 5 mmol) and

DMSO (150 mL). The mixture was stirred under air at 190°C. The progress of the reaction was monitored by GLC and after 2 h the conversion was found complete. The reaction mixture was poured into water and the resulting white-greenish precipitate was recovered by filtration, purified by crystallization in ethanol giving **8** as a white solid (1.34 g, 92%), m.p. 51-53 °C. ^{1}H NMR (200 MHz, CDCl$_3$): d 8.09e8.05 (m, 1H), 8.00-7.89 (m, 3H), 7.66-7.60 (m, 2H), 7.51(dt,J^1 = 8Hz,J^2 = 1.4Hz,1H),7.40(dt,J^1 = 8Hz,J^2 = 1.4Hz,1H) ppm. MS (EI): m/z (%) = 291 (100), 290 (20), 289 (99), 210 (30), 108 (19). The spectral properties of this compound are in agreement with those previously reported.[100]

3.4 2-(4-Bromophenyl)-6-methylbenzo[d]thiazole (8c)[158, 159]

According to a reported procedure,[159] in a three-necked 500 mL flask equipped with mechanic stirrer and dropping fun- nel were added 125 mL of glacial acetic acid that were cooled at 5 °C. A mixture of KSCN (5.83 g, 60 mmol) and *p*-toluidine (6.43 g, 60 mmol) was added to the precooled acetic acid giving a brownish solution. Then, a bromine solution (60 mmol of Br$_2$ in 60 mL glacial acetic acid) was added very slowly with constant stirring so that temperature did not rise above 5 °C. The reaction mixture was still stirred for additional 3 h. The hydrobromide salt obtained was filtered, the solid was dissolved in 150 mL of hot water and filtered once more. The solution was neutralized with ammonia and white crystals formed of 6-methylbenzo[d]thiazol-2-amine were collected. Afterwards, the intermediate obtained was refluxed with an aqueous solution of NaOH (5 times by weight of benzothiazole) until its own complete depletion. The solution was filtered and neutralized with glacial acetic acid. The separated yellowish semisolid formed was extracted with diethyl ether and dried over Na$_2$SO$_4$. The evaporation of the solvent and crystallization from MeOH/H$_2$O afforded 2,2'-disulfanediyilbis (4-methylaniline) as yellowish needle-shaped crystals (3.92 g, 47%), m.p. 84-85 °C. ^{1}H NMR (400, CDCl$_3$): d 6.98-6.95 (m, 4H), 6.64 (d, 2H, J = 8 Hz), 4.18 (bs, 4H, NH$_2$), 2.13 (s, 6H, CH$_3$) ppm. ^{13}C NMR (100 MHz): d 146.3, 137.14, 132.4, 127.6, 119.0, 115.4, 20.1 ppm. MS (EI): m/z (%) = 277 (8), 276 (48), 139 (24), 138 (100), 94 (24), 77 (8).

2,2'-Disulfanediyilbis (4-methylaniline) (3.59 g, 13 mmol), bromobenzaldehyde (4.88 g, 26.4 mmol) and sodium metabisulfite (2.52 g, 13.26 mmol) were dissolved in DMSO (100 mL). The resulting orange reaction mixture was stirred at 120 C and the formation of the desired product monitored by TLC and GC analyses. After 4 h, the reaction mixture was cooled at room temperature, water was added (200 mL) and the resulting precipitate was collected by vacuum filtration. Afterwards, the solid was well washed with excess water (150 mL) in order to remove residual DMSO, re-dissolved in CH$_2$Cl$_2$ and finally washed with brine. The organic layer was dried over Na$_2$SO$_4$ and the solvent removed in vacuo giving compound **8c** as a yellow solid (5.14 g, 64%), m.p.

175-178 °C. ^{1}H NMR (400, CDCl$_3$): d 7.95-7.93 (m, 3H), 7.69 (s, 1H), 7.62(d,2H,J = 8Hz), 7.31 (dd,1H,J^1 = 8Hz,J^2 = 2Hz), 2.50 (s,3H) ppm. ^{13}C NMR (100 MHz, CDCl$_3$) 165.6, 152.2, 135.6, 135.2, 132.7, 132.2, 129.1, 128.2, 125.1, 123.3, 121.4, 21.6 ppm. MS (EI): m/z (%) = 306 (17), 305 (100), 304 (36), 303 (95), 302 (21). The spectral properties of this compound are in agreement with those previously reported.[158]

3.5 2-(4-Bromophenyl)benzo[d]thiazole-6-carbaldehyde (8b)

A two-necked 1 L flask equipped with condenser was charged with 2-(4-bromophenyl)-6-methylbenzo [d]thiazole (**8c**) (5 g, 16.4 mmol), N-bromosuccinimide (6.12 g, 34.4 mmol) and AIBN (0.43 g, 2.6 mmol). The reaction vessel was fitted with a silicon septum, then evacuated and back-filled with argon for three times. After that, degassed benzene (320 mL) was added and the reaction mixture was left to reflux 6 h. The reaction was filtered and the solvent was removed *in vacuo*. The solid obtained was dissolved in CH$_2$Cl$_2$, washed with water (3 times) and brine, thus dried over Na$_2$SO$_4$. The crude product was a mixture of monobrominated and dibrominated compound (30:70, respectively) as shown by ^{1}H NMR. The mixture of brominated products obtained (7.52 g) was added without further purification to a two-necked 500 mL flask equipped with a condenser and magnetic stirrer. The reaction vessel was evacuated and back-filled with argon for three times. AgNO$_3$ (6.27 g, 36.9 mmol) and 200 mL anhydrous 1,2-dimethoxyethane were then added and the reaction mixture was allowed to reflux until the complete disappearance of the precursor. Anhydrous triethylamine (23 mL, 164 mmol) was finally added and the reaction was refluxed 2 h more. Afterwards, CH$_2$Cl$_2$ was poured to the reaction mixture that was filtered on a layer of Celite. The solvent was removed and the crude product was dissolved again in CH$_2$Cl$_2$, washed with water (3 times) and brine and dried over Na$_2$SO$_4$. The solid obtained after evaporation of the solvent was recrystallized from CH$_2$Cl$_2$/hexane giving product **8b** as an off- white solid (3.28 g, 63%), m.p. 305e309 C. ^{1}H NMR (400, CDCl$_3$): δ10.12(s,1H,CHO),8.45(d,1H,J1⁄42Hz),8.17(d,1H,J1⁄48Hz),8.03 (dd,1H,J^1 = 8Hz,J^2 1⁄42MHz),7.99(m,2H),7.67(m,2H)ppm. ^{13}C NMR (100 MHz, CDCl$_3$): δ 191.1, 171.3, 158.1, 135.8, 133.6, 132.6 (2C), 132.1, 129.3 (2C), 127.6, 126.6, 124.5, 123.9 ppm. MS (EI): m/z (%) = 319 (100), 318 (79), 317 (94), 316 (64), 209 (32). Elemental analysis calcd (%) for C$_{14}$H$_8$BrNOS: C 52.85, H 2.53; found: C 52.89, H 2.52.

3.6 General procedures for the Pd-catalysed C-2 arylation of 5- aryl-imidazoles (7a-d and 7g) and 5-aryl-thiazoles (7e-f) with bromides 8a and 8b

Method A.[90, 91, 109]

A two-necked flask equipped with a magnetic stirrer and a reflux condenser was charged with the appropriate 5-aryl-1-methyl-1H-imidazole **7a-c** (1 mmol) or 5-aryl-thiazoles **7d-f** (1 mmol), 2-(4-bromophenyl)benzo [d]thiazole (**8a**) (1.1 mmol), Pd(OAc)$_2$ (11.2 mg, 0.05 mmol) and CuI (381 mg, 2 mmol). The apparatus was fitted with a silicon septum, evacuated and back- filled with argon three times. Anhydrous DMA (5 mL) was added by syringe against a positive pressure of argon. The reaction mixture was stirred at 160 °C. The reaction evolution was followed by GLC and GLC-MS analyses. After cooling at room temperature, the reaction mixture was diluted with CH$_2$Cl$_2$ (200 mL) and poured into a saturated aqueous NH$_4$Cl solution to which 5 mL of concentrated aqueous ammonia had been added. The resulting mixture was stirred in the open air for 30 min and then extracted with CH$_2$Cl$_2$. The organic extracts were washed with saturated brine, dried, concentrated under reduced pressure, and the resulting crude reaction product was purified as described below. This procedure was used to prepare compounds **2a-c** and **3a-c**.

Method B.[83]

A two-necked flask equipped with a magnetic stirrer and a reflux condenser was charged with the 5-aryl-1-methyl-1H-imidazole **7a**, or **7g** (1 mmol), 2-(4-bromophenyl)benzo [d]thiazole (**8a**) or 2-(4-bromophenyl)benzo [d]thiazole-6-carbaldehyde (**8b**) (1.1 mmol), Pd(OAc)$_2$ (11.2 mg, 0.05 mmol), Bu$_4$NOAc (0.60 g, 2 mmol) and CuI (380.9 mg, 2 mmol). The apparatus was fitted with a silicon septum, evacuated and back-filled with argon three times. Anhydrous DMA (5 mL) was added by syringe against a positive pressure of argon. The reaction mixture was stirred at 110 °C for 24 h. The reaction evolution was followed by TLC analysis. After cooling at room temperature, the reaction mixture was diluted with CH$_2$Cl$_2$ (100 mL) and poured into a saturated aqueous NH$_4$Cl solution to which 5 mL of concentrated aqueous ammonia had been added. The resulting mixture was stirred in the open air for 30 min and the organic layer was extracted. The solvent was removed and the solid crude product was well washed with water in order to remove the excess of Bu$_4$NOAc, filtered, re-dissolved in CH$_2$Cl$_2$, washed with saturated brine, dried and concentrated under reduced pressure. The resulting crude reaction product was purified by crystallization. This procedure was used to prepare compounds **2d** and **2e**.

3.6.1. 2-(4-(5-(4-Methoxyphenyl)-1-methyl-1H-imidazol-2-yl) phenyl)benzo[d]thiazole (2a)

The crude reaction product obtained by Pd- and Cu-mediated reaction of **7a** and **8a** according to

Method A was purified by treatment with a hot mixture of toluene and AcOEt (70:30), followed by filtration. The solid recovered (0.09 g) resulted to be pure **2a**, while the filtrate was further purified by flash chromatography on silica gel using a mixture of toluene and AcOEt (70:30) as eluent. The chromatographic fractions containing the product were collected, concentrated and added to the solid previously recovered by filtration. In this way pure **2a** was obtained as a yellow solid (0,14 g, 66%), m.p. 244-248 °C. ^{1}H NMR (200 MHz, CDCl$_3$): δ 8.21 (m, 2H), 8.10 (d, J ¼ 8.0 Hz, 1H), 7.93 (d, J ¼ 8.0 Hz, 1H), 7.86 (m, 2H), 7.55e7.37 (m, 4H), 7.20 (s, 1H), 7.01 (m, 2H), 3.87 (s, 3H), 3.71 (s, 3H) ppm. ^{13}C NMR (50.3 MHz, CDCl$_3$): δ 167.2, 159.5, 154.1, 147.9, 135.9, 135.1, 133.4, 133.3, 130.2, 129.0, 127.7, 127.5, 126.4, 125.3, 123.3, 122.3, 121.7, 114.3, 55.4, 34.0 ppm. MS (EI): m/z (%) = 398 (30), 397 (100), 396 (27), 382 (15), 198 (13). Elemental analysis calcd (%) for C$_{24}$H$_{19}$N$_3$OS: C 72.52, H 4.82; found: C 72.49, H 4.80.

3.6.2. 2-(4-(1-Methyl-5-(p-tolyl)-1H-imidazol-2-yl)phenyl)benzo [d]thiazole (2b)

The crude reaction product obtained by Pd- and Cu-mediated reaction of **7b** and **8a** according to *Method A* was purified by flash chromatography on silica gel with a mixture of toluene and AcOEt (60:40) as eluent to give **2b** as an iridescent yellow-greenish solid (0.12 mg, 66%), m.p. 204-206 °C. ^{1}H NMR (200 MHz, CDCl$_3$): δ 8.21 (m, 2H), 8.10 (dd, J^1 = 8.0 Hz, J^2 = 0.6 Hz, 1H), 7.93 (m, 1H), 7.86 (m, 2H), 7.56-7.23 (m, 8H), 3.74 (s, 3H), 2.42 (s, 3H) ppm. ^{13}C NMR (50.3 MHz, CDCl$_3$): δ 167.2, 154.1, 148.1, 138.0, 136.2, 135.1, 133.4, 133.2, 129.5, 129.0, 128.8, 128.6, 127.7, 127.0, 126.4, 125.3. 123.3, 121.6, 34.0, 21.3 ppm. MS (EI): m/z (%) = 383 (9), 382 (30), 381 (100), 380 (49), 190 (14). Elemental analysis calcd (%) for C$_{24}$H$_{19}$N$_3$S: C 75.56, H 5.02; found: C 75.59, H 5.03.

3.6.3. 4-(2-(4-(Benzo[d]thiazol-2-yl)phenyl)-1-methyl-1H- imidazol-5- yl)benzonitrile (2c)

The crude reaction product obtained by Pd- and Cu-mediated reaction of **7c** and **8a** according to *Method A* was purified by flash chromatography on silica gel with a mixture of toluene and AcOEt (40:60) as eluent to give **2c** as a yellow solid (0.15 g, 83%), m.p. 217-220 °C. ^{1}H NMR (200 MHz, CDCl$_3$): δ 8.24 (m, 2H), 8.11 (d, J = 7.4 Hz, 1H), 7.94 (d, J = 8.4 Hz, 1H), 7.86 (m, 2H), 7.77 (m, 2H), 7.60 (m, 2H), 7.53e7.37 (m, 3H), 3.78 (s, 3H) ppm. ^{13}C NMR (50.3 Hz, CDCl$_3$): δ 166.9, 154.1, 150.0, 135.1, 134.4, 134.3, 134.0, 132.7, 132.4, 129.7, 129.3, 128.5, 127.8, 126.5, 125.5, 123.4, 121.7, 118.5, 111.4, 34.4 ppm. MS (EI): m/z (%) = 394 (9), 393 (27), 392 (100), 391 (66), 196 (10). Elemental analysis calcd (%) for C$_{24}$H$_{16}$N$_4$S: C 73.45, H 4.11; found: C 73.50, H 4.09.

3.6.4 4-(2-(4-(Benzo[d]thiazole-2-yl)phenyl)-1-methyl-1H- imidazol-5-yl)-N,N-dimethylaniline (2d)

The crude reaction product obtained by Pd- and Cu-mediated reaction of **7g** and **8a** according to *Method B* was purified by crystallization from toluene to give **2d** as a yellow solid (0.19 g, 46%),

m.p. 220-225 °C. ^{1}H NMR (400 MHz, CDCl$_3$): δ 8.19 (m, 2H), 8.09 (d, J = 8Hz,1H), 7.92(d, J = 8Hz,1H),7.86(m,2H),7.51(t,J = 8Hz,1H), 7.40 (t, J = 8 Hz, 1H), 7.33 (m, 2H), 7.16 (s, 1H), 6.80 (m, 2H), 3.71 (s, 3H), 3.01 (s, 6H) ppm. ^{13}C NMR (50.3 MHz, CDCl$_3$): δ 167.5, 154.3, 150.3, 147.7, 137.0, 135.2, 133.7, 133.3, 129.9, 129.0, 127.8, 127.1, 126.5, 125.4, 123.4, 122.4, 121.8, 117.6, 112.4, 40.5, 34.0 ppm. HRMS (ESI) m/ z found [M+H]$^+$ 411.1645; C$_{25}$H$_{22}$N$_4$S requires [M+H]$^+$ 411.1638.

3.6.5   2-(4-(5-(4-Methoxyphenyl)-1-methyl-1H-imidazol-2-yl)   phenyl)benzo[d]thiazole-6-carbaldehyde (2f)

The crude reaction product obtained by Pd- and Cu-mediated reaction of **7a** and **8d** according to *Method B* was purified by crys- tallization from AcOEt to give **2f** as a yellow solid (0.44 g, 68%), m.p. 254-257 °C. ^{1}H NMR (400 MHz, CDCl$_3$): δ 10.13 (s, 1H), 8.48 (d, J 1⁄4 2 Hz,1H), 8.25 (m, 2H), 8.20 (d, J = 8 Hz,1H), 8.03 (dd, J^1 1⁄48 Hz, J^2 = 2 Hz, 1H), 7.90 (m, 2H), 7.40 (m, 2H), 7.20 (s, 1H), 7.01 (m, 2H), 3.88 (s, 3H), 3.73 (s, 3H) ppm. ^{13}C NMR (100 MHz, CDCl$_3$): δ 191.2, 171.9, 159.8, 158.2, 147.8, 136.3, 135.8, 134.3, 133.5, 132.9, 130.3, 129.2, 128.1, 127.8, 127.6, 124.6, 123.9, 114.5, 55.5, 34.1 ppm. HRMS (ESI) m/z found [M+H]$^+$ 426.1276; C$_{25}$H$_{19}$N$_3$O$_2$S requires [M+H]$^+$ 426.1271.

3.6.6 2-(4-(5-(4-Methoxyphenyl)thiazol-2-yl)phenyl)benzo[d] thiazole (3a)

The crude reaction product obtained by Pd- and Cu-mediated reaction of **7d** and **8a** according to Method A was treated with hot AcOEt and filtered. The solid recovered by filtration was further treated with hot CH$_2$Cl$_2$, filtered and concentrated. In this way a first aliquot of **3a** was recovered (26 mg). The solution obtained from the first filtration was purified by flash chromatography on silica gel with a mixture of CH$_2$Cl$_2$ and AcOEt (96:4) as eluent. The chromatographic fractions containing the product were collected, concentrated and added to the first aliquot of **3a**, to give the required product as an iridescent yellow solid (0.14 g, 72%), m.p. 196-199 °C. ^{1}H NMR (200 MHz, CDCl$_3$): δ 8.20-8.05 (m, 5H), 7.97-7.91 (m, 2H), 7.58-7.37 (m, 4H), 6.96 (m, 2H), 3.86 (s, 3H) ppm. ^{13}C NMR (100 MHz, acquired at 40 °C, CDCl^3): δ 167.2, 165.1, 160.2, 154.5, 140.3, 138.9, 136.1, 135.4, 134.8, 128.3, 126.9, 126.6, 125.6, 124.1, 123.6, 121.8, 114.8, 55.6 ppm. MS (EI): m/z (%) = 400 (100), 281 (22), 207 (38), 149 (32), 44 (24). Elemental analysis calcd (%) for C$_{23}$H$_{16}$N$_2$OS$_2$: C 68.97, H 4.03; found: C 68.89 and H 4.02.

3.6.7 2-(4-(5-(p-Tolyl)thiazol-2-yl)phenyl)benzo[d]thiazole (3b)

The crude reaction product obtained by Pd- and Cu-mediated reaction of **7b** and **8a** according to *Method A* was purified adding a mixture of toluene and AcOEt (95:5), filtrating an insoluble re- sidual and performing a flash chromatography on silica gel of the filtrate to give **3b** as a yellow solid (47 mg, 25%), m.p. 207-210 °C. ^{1}H NMR (200 MHz, CDCl$_3$): δ 8.21-8.16 (m, 2H), 8.12-8.06 (m, 3H),

8.03 (s, 1H), 7.93 (d, J = 8.0 Hz, 1H), 7.56-7.40 (m, 4H), 7.24 (m, 2H), 2.40 (s, 3H) ppm. ^{13}C NMR (100 MHz, CDCl$_3$): δ 167.2, 165.5, 154.4, 140.5, 139.3, 138.8, 136.0, 135.3, 134.8, 130.0, 128.5, 128.3, 126.9, 126.8, 126.7, 125.6, 123.5, 121.8, 21.4 ppm. MS (EI): m/z (%) = 385 (26), 384 (100), 192 (12), 148 (26), 147 (31). Elemental analysis calcd (%) for C$_{23}$H$_{16}$N$_2$S$_2$: C 71.84, H 4.19; found: C 71.78, H 4.20.

3.6.8 4-(2-(4-(Benzo[d]thiazol-2-yl)phenyl)thiazol-5-yl) benzonitrile (3c)

The crude reaction product obtained by Pd- and Cu-mediated reaction of **7c** and **8a** according to *Method A* was treated with boiling CH$_2$Cl$_2$ for 2 h, filtered and concentrated, to give **3c** as a yellow solid (96 mg, 53%), m.p. 233-235 °C. ^{1}H NMR (200 MHz, acquired at 40 °C, CDCl$_3$): δ 8.23-8.08 (m, 6H), 7.93 (d, J = 7.6 Hz, 1H), 7.71 (s, 4H), 7.56-7.38 (m, 2H) ppm. ^{13}C NMR (100 MHz, acquired at 40 °C, CDCl$_3$): δ 168.0, 166.9, 154.4, 141.5, 138.0, 135.9, 135.7, 135.4, 133.13, 128.4, 127.3, 127.2, 126.7, 125.8, 123.7, 121.9, 118.5, 112.1 ppm. MS (EI): m/z (%) = 397 (12), 396 (29), 395 (100), 197 (8), 159 (52). Elemental analysis calcd (%) for C$_{23}$H$_{13}$N$_3$S$_2$: C 69.85, H 3.31; found: C 69.79, H 3.29.

3.6.9 Ethyl 2-cyano-3-(2-(4-(5-(4-methoxyphenyl)-1-methyl-1H- imidazol)phenyl)benzo[d]thyazol-6-yl)acrylate (2e)

According to a reported procedure,[123] a two-necked 10 mL flask equipped with a condenser was charged with compound 1e (64 mg, 0.15 mmol) and imidazole (2 mg, 0.03 mmol). The reaction vessel was fitted with a silicon septum, then evacuated and back- filled with argon for three times. Then, dichloromethane (1 mL) and ethyl 2-cyanoacetate (16 mL, 0.15 mmol) were added and the reaction mixture was heated to reflux overnight. The yellow crude product was worked-up by diluting with CH$_2$Cl$_2$ and washing with water three times. The organic layer was dried over Na$_2$SO$_4$, the solvent was evaporated and the crude product was purified by washing with 5 mL of diethyl ether, giving compound **2e** as a yellow-orange solid (70 mg, 90%), m.p. 231-235 °C. ^{1}H NMR (200 MHz, CDCl$_3$): δ 8.67 (d, J 1/4 2 Hz, 1H), 8.36 (s, 1H), 8.24 (m, 2H), 8.16 (d, J 1/4 8 Hz,1H), 8.09 (dd, J^1 = 8 Hz, J^2 = 2 Hz,1H), 7.89 (m, 2H), 7.40 (m, 2H), 7.20 (s, 1H), 7.02 (m, 2H), 4.42 (q, J = 8 Hz, 2H), 3.87 (s, 3H), 3.73 (s, 3H), 1.42 (t, J 1/4 8 Hz, 3H) ppm. ^{13}C NMR (100 MHz, CDCl$_3$): δ 171.8, 162.7, 159.9, 157.3, 154.3, 147.8, 136.4, 136.3, 134.4, 132.9, 130.4, 129.8, 129.3, 128.6, 128.2, 127.8, 124.9, 124.0, 122.4, 115.9, 114.5, 102.7, 63.0, 55.5, 34.1, 14.3 ppm. HRMS (ESI) m/z found [M+H]$^+$ 521.1646; C$_{30}$H$_{24}$N$_4$O$_3$S requires [M+H]$^+$ 521.1642.

3.7 General procedure for the one-pot C5 halogenation/ alkynylation of 2-aryl-1-methyl-1H-imidazoles 11a,b: synthesis of fluorophores 4a-d

N,N-Dimethylformamide (DMF) and *N,N*-dimethylacetamide (DMA) were dried by distillation at reduced pressure over CaH$_2$. 1-Methyl-1H-imidazole (4) was purified by distillation at reduced pressure. Phenylacetylene (7a), 4-ethynylanisole (**13b**), and piperidine were purified by distillation at reduced pressure over CaH$_2$. *N*-Bromosuccinimide (NBS) was purified by crystallization. All the other commercially available reagents and solvents were used as received. Ethyl 4-(1-methyl-1H-imidazol-2-yl)benzoate (**11b**) was prepared by the Pd/Cu-mediated direct C2–H arylation of 1-methyl-1H-imidazole (**10a**) with ethyl 4-bromobenzoate (**9f**) as previously reported.[86]

To a solution of 2-aryl-1-methyl-1H-imidazole **11** (1 mmol) in DMF (5 mL), NBS (169 mg, 0,95 mmol) was added and the resulting reaction mixture was stirred in the dark at room temperature for 5 h. Then, Pd(PPh$_3$)$_2$Cl$_2$ (14 mg, 0.02 mmol, 2 mol%), CuI (8 mg, 0.04 mmol, 4 mol%), an alkyne **13** (1, 1 mmol) and piperidine (300 mL, 255 mg, 3 mmol) were added and the resulting reaction mixture was stirred at 80 °C for 3 h. The reaction mixture was diluted with EtOAc (100 mL), then saturated aqueous NH$_4$Cl (100 mL) was added. The resulting mixture was stirred for 30 minutes and extracted with EtOAc (3 × 25 mL). The organic extracts were washed with water (3 × 25 mL) and brine (1 × 25 mL), dried over anhydrous Na$_2$SO$_4$, filtered and concen- trated under reduced pressure. The residue was purified by flash chromatography on silica gel. This procedure was employed to prepare compounds **4a-d**. GLC analysis showed that all these compounds had chemical purity higher than 98%.

3.7.1 1-Methyl-2-(4-nitrophenyl)-5-(phenylethynyl)-1H-imidazole (4a)

The crude reaction product obtained by the one-pot halogenation/alkynylation reaction of 1-methyl-2-(4-nitrophenyl)-1H-imidazole (**11a**) with phenylacetylene (**13a**) was purified by flash chromatography on silica gel with a mixture of toluene and EtOAc (90 : 10) as eluent to give **4a** as an orange solid (205 mg, 81%), m.p.: 154–157 °C. EIMS, m/z (%) = 304 (21), 303 (100), 257 (19), 256 (13), 255 (9). ^{1}H NMR (200 MHz, CDCl$_3$): δ 8.34 (m, 2H), 7.90 (m, 2H), 7.55 (m, 2H), 7.49 (s, 1H), 7.39 (m, 3H), 3.89 (s, 3H) ppm. ^{13}C NMR (50.3 MHz, CDCl$_3$): δ 147.5, 145.8, 136.1, 134.5, 131.3 (2C), 129.0 (2C), 128.9, 128.5 (2C), 123.9 (2C), 122.1, 119.5, 97.8, 77.1, 33.3 ppm. Anal. calcd found: C, 71.35; H, 4.33; N, 13.88. Calcd for C$_{18}$H$_{13}$N$_3$O$_2$: C, 71.28; H, 4.32; N, 13.85.

3.7.2 5-((4-Methoxyphenyl)ethynyl)-1-methyl-2-(4-nitrophenyl)- 1H-imidazole (4b)

The crude reaction product obtained by one-pot halogenation/alkynylation reaction of 1-methyl-2-(4-nitrophenyl)-1H-imidazole (**11a**) with 4-ethynylanisole (**13b**) was purified by flash

chromatography on silica gel with a mixture of toluene and EtOAc (90 :10) as eluent to give **4b** as a red solid (144 mg, 72%), m.p.: 168– 171 °C. EIMS, m/z (%) = 334 (22), 333 (100), 318 (13), 303 (10), 287 (10). ^{1}H NMR (200 MHz, CDCl$_3$): δ 8.33 (m, 2H), 7.89 (m, 2H), 7.48 (m, 2H), 7.27 (s, 1H), 6.91 (m, 2H), 3.88 (s, 3H), 3.85 (s, 3H) ppm. ^{13}C NMR (50.3 MHz, CDCl$_3$): δ 160.1, 147.5, 145.6, 136.2, 134.1, 132.9 (2C), 128.9 (2C), 123.9 (2C), 119.9, 114.2 (2C), 97.8, 75.8, 55.4, 33.3 ppm. Anal. calcd found: C, 68.50; H, 4.55; N, 12.59. Calcd for C$_{19}$H$_{15}$N$_3$O$_3$: C, 68.46; H, 4.54; N, 12.61.

3.7.3 Ethyl 4-(1-methyl-5-(phenylethynyl)-1H-imidazol-2- yl)benzoate (4c)

The crude reaction product obtained by one-pot halogenation/alkynylation reaction of ethyl 4-(1-methyl-1H-imidazol- 2-yl)benzoate (**11b**) with phenylacetylene (**13a**) was purified by flash chromatography on silica gel with a mixture of toluene and EtOAc (90:10) as eluent to give **4c** as a brown solid (211 mg, 74%), m.p.: 123–126 °C. EIMS, m/z (%) = 330 (100), 302 (15), 301 (17), 257 (8), 128 (8). ^{1}H NMR (200 MHz, CDCl$_3$): δ 8.15 (m, 2H), 7.77 (m, 2H), 7.52 (m, 2H), 7.47 (s, 1H), 7.36 (m, 2H), 4.40 (q, J = 7.1 Hz, 2H), 3.82 (s, 3H), 1.41 (t, J = 7.1, 3H) ppm. ^{13}C NMR (50.3 MHz, CDCl$_3$): δ 165.8, 147.1, 134.1, 134.0, 131.1 (2C), 130.4, 129.6 (2C), 128.5, 128.3 (2C), 128.1 (2C), 122.2, 118.5, 97.1, 77.5, 61.0, 33.0, 14.2 ppm. Anal. calcd found: C, 76.38; H, 5.50; N, 20.63. Calcd for C$_{21}$H$_{18}$N$_2$O$_2$: C, 76.34; H, 5.49; N, 20.65.

3.7.4 Ethyl 4-(5-((4-methoxyphenyl)ethynyl)-1-methyl-1H- imidazol-2-yl)benzoate (4d)

The crude reaction product obtained by one-pot halogenation/alkynylation reaction of ethyl 4-(1-methyl-1H-imidazol-2-yl)benzoate (**11b**) with 4-ethynylanisole (**13b**) was purified by flash chromatography on silica gel with a mixture of toluene and EtOAc (80:20) as eluent to give **4d** as a yellow solid (158 mg, 90%), m.p.: 141–145 °C. EIMS, m/z (%) = 361 (25), 360 (100), 345 (7), 332 (11), 317 (14). ^{1}H NMR (200 MHz, CDCl$_3$): δ 8.15 (m, 2H), 7.76 (m, 2H), 7.47 (m, 2H), 7.43 (s, 1H), 6.89 (m, 2H), 4.40 (q, J = 7.4 Hz, 2H), 3.83 (s, 3H), 3.82 (s, 3H), 1.41 (t, J = 7.4 Hz, 3H) ppm. ^{13}C NMR (50.3 MHz, CDCl$_3$): δ 165.9, 159.9, 147.0, 134.3, 133.7, 132.8 (2C), 130.4, 129.7 (2C), 128.2 (2C), 118.9, 114.3, 114.1 (2C), 97.1, 76.1, 61.1, 55.3, 33.1, 14.3 ppm. Anal. calcd found: C, 73.37; H, 5.58; N, 7.79. Calcd for C$_{22}$H$_{20}$N$_2$O$_3$: C, 73.32; H, 5.59; N, 7.77.

3.8 General procedure for the synthesis of 2,5-diaryl-1-methyl-1*H*-imidazoles 5 by one-pot C5 and C2 direct arylation

In a flame-dried reaction vessel were placed the appropriate aryl bromide **9** (3.0 mmol), Pd(OAc)$_2$ (11.2 mg, 0.050 mmol) and CsOAc (0.384 g, 2.00 mmol). The reaction vessel was fitted with a silicon septum, evacuated, and back-filled with argon. This sequence was repeated twice. DMA (5 mL) and

1-methyl-1*H*-imidazole (**10a**) (80 μL, 80.2 mg, 1.0 mmol) were then added successively under a stream of argon by syringe at room temperature. The resulting mixture was stirred at 110 °C under argon for 24 h. CuI (0.38 g, 2.0 mmol) was then added to the resulting pale yellow mixture under a stream of argon. The reaction mixture was heated to 140 °C and stirred at this temperature for 24 h. After cooling to room temperature, the reaction mixture was diluted with AcOEt and poured into a saturated aqueous NH_4Cl solution. The resulting mixture was basified with a few drops of aqueous NH_4OH, stirred in the open air for 0.5 h, and then extracted with AcOEt. The organic extract was washed with water, dried, and concentrated under reduced pressure, and the residue was purified by flash chromatography on silica gel. The chromatographic fractions containing the required compound were collected and concentrated. This procedure was employed to prepare 2,5-diaryl-1-methyl-1*H*-imidazoles **5a** and **5b** in 77 and 37% yields, respectively.

3.8.1 4,4'-(1-Methyl-1H-imidazole-2,5-diyl)dibenzaldehyde (5a)

The crude reaction product obtained by Pd-catalyzed and Cu-mediated one pot direct arylation reactions involving **9e** was purified by flash chromatography on silica gel with AcOEt as eluant to give **5a** (0.226 g, 77%) as a bright yellow solid, m.p.: 164–165 °C. ^{1}H NMR ($CDCl_3$) δ 10.12 (s, 1H), 10.10 (s, 1H), 8.05 (m, 2H), 8.03 (m, 2H), 7.94 (m, 2H), 7.68 (m, 2H), 7.28 (s, 1H), 3.85 (s, 3H). EIMS: m/z 290 (M^+, 100), 289 (66), 158 (11), 130 (8), 103 (7), 89 (7). GLC analysis showed that **5a** had chemical purity higher than 98%. The NMR spectroscopic data of this compound were in satisfactory agreement with those previously reported.[150]

3.8.2 1-Methyl-2,5-bis(4-nitrophenyl)-1H-imidazole (5b)

The crude reaction product obtained by Pd-catalyzed and Cu-mediated one pot direct arylation reactions involving **9g** was purified by flash chromatography on silica gel with a mixture of toluene and AcOEt (70:30) as eluant to give **5b** (0.120 g, 37%) as a bright yellow solid. ^{1}H NMR ($CDCl_3$) δ 8.40 (m, 2H), 8.38 (m, 2H), 7.96 (m, 2H), 7.68 (m, 2H), 7.45 (s, 1H), 3.83 (s, 3H). EIMS: m/z 324 (M^+,69), 323 (19), 281 (33), 232 (17), 208 (30), 207 (100). GLC analysis showed that **5b** had chemical purity higher than 98%. The NMR spectroscopic data of this compound were in satisfactory agreement with those previously reported.[150]

3.8.3 2,2'-(((1-Methyl-1H-imidazole-2,5-diyl)bis(4,1-phenylene))bis(methanylylidene))dimalononitrile (5c)

According to a previously reported procedure,[160] a reaction vessel was charged with 2,5-diarylated imidazole **5a** (0.100 g, 0.33 mmol). The reaction vessel was fitted with a silicon septum, then

evacuated and back- filled with argon for three times. Then, CH_2Cl_2 (24 mL), malononitrile (46 mg, 0.7 mmol), and Et_3N (4 drops) were added and the reaction mixture was stirred at room temperature overnight. The orange crude product was worked-up by diluting with CH_2Cl_2, and the solvent was evaporated in vacuo giving compound **5c** as a red powder (87 mg, 68%), m.p. 165-167°C. ^{1}H NMR (400 MHz, DMSO-d_6) δ 8.65 (m, 2H), 8.19 (s, 1H), 8.17 (s, 1H), 8.16 (m, 2H), 8.09 (m, 2H), 7.92 (m, 2H), 7.61 (s, 1H), 3.90 (s, 3H). Anal. Calcd for $C_{24}H_{14}N_6$: C, 74.60; H, 3.65. Found: C, 74.67; H, 3.64.

3.8.4 Diethyl 3,3'-((1-methyl-1H-imidazole-2,5-diyl)bis(4,1-phenylene))-bis(2-cyanoacrylate) (5d)

According to a previously reported procedure,[123] a reaction vessel was charged with 2,5-diarylated imidazole **5a** (0.100 g, 0.33 mmol) and imidazole (0.68 mg, 1.0 mmol). The reaction vessel was fitted with a silicon septum, then evacuated and back- filled with argon for three times. Then, CH_2Cl_2 (5 mL) and ethyl cyanoacetate (0.1 mL, 1.0 mmol) were added and the reaction mixture was heated to reflux for 36 h. The yellow crude product was worked-up by diluting with CH_2Cl_2 and washing with water three times. The organic layer was dried over Na_2SO_4, the solvent was evaporated giving compound **5d** as a bright orange fluorescent powder (94 mg, 58%), m.p. 230-232 °C. ^{1}H NMR (400 MHz, DMSO-d_6) δ 8.65 (m, 2H), 8.19 (s, 1H), 8.17 (s, 1H), 8.16 (m, 2H), 8.09 (m, 2H), 7.92 (m, 2H), 7.61 (s, 1H), 3.90 (s, 3H). Anal. Calcd for $C_{28}H_{24}N_4O_4$: C, 69.99; H, 5.03. Found: C, 70.05; H, 5.04.

3.8.5 2,2'-(((1-Methyl-1H-imidazole-2,5-diyl)bis(4,1-phenylene))bis(methanylylidene))bis(1H-indene-1,3(2H)-dione) (5e)

According to a previously reported procedure,[161] to a solution of 2,5-diarylimidazole **5a** (86 mg, 0.29 mmol) in 3 mL of MeOH and 3 mL of CH_2Cl_2, 1,3-indanedione (146 mg, 1.0 mmol), *L*-proline (12 mg, 0,1 mmol) were added and the reaction mixture was stirred at room temperature for 24 h. The crude product **5e** was recovered by filtration, as a bright red fluorescent powder (156 mg, 96%), m.p. 170-171 °C. ^{1}H NMR (400 MHz, DMSO-d_6) δ 8.65 (m, 2H), 8.19 (s, 1H), 8.17 (s, 1H), 8.16 (m, 2H), 8.09 (m, 2H), 7.92 (m, 2H), 7.61 (s, 1H), 3.90 (s, 3H). Anal. Calcd for $C_{28}H_{24}N_4O_4$: C, 69.99; H, 5.03. Found: C, 70.05; H, 5.04.

3.9 Preparation of polymer films for optical studies

Different dye/PMMA thin films were prepared by drop casting, *i.e.* pouring a 0.8 mL chloroform solution containing 30 mg of the polymer and the proper amount of dye to obtain concentrations in the range of 0.05–2.2 wt% over a 35×50 mm area of a glass surface. The glass slides were cleaned with chloroform and immerged in 6 M HCl for at least 12 h, then they were rinsed with water, acetone

and isopropanol and dried for 8 h at 120 °C. Solvent evaporation was performed on a warm hot plate (about 30 °C) and in a closed environment. The film thickness was measured by a Starrett micrometer to be 25 ± 5 mm. The PMMA films were easily removed with a spatula after immersion in water so that they can be stored for successive measurements and comparison by attaching them on 50 × 50 × 3 mm optically pure glass substrate (Edmund Optics Ltd BOROFLOAT window 50 50 TS) with a high-purity silicone oil with a refractive index comparable to PMMA and glass (*i.e.*, poly(methylphenyl siloxane), 710 fluid, Aldrich, refractive index n = 1.5365). Absorption and emission properties of such devices showed negligible differences with the freshly prepared ones.

3.9.1 Apparatus and methods

Absorption spectra were recorded at room temperature on a Perkin-Elmer Lambda 650 spectrometer. Fluorescence spectra were measured at room temperature on a Horiba Jobin-Yvon Fluorolog®-3 spectrofluorometer and equipped with a 450 W xenon arc lamp, double-grating excitation and single- grating emission monochromators. The fluorescence of dye/ PMMA films were recorded by using the Solid-Sample Holder and collecting the front-face emission at 30°. The fluorescence quantum yield (Φ_f) in tetrahydrofuran (THF) was determined at room temperature relative to quinine sulphate ($\Phi^s_f = 0.54$ in 0.1 M H_2SO_4) using the following relation:

$$\Phi_x = \Phi_{st}\left(\frac{Grad_x}{Grad_{st}}\right)\left(\frac{\eta_x^2}{\eta_{st}^2}\right)$$

where the subscripts ST and X are standard and dye respectively, ''Grad'' is the gradient from the plot of integrated fluorescence intensity versus absorbance for different solutions of standard and dyes. In order to minimise re-absorption effects concentration was kept low, so absorbances never exceed 0.1 at and above the excitation wavelength. Z is the refractive index of the solvent, *i.e.* 1.405 for THF and 1.333 for water.[162] A thin film of about 10^{-3} M 9,10-diphenylanthracene in PMMA was used as a standard (($\Phi^s_f = 0.83$)[163] for the quantum yield measurement of dye/PMMA films.

3.9.2 Photocurrent measurements

A proper apparatus was built, made of a plywood wooden box 15 × 15 × 30 cm with walls 1.5 cm thick. A removable cover hosting a housing for a solar lamp is present at the top. During the measurement a solar lamp TRUE-LIGHT® ESl E27 20 W was used. Two 50 × 3 mm slits were carved out at 5 cm from the bottom of the box to exactly fit the LSC systems (dimensions 50 × 50 × 3 mm) so that a minimum amount of light would come out during the measurements. On the outer side of the slit, a set of three 1 × 1 cm photodiodes (THORLABS FDS1010 Si photodiode, with an active

area of 9.7 ×9.7 mm and high responsivity (A/W) in the spectral range of 400–1100 nm) connected in parallel fashion was placed and coupled to a multimeter (KEITHLEY Mod. 2700) for photocurrent measuring.

3.9.3 Efficiency measurement using a PV-cell

A different set of LSC samples was prepared to measure the concentration efficiency attaching a Si-PV cell (IXYS SLMD121H08L mono solar cell 86 × 14 mm, with a solar cell efficiency of 22% and a fill factor 470%) to one edge of the sample. This set of samples was made covering the full 50 × 50 mm area of the previously introduced optically pure glass slabs with a 24 × 5 mm dye/ PMMA thick film. One edge of the LSC was connected to a Si-based PV cell masked to cover just the LSC edge (50 × 3 mm) using silicone grease while the remaining edges were covered with an aluminum tape. These devices were then placed over a white poly(ethylene terephthalate) scattering sheet (Microcellular® MCPET reflective sheet, ERGA TAPES Srl) and placed about 20 cm under a solar lamp (TRUELIGHT®ESL E27 20 W, with a correlated color temperature of 5500 K). The efficiency is reported as Z_{opt}, which is the ratio between the short circuit current of the PV cell attached the LSC edges under illumination of a light source (I_{LSC}) and the short circuit current of the bare cell put perpendicular to the light source (I_{SC}).

3.10 Computational methods

Quantum mechanical (QM) calculations on fluorophores have been performed at the density functional theory (DFT) and its time-dependent extension (TD-DFT) levels of theory.[111-114] Due to the likely presence of long-distance charge transfers, the CAM-B3LYP functional[115] has been chosen, together with the SNSD basis set,[116] which was developed for spectroscopic studies of medium-to-large molecular systems. The SNSD basis set allows cost-effective predictions for a broad range of spectroscopic properties, including electronic absorption and emission spectra.[24, 117] Vertical excitation energies (VE) and excited state equilibrium geometries have been calculated with TD-DFT.[164] As a matter of fact, the TD-CAM-B3LYP computations have already shown very good performance for a broad range of excited electronic states,[165, 166] and in conjunction with the SNSD or N07D-aug basis sets they have been extensively tested for spectro- scopic properties of different p-conjugated chromophores.[22, 32, 167]

In order to match experimental conditions, environmental effects simulating solvent (THF) and polymeric matrix (PMMA) have been accounted for with the polarizable continuum model (PCM)[168, 169] and more precisely its Conductor-like (C-PCM) variant.[170] The molecule-shaped cavity surrounding the solute molecule has been built by interlocking spheres centered on heavy atoms,

exploiting the default set of sphere radii implemented in Gaussian.[171] Non-equilibrium solvent effects on the vertical excitation energies have been computed with the linear response LR-PCM/TD-DFT approach,[164] where the excitation energies are directly determined without computing the exact excited electron density. This solvation model provides reliable results at a relatively low computational cost and can be extended to several spectroscopic properties,[172] with further consideration of spectral line shapes.[22, 32]

The TD-CAM-B3LYP/PCM(THF) method has been validated and compared to the TD-B3LYP results based on the computation of vertical absorption energies and the simulation of absorption spectra with respect to their experimental counterparts (see the Results section). Details about the nature of the electronic transitions have been revealed by computation of the electronic densities at the ground and excited states, and the subsequent natural bond orbital (NBO) analysis.[173]

In a first approximation, the electronic spectra can be simulated with the commonly used basic vertical energy approach, which relies on the computation of vertical excitation energies, giving rise to a single peak per electronic transition with the intensity determined by the corresponding electronic transition dipole moment. The line-shapes are then obtained by applying a symmetric distribution functions to simulate the broadening observed experimentally. Nevertheless, the computation of electronic spectra with the VE approach completely neglects the influence of nuclear motions. Therefore, this approach is not able to simulate the vibrational structure present in experimental spectra and, consequently, accurately reproduce the typical asymmetry of the experimental bands, which is often required in order to get more accurate absorption and emission maxima and to be able to correctly interpret the experimental results.[24, 167] In this regard, several approaches to include vibronic contributions have recently become feasible for medium-to-large systems, following the time-independent or time-dependent[174] frameworks. Here we employ the time- independent Franck–Condon Vertical-Gradient (FC|VG) and Adiabatic-Shift (FC|AS) models, which allow to avoid the expensive computations of excited state frequencies. Within the framework of the Franck–Condon principle,[175-177] the transition dipole moment is assumed to remain constant during the electronic transition, equal to its value at the equilibrium geometry. This approximation is generally valid for fully allowed transitions, such as the ones considered in this work. The spectrum is simulated based on the computation of overlap integrals (Franck-Condon integrals) between the vibrational wavefunctions of the electronic states involved in the transition, which within sum-over-states approach are treated. Finally the resulting stick spectrum is convoluted by mean of distribution functions.

In order to compute vibrationally resolved electronic spectra different models are now available,

which differ by their conceptual approach to the electronic transition, vertical or adiabatic.[32, 178] In this work we simulated absorption spectra by means of the vertical gradient model, which focuses on the final-state PES at the equilibrium geometry of the initial state, *i.e.*, the region corresponding to the most intense transitions (FC|VG). This is also known in literature as the linear coupling model (LCM).[179] The adiabatic approach has been applied as well in order to estimate Franck-Condon factors of the emission spectra and simulate fluorescence spectra in polymer matrix, within the Adiabatic Shift (AS) model. Those models (VG and AS) have been applied assuming that the computation of the excited- state energy gradients (at the ground-state equilibrium structure) or excited-state geometry optimizations, are sufficient to describe the PES of excited states in vertical region (absorption, VG) or at its equilibrium (emission, AS).

The simulated VG and AS stick spectra have been convoluted using Gaussian functions with half-widths at half-maximum (HWHM) of 750 cm^{-1}. This value has been chosen to match the reference experimental absorption spectra.

All computations were performed using a locally modified version of the Gaussian package.[171] A graphical user interface (VMS-Draw)[180] was used to analyze in detail the outcome of vibronic computations and plot electronic spectra.

Bibliography

1.   Forrest, S. M.; Thompson, M. E. *Chemical Reviews* **2007,** *107*, 923-1386.

2.   Miller, R. D.; Chandross, E. A. *Chemical Reviews* **2010,** *110*, 1-574.

3.   Mayor, M. *Chimia* **2010,** *64*, 348-349.

4.   Batail, P. *Chemical Reviews* **2004,** *104*, 4887-4890.

5.   Bredas, J. L.; Durrant, J. R. *Acc Chem Res* **2009,** *42*, 1689-90.

6.   Lin, Y.; Li, Y.; Zhan, X. *Chem Soc Rev* **2012,** *41*, 4245-72.

7.   Nozik, A. J.; Miller, J. *Chem Rev* **2010,** *110*, 6443-5.

8.   Ohmori, Y. *Laser & Photonics Reviews* **2009,** *4*, 300-310.

9.   Roncali, J. *Acc Chem Res* **2009,** *42*, 1719-30.

10.   Hains, A. W.; Liang, Z.; Woodhouse, M. A.; Gregg, B. A. *Chem Rev* **2010,** *110*, 6689-735.

11.   Sark, W. G. J. H. M. v.; Barnham, K. W. J.; Slooff, L. H.; Chatten, A. J.; Büchtemann, A.; Meyer, A.; McCormack, S. J.; Koole, R.; Farrell, D. J.; Bose, R.; Bende, E. E.; Burgers, A. R.; Budel, T.; Quilitz, J.; Kennedy, M.; Meyer, T.; Donegá, C. D. M.; Meijerink, A.; Vanmaekelbergh, D. *Optics Express* **2008,** *16*, 21773.

12.   van Sark, W. G. J. H. M. *Renewable Energy* **2013,** *49*, 207-210.

13.   Barone, V.; Bellina, F.; Biczysko, M.; Bloino, J.; Fornaro, T.; Latouche, C.; Lessi, M.; Marianetti, G.; Minei, P.; Panattoni, A.; Pucci, A. *Phys Chem Chem Phys* **2015,** *17*, 26710-23.

14.   Kivala, M.; Diederich, F. *Acc Chem Res* **2009,** *42*, 235-48.

15.   Kato, S.; Diederich, F. *Chem Commun (Camb)* **2010,** *46*, 1994-2006.

16.   Meier, H. *Angew Chem Int Ed Engl* **2005,** *44*, 2482-506.

17.   Kuzyk, M. G. *Journal of Materials Chemistry* **2009,** *19*, 7444.

18.   Bures, F.; Schweizer, W. B.; May, J. C.; Boudon, C.; Gisselbrecht, J. P.; Gross, M.; Biaggio, I.; Diederich, F. *Chemistry* **2007,** *13*, 5378-87.

19.   May, J. C.; Biaggio, I.; Bures, F.; Diederich, F. o. *Applied Physics Letters* **2007,** *90*, 251106.

20.   Bureš, F.; Pytela, O.; Kivala, M.; Diederich, F. *Journal of Physical Organic Chemistry* **2011,** *24*, 274-281.

21.   De Proft, F.; Geerlings, P. *Chemical Reviews* **2001,** *101*, 1451-1464.

22.   Prampolini, G.; Bellina, F.; Biczysko, M.; Cappelli, C.; Carta, L.; Lessi, M.; Pucci, A.; Ruggeri, G.; Barone, V. *Chemistry* **2013,** *19*, 1996-2004.

23.   Lessi, M.; Manzini, C.; Minei, P.; Perego, L. A.; Bloino, J.; Egidi, F.; Barone, V.; Pucci, A.; Bellina, F. *ChemPlusChem* **2014,** *79*, 366-370.

24.   Barone, V.; Baiardi, A.; Biczysko, M.; Bloino, J.; Cappelli, C.; Lipparini, F. *Phys Chem Chem Phys* **2012,** *14*, 12404-22.

25.   Dreuw, A.; Head-Gordon, M. *Chem Rev* **2005,** *105*, 4009-37.

26.   Jacquemin, D.; Perpete, E. A.; Ciofini, I.; Adamo, C. *Acc Chem Res* **2009,** *42*, 326-34.

27.   Laurent, A. D.; Adamo, C.; Jacquemin, D. *Phys Chem Chem Phys* **2014,** *16*, 14334-56.

28.   Cammi, B. M. a. R., *Continuum Solvation Models in Chemical Physics: Theory and Applications*. Wiley2007.

29.   Pedone, A.; Prampolini, G.; Monti, S.; Barone, V. *Chemistry of Materials* **2011,** *23*, 5016-5023.

30.   Pedone, A.; Bloino, J.; Barone, V. *The Journal of Physical Chemistry C* **2012,** *116*, 17807-17818.

31.   De Mitri, N.; Prampolini, G.; Monti, S.; Barone, V. *Phys Chem Chem Phys* **2014,** *16*, 16573-87.

32.   Barone, V.; Biczysko, M.; Bloino, J.; Carta, L.; Pedone, A. *Computational and Theoretical Chemistry* **2014,** *1037*, 35-48.

33.   Bureš, F. *RSC Advances* **2014,** *4*, 58826-58851.

34.   Kulhánek, J.; Bureš, F.; Opršal, J.; Kuznik, W.; Mikysek, T.; Růžička, A. *Asian Journal of Organic Chemistry* **2013,** *2*, 422-431.

35.   Perepichka, I. F.; D. F, P. **2009**, i-xxii.

36.   Kulhanek, J.; Bures, F.; Kuznik, W.; Kityk, I. V.; Mikysek, T.; Ruzicka, A. *Chem Asian J* **2013,** *8*, 465-75.

37.   Togni, A.; Rihs, G. *Organometallics* **1993,** *12*, 3368-3372.

38.   Achelle, S.; Baudequin, C.; Plé, N. *Dyes and Pigments* **2013,** *98*, 575-600.

39.   Hrobarikova, V.; Hrobarik, P.; Gajdos, P.; Fitilis, I.; Fakis, M.; Persephonis, P.; Zahradnik, P. *J Org Chem* **2010,** *75*, 3053-68.

40.   Kulhanek, J.; Bures, F. *Beilstein J Org Chem* **2012,** *8*, 25-49.

41.   Hansch, C.; Leo, A.; Taft, R. W. *Chemical Reviews* **1991,** *91*, 165-195.

42.   Pytela, O. *Collection of Czechoslovak Chemical Communications* **1996,** *61*, 704-712.

43.   Ramirez, M. A.; Cuadro, A. M.; Alvarez-Builla, J.; Castano, O.; Andres, J. L.; Mendicuti, F.; Clays, K.; Asselberghs, I.; Vaquero, J. J. *Org Biomol Chem* **2012,** *10*, 1659-69.

44.   Wu, W.; Wang, C.; Zhong, C.; Ye, C.; Qiu, G.; Qin, J.; Li, Z. *Polym. Chem.* **2013,** *4*, 378-386.

45.   Kang, H.; Evmenenko, G.; Dutta, P.; Clays, K.; Song, K.; Marks, T. J. *J Am Chem Soc* **2006,** *128*, 6194-205.

46.   Roncali, J. *Macromolecular Rapid Communications* **2007,** *28*, 1761-1775.

47.   Roncali, J. *Chemical Reviews* **1997,** *97*, 173-206.

48.   Perepichka, D. F.; Bryce, M. R. *Angew Chem Int Ed Engl* **2005,** *44*, 5370-3.

49.   PAC, *Glossary of terms used in photochemistry, 3rd edition (IUPAC Recommendations 2006).* 2007.

50.   Valeur, B.; Berberan-Santos, M. N., *Molecular fluorescence: principles and applications*. WILEY-VCH2012; Vol. 8.

51.   Gratzel, M. *Inorg Chem* **2005,** *44*, 6841-51.

52.   Yang, J.; Ganesan, P.; Teuscher, J.; Moehl, T.; Kim, Y. J.; Yi, C.; Comte, P.; Pei, K.; Holcombe, T. W.; Nazeeruddin, M. K.; Hua, J.; Zakeeruddin, S. M.; Tian, H.; Gratzel, M. *J Am Chem Soc* **2014,** *136*, 5722-30.

53.   Lakowicz, J. R., *Principles of Fluorescence Spectroscopy*. Springer2006.

54.   Jayabharathi, J.; Thanikachalam, V.; Sathishkumar, R.; Jayamoorthy, K. *Spectrochim Acta A Mol Biomol Spectrosc* **2013,** *101*, 249-53.

55.   Zhang, M.; Li, M.; Zhao, Q.; Li, F.; Zhang, D.; Zhang, J.; Yi, T.; Huang, C. *Tetrahedron Letters* **2007,** *48*, 2329-2333.

56.   Chen, F.; Zhang, J.; Wan, X. *Chemistry* **2012,** *18*, 4558-67.

57.   Ooyama, Y.; Harima, Y. *Journal of Materials Chemistry* **2011,** *21*, 8372.

58.   Pucci, A.; Ruggeri, G. *Journal of Materials Chemistry* **2011,** *21*, 8282.

59.   Pucci, A.; Bizzarri, R.; Ruggeri, G. *Soft Matter* **2011,** *7*, 3689.

60.   Weber, W. H.; Lambe, J. *Appl Opt* **1976,** *15*, 2299-300.

61.   Rowan, B. C.; Wilson, L. R.; Richards, B. S. *IEEE Journal of Selected Topics in Quantum Electronics* **2008,** *14*, 1312-1322.

62.   Granqvist, C.-G.; Zastrow, A.; Wittwer, V.; Lampert, C. M.; Mason, J. J.; Wittwer, V. **1986,** *0653*, 93-100.

63.   Goetzberger, A. *Applied Physics* **1978,** *16*, 399-404.

64.   Hermann, A. M. *Solar Energy* **1982,** *29*, 323-329.

65.   Wittwer, V.; Stahl, W.; Goetzberger, A. *Solar Energy Materials* **1984,** *11*, 187-197.

66.   Deb, S. K.; Friedman, P. S. **1980,** *0248*, 97-104.

67.   Slooff, L. H.; Bende, E. E.; Burgers, A. R.; Budel, T.; Pravettoni, M.; Kenny, R. P.; Dunlop, E. D.; Büchtemann, A. *physica status solidi (RRL) - Rapid Research Letters* **2008,** *2*, 257-259.

68.   Carey, F. A.; Sundberg, R. J., *Advanced Organic Chemistry: Part A: Structure and Mechanisms.* Springer Science & Business Media2007.

69.   Moylan, C. R.; Miller, R. D.; Twieg, R. J.; Betterton, K. M.; Lee, V. Y.; Matray, T. J.; Nguyen, C. *Chemistry of Materials* **1993,** *5*, 1499-1508.

70.   Miller, R. D.; Lee, V. Y.; Moylan, C. R. *Chemistry of Materials* **1994,** *6*, 1023-1032.

71.   Shaker, R. M. *Arkivoc* **2011,** *2012*, 1.

72.   Fridman, N.; Speiser, S.; Kaftory, M. *Crystal Growth & Design* **2006,** *6*, 1653-1662.

73.   Mahadik, S. T.; Sunthankar, S. V. *Indian J. Chem.* **1975,** *13*, 1369-1370.

74.   Jadhav, S. D.; Kokare, N. D.; Jadhav, S. D. *Journal of Heterocyclic Chemistry* **2008,** *45*, 1461-1464.

75.   Song, G.-L.; Zhu, H.-J.; Chen, L.; Liu, S.; Luo, Z.-H. *Helvetica Chimica Acta* **2010,** *93*, 2397-2405.

76.   Song, G.; He, G.; Wang, S.; Zhu, H. *Journal of Luminescence* **2013,** *143*, 566-573.

77.   H. Erlenmeyer, W. B., and H. Lehr. *Helv. Chim. Acta* **1944,** *27*, 969-970.

78.   Trosken, O. 1955.

79.   Andreeshchev, E. A.; Viktorova, V. S.; Kilin, S. F.; Kovyrzina, K. A.; Kosyakina, L. N.; Kushakevich, Y. P.; Rozman, I. M.; Chkhikvadze, Y. G. *Chemistry of Heterocyclic Compounds* **1986,** *22*, 1262-1266.

80.   Noei, J.; Khosropour, A. R. *Ultrason Sonochem* **2009,** *16*, 711-7.

81.   Noei, J.; Khosropour, A. R. *Bulletin of the Korean Chemical Society* **2010,** *31*, 3073-3074.

82.   Bellina, F.; Rossi, R. *Advanced Synthesis & Catalysis* **2010,** *352*, 1223-1276.

83.   Bellina, F.; Lessi, M.; Manzini, C. *European Journal of Organic Chemistry* **2013,** *2013*, 5621-5630.

84.   Campeau, L. C.; Fagnou, K. *Chem Commun (Camb)* **2006,** 1253-64.

85.   Krishnamurthy, N. V.; Reddy, A. R.; Bhudevi, B. *J Fluoresc* **2008,** *18*, 29-34.

86.   Bellina, F.; Lessi, M.; Marianetti, G.; Panattoni, A. *Tetrahedron Letters* **2015,** *56*, 3855-3857.

87.   Carlotti, M.; Ruggeri, G.; Bellina, F.; Pucci, A. *Journal of Luminescence* **2016,** *171*, 215-220.

88.   Inoh, J.-I.; Satoh, T.; Pivsa-Art, S.; Miura, M.; Nomura, M. *Tetrahedron Letters* **1998,** *39*, 4673-4676.

89.   Adam, W.; Grimison, A. *Tetrahedron* **1966,** *22*, 835-839.

90.   Bellina, F.; Cauteruccio, S.; Di Fiore, A.; Marchetti, C.; Rossi, R. *Tetrahedron* **2008,** *64*, 6060-6072.

91.   Bellina, F.; Cauteruccio, S.; Mannina, L.; Rossi, R.; Viel, S. *J Org Chem* **2005,** *70*, 3997-4005.

92.   Catalan, J.; Elguero, J. **1987,** *41*, 187-274.

93.   Lafrance, M.; Fagnou, K. *J Am Chem Soc* **2006,** *128*, 16496-7.

94.   Gorelsky, S. I. *Coordination Chemistry Reviews* **2013,** *257*, 153-164.

95.   Petit, A.; Flygare, J.; Miller, A. T.; Winkel, G.; Ess, D. H. *Org Lett* **2012,** *14*, 3680-3.

96.   Gorelsky, S. I. *Organometallics* **2012,** *31*, 794-797.

97.   Liegault, B.; Lapointe, D.; Caron, L.; Vlassova, A.; Fagnou, K. *J Org Chem* **2009,** *74*, 1826-34.

98.   Chuvylkin, L. I. B. k. a. N. D. *Khimiya Geterotsiklicheskikh Soedin.* **1996,** 1535–1563.

99.   L. Chen, C. Y., S. Li, and J. Qin. *Spectrochim. Acta. A. Mol. Biomol. Spectrosc.* **2007,** *68*, 317–322.

100.   Wang, H.; Chen, G.; Xu, X.; Chen, H.; Ji, S. *Dyes and Pigments* **2010,** *86*, 238-248.

101.   Bellina, F.; Cauteruccio, S.; Rossi, R. *J Org Chem* **2007,** *72*, 8543-6.

102.   Li, Y.; Jin, J.; Qian, W.; Bao, W. *Org Biomol Chem* **2010,** *8*, 326-30.

103.   Zhu, M.; Fujita, K.; Yamaguchi, R. *Chem Commun (Camb)* **2011,** *47*, 12876-8.

104.   Qin, X.; Feng, B.; Dong, J.; Li, X.; Xue, Y.; Lan, J.; You, J. *J Org Chem* **2012,** *77*, 7677-83.

105.   Chodowska-Palicka, J.; Nilsson, M. *Synthesis* **1974,** *1974*, 128-129.

106.   Sonogashira, K. *Journal of Organometallic Chemistry* **2002,** *653*, 46-49.

107.   S. De Ornellas, T. E. S., T. J. Williams, C. G. Baumann, and I. J.S.; Fairlamb. *Curr. Org. Synth.* **2011,** *8*, 79-101.

108.   Bellina, F.; Cauteruccio, S.; Rossi, R. *European Journal of Organic Chemistry* **2006,** *2006*, 1379-1382.

109.   Bellina, F.; Calandri, C.; Cauteruccio, S.; Rossi, R. *Tetrahedron* **2007,** *63*, 1970-1980.

110.   Heimel, G.; Daghofer, M.; Gierschner, J.; List, E. J.; Grimsdale, A. C.; Mullen, K.; Beljonne, D.; Bredas, J. L.; Zojer, E. *J Chem Phys* **2005,** *122*, 54501.

111.   Hohenberg, P.; Kohn, W. *Physical Review* **1964,** *136*, B864-B871.

112.   Kohn, W.; Sham, L. J. *Physical Review* **1965,** *140*, A1133-A1138.

113.   Burke, K.; Werschnik, J.; Gross, E. K. *J Chem Phys* **2005,** *123*, 62206.

114.   Casida, M. E. *Journal of Molecular Structure: THEOCHEM* **2009,** *914*, 3-18.

115.   Yanai, T.; Tew, D. P.; Handy, N. C. *Chemical Physics Letters* **2004,** *393*, 51-57.

116.   Barone, V.; Biczysko, M.; Bloino, J. *Phys Chem Chem Phys* **2014,** *16*, 1759-87.

117.   Bloino, J.; Biczysko, M.; Santoro, F.; Barone, V. *Journal of Chemical Theory and Computation* **2010,** *6*, 1256-1274.

118.   Iliashenko, R. Y.; Gorobets, N. Y.; Doroshenko, A. O. *Tetrahedron Letters* **2011,** *52*, 5086-5089.

119.   Jacquemin, D.; Perpete, E. A.; Scuseria, G. E.; Ciofini, I.; Adamo, C. *J Chem Theory Comput* **2008,** *4*, 123-35.

120.   Lee, S. U. *Bulletin of the Korean Chemical Society* **2013,** *34*, 2276-2280.

121.   Jacquemin, D.; Perpete, E. A.; Scalmani, G.; Frisch, M. J.; Assfeld, X.; Ciofini, I.; Adamo, C. *J Chem Phys* **2006,** *125*, 164324.

122.   Bellina, F.; Manzini, C.; Marianetti, G.; Pezzetta, C.; Fanizza, E.; Lessi, M.; Minei, P.; Barone, V.; Pucci, A. *Dyes and Pigments* **2016,** *134*, 118-128.

123.   Heravi, M. M.; Tehrani, M. H.; Bakhtiari, K.; Oskooie, H. A. *Journal of Chemical Research* **2006,** *2006*, 561-562.

124.   Carlotti, M.; Fanizza, E.; Panniello, A.; Pucci, A. *Solar Energy* **2015,** *119*, 452-460.

125.   Griffini, G.; Levi, M.; Turri, S. *Renewable Energy* **2015,** *78*, 288-294.

126.   Minei, P.; Fanizza, E.; Rodríguez, A. M.; Muñoz-García, A. B.; Cimino, P.; Pavone, M.; Pucci, A. *RSC Adv.* **2016,** *6*, 17474-17482.

127.   De Clercq, E.; Cools, M.; Balzarini, J.; Snoeck, R.; Andrei, G.; Hosoya, M.; Shigeta, S.; Ueda, T.; Minakawa, N.; Matsuda, A. *Antimicrobial Agents and Chemotherapy* **1991,** *35*, 679-684.

128.   Minei, P.; Battisti, A.; Barondi, S.; Lessi, M.; Bellina, F.; Ruggeri, G.; Pucci, A. *ACS Macro Letters* **2013,** *2*, 317-321.

129.   Mahuteau-Betzer, F.; Piguel, S. *Tetrahedron Letters* **2013,** *54*, 3188-3193.

130.   Kobayashi, H.; Ogawa, M.; Alford, R.; Choyke, P. L.; Urano, Y. *Chem Rev* **2010,** *110*, 2620-40.

131.   Siejak, P.; Frackowiak, D. *J Phys Chem B* **2005,** *109*, 14382-6.

132.   Freundlich, A.; Guillemoles, J.-F.; Digaum, J.; Kuebler, S. M. *Proc. SPIE* **2014,** *8981*, 89810E.

133.   Bellina, F.; Guazzelli, N.; Lessi, M.; Manzini, C. *Tetrahedron* **2015,** *71*, 2298-2305.

134. Schnürch, M.; Flasik, R.; Khan, A. F.; Spina, M.; Mihovilovic, M. D.; Stanetty, P. *European Journal of Organic Chemistry* **2006,** *2006*, 3283-3307.

135. Ohta, A.; late) Yasuo, A. *Heterocycles* **1990,** *31*, 1951.

136. Rossi, R.; Bellina, F.; Lessi, M.; Manzini, C. *Advanced Synthesis & Catalysis* **2014,** *356*, 17-117.

137. He, M.; Soulé, J.-F.; Doucet, H. *ChemCatChem* **2014,** *6*, 1824-1859.

138. Ohta, A.; Aoyagi, Y.; Inoue, A.; Koizumi, I.; Hashimoto, R.; Tokunaga, K.; Gohma, K.; Komatsu, J.; Sekine, K.; Miyafuji, A.; Kunoh, J.; Honma, R.; late) Yasuo, A. *Heterocycles* **1992,** *33*, 257.

139. Kondo, Y.; Komine, T.; Sakamoto, T. *Organic Letters* **2000,** *2*, 3111-3113.

140. Toure, B. B.; Lane, B. S.; Sames, D. *Org Lett* **2006,** *8*, 1979-82.

141. Chiong, H. A.; Daugulis, O. *Org Lett* **2007,** *9*, 1449-51.

142. Skogh, A.; Fransson, R.; Skold, C.; Larhed, M.; Sandstrom, A. *J Org Chem* **2013,** *78*, 12251-6.

143. Cerna, I.; Pohl, R.; Klepetarova, B.; Hocek, M. *Org Lett* **2006,** *8*, 5389-92.

144. Majumdar, K. C.; Debnath, P.; Taher, A.; Pal, A. K. *Canadian Journal of Chemistry* **2008,** *86*, 325-332.

145. Mori, A.; Arai, N.; Takahashi, M.; Mitani, M. *Synlett* **2006,** *2006*, 3170-3172.

146. Kumar, P. V.; Lin, W.-S.; Shen, J.-S.; Nandi, D.; Lee, H. M. *Organometallics* **2011,** *30*, 5160-5169.

147. Shibahara, F.; Yamaguchi, E.; Murai, T. *Chem Commun (Camb)* **2010,** *46*, 2471-3.

148. Shibahara, F.; Yamaguchi, E.; Murai, T. *J Org Chem* **2011,** *76*, 2680-93.

149. Pivsa-Art, S.; Satoh, T.; Kawamura, Y.; Miura, M.; Nomura, M. *Bulletin of the Chemical Society of Japan* **1998,** *71*, 467-473.

150. Takfaoui, A.; Zhao, L.; Touzani, R.; Soulé, J.-F.; Dixneuf, P. H.; Doucet, H. *Tetrahedron* **2014,** *70*, 8316-8323.

151. Bellina, F.; Cauteruccio, S.; Mannina, L.; Rossi, R.; Viel, S. *European Journal of Organic Chemistry* **2006,** *2006*, 693-703.

152. Pandey, S.; Ali, M.; Kamath, G.; Pandey, S.; Baker, S. N.; Baker, G. A. *Anal Bioanal Chem* **2012,** *403*, 2361-6.

153. Roger, J.; Doucet, H. *Tetrahedron* **2009,** *65*, 9772-9781.

154. Primas, N.; Bouillon, A.; Lancelot, J.-C.; El-Kashef, H.; Rault, S. *Tetrahedron* **2009,** *65*, 5739-5746.

155. Jensen, J.; Skjaerbaek, N.; Vedsø, P. *Synthesis* **2001,** *2001*, 0128-0134.

156. Roger, J.; Pozgan, F.; Doucet, H. *J Org Chem* **2009,** *74*, 1179-86.

157. Chen, L.; Yang, C.; Li, S.; Qin, J. *Spectrochim Acta A Mol Biomol Spectrosc* **2007,** *68*, 317-22.

158. Weekes, A. A.; Bagley, M. C.; Westwell, A. D. *Tetrahedron* **2011,** *67*, 7743-7747.

159. Kalwania, G. C., S.; Choudhary S. *Asian Journal of Chemistry* **2011,** *23*, 5133.

160. Zheng, W.; He, X.; Chen, H.; Gao, Y.; Li, H. *Spectrochim Acta A Mol Biomol Spectrosc* **2014,** *124*, 97-101.

161. Lee, C. J.; Sheu, C. N.; Tsai, C. C.; Wu, Z. Z.; Lin, W. *Chem Commun (Camb)* **2014,** *50*, 5304-6.

162. Crosby, G. A.; Demas, J. N. *The Journal of Physical Chemistry* **1971,** *75*, 991-1024.

163. Guilbault, G. G. *General Aspects of Luminescene Spectro- scopy* **1990**, 1-41.

164. Scalmani, G.; Frisch, M. J.; Mennucci, B.; Tomasi, J.; Cammi, R.; Barone, V. *J Chem Phys* **2006,** *124*, 94107.

165. Peach, M. J.; Helgaker, T.; Salek, P.; Keal, T. W.; Lutnaes, O. B.; Tozer, D. J.; Handy, N. C. *Phys Chem Chem Phys* **2006,** *8*, 558-62.

166. Isegawa, M.; Peverati, R.; Truhlar, D. G. *The Journal of Chemical Physics* **2014,** *140*, 129901.

167. Barone, V.; Biczysko, M.; Borkowska-Panek, M.; Bloino, J. *Chemphyschem* **2014,** *15*, 3355-64.

168. Tomasi, J.; Mennucci, B.; Cammi, R. *Chem Rev* **2005,** *105*, 2999-3093.

169.	Cramer, C. J.; Truhlar, D. G. *Chemical Reviews* **1999,** *99*, 2161-2200.

170.	Cossi, M.; Rega, N.; Scalmani, G.; Barone, V. *J Comput Chem* **2003,** *24*, 669-81.

171.	M. J. Frisch, G. W. T., H. B. Schlegel, G. E. Scuseria, M. A. Robb, J. R. Cheeseman, G. Scalmani, V. Barone, B. Mennucci, G. A. Petersson, H. Nakatsuji, M. Caricato, X. Li, H. R. Hratchian, A. F. Izmaylov, J. Bloino, G. Zheng, J. L. Sonnenberg, M. Hada, M. Ehara, K. Toyota, R. Fukuda, J. Hasegawa, M. Ishida, T. Nakajima, Y. Honda, O. Kitao, H. Nakai, T. Vreven, J. R. Montgomery Jr., J. A. Peralta, F. Ogliaro, M. Bearpark, J. J. Heyd, E. Brothers, K. N. Kudin, V. N. Staroverov, R. Kobayashi, J. Normand, K. Raghavachari, A. Rendell, J. C. Burant, S. S. Iyengar, J. Tomasi, M. Cossi, N. Rega, J. M. Millam, M. Klene, J. E. Knox, J. B. Cross, V. Bakken, C. Adamo, J. Jaramillo, R. Gomperts, R. E. Stratmann, O. Yazyev, A. J. Austin, R. Cammi, C. Pomelli, J. W. Ochterski, R. L. Martin, K. Morokuma, V. G. Zakrzewski, G. A. Voth, P. Salvador, J. J. Dannenberg, S. Dapprich, A. D. Daniels, O. Farkas, J. B. Foresman, J. V. Ortiz, J. Cioslowski and D. J. Fox, Gaussian 09 Revision D.01. Gaussian Inc., Wallingford CT, 2009.

172.	Marenich, A. V.; Cramer, C. J.; Truhlar, D. G.; Guido, C. A.; Mennucci, B.; Scalmani, G.; Frisch, M. J. *Chemical Science* **2011,** *2*, 2143.

173.	Reed, A. E.; Curtiss, L. A.; Weinhold, F. *Chemical Reviews* **1988,** *88*, 899-926.

174.	Baiardi, A.; Bloino, J.; Barone, V. *J Chem Theory Comput* **2013,** *9*, 4097-115.

175.	Dymond, J. F. a. E. G. *Trans. Faraday Soc.* **1926,** *21*, 536-542.

176.	Condon, E. U. *Physical Reviews* **1926**, 1182-1210.

177.	Condon, E. U. *Physical Reviews*
1928, 858-872.

178.	Avila Ferrer, F. J.; Santoro, F. *Phys Chem Chem Phys* **2012,** *14*, 13549-63.

179.	Macak, P.; Luo, Y.; Ågren, H. *Chemical Physics Letters* **2000,** *330*, 447-456.

180.	Licari, D.; Baiardi, A.; Biczysko, M.; Egidi, F.; Latouche, C.; Barone, V. *J Comput Chem* **2015,** *36*, 321-34.

Acknowledgements